Impact of Soil Moisture and Vegetation Distribution on July 1989 Climate Using a Regional Climate Model

By
Jeffrey H. Copeland

P.I. Roger A. Pielke

Department of Atmospheric Science
Colorado State University
Fort Collins, Colorado

NPS CA 1268-2-9004 CEGR-R92-0193 and COLR-R92-0204
CSMP (UCAR) S9361
USGS grant 1434-94-A-1275

Colorado State University

Department of Atmospheric Science

Paper No. 574

IMPACT OF SOIL MOISTURE AND VEGETATION DISTRIBUTION ON JULY 1989 CLIMATE USING A REGIONAL CLIMATE MODEL

Jeffrey H. Copeland

Department of Atmospheric Science
Colorado State University
Fort Collins, Colorado
Spring 1995

Atmospheric Science Paper No. 574

ABSTRACT

IMPACT OF SOIL MOISTURE AND VEGETATION DISTRIBUTION ON JULY 1989 CLIMATE USING A REGIONAL CLIMATE MODEL

Anyone who has ever walked from a closed forest into an open meadow knows that vegetation can have a significant effect on the atmosphere. Additionally, anyone who has tried gardening is also aware of the role the atmosphere can have on the success or failure of that hobby. It is fairly well understood, at least in a broad sense, how the earth's surface and the planetary boundary layer interact on the local scale. What is less known is how changes in the characteristics of the earth's surface feed back up to larger scales such as regional or global. This has important consequences in understanding how changes in surface characteristics due to natural or anthropogenic causes impact the climate. Perhaps even more important, is understanding the sensitivity of our parameterizations of atmosphere-landsurface interactions to the specification of the earth's surface.

The Regional Atmospheric Modeling System has been modified for use in regional climate studies (CLIMRAMS). The model has been verified for July 1989 and has shown that the simulated screen height temperatures over 70% of the model domain were within 1°C of observations. The the simulated precipitation was generally within a factor of two of the observations. The United States average daily precipitation was 2.3mm·day^{-1} while the simulated rate was 1.9mm·day^{-1}.

The model was also applied to sensitivity studies to assess the impact of soil moisture and vegetation distribution. Results from the soil moisture studies indicate that the initial specification of the soil moisture content can have small but significant effects on screen height quantities and precipitation for time periods up to a month. Results from a homogeneous grassland study demonstrate that regionally there can be cooling due to increased albedo or warming due to decreased latent heat flux. Finally, CLIMRAMS was applied to study the effect of lost forest and grassland ecosystems to agricultural usage. The results of the final study suggest the possibility that the current landuse has caused summertime surface conditions to be warmer and drier than the natural landscape would indicate.

Jeffrey H. Copeland
Department of Atmospheric Science
Colorado State University
Fort Collins, Colorado 80523
Spring 1995

ACKNOWLEDGEMENTS

I would first like to thank my thesis advisor, Dr. Roger A. Pielke, for his continued support and insight; and for allowing me the freedom to chart my own course during my studies. I would also like to thank my co-advisor, Dr. William R. Cotton for bringing me to Colorado State University originally. Thanks are also due to my remaining committee members, Drs. Richard Johnson, Tom Vonderhaar, and Dennis Ojima. Special thanks are given to Dennis for being able to join the committee at such a late juncture.

I would also like to thank Dr. Timothy Kittel of the Climate Systems Modeling Program and all the other scientists and students at CSU, UW, and OSU/EPA/USFS working on the Central Grasslands Climate Change Project for their helpful and enlightening discussions on ecosystems, botany, and hydrology. Tom Chase, who worked on the parallel Colorado Rockies Project, I pass on to him the "green briefcase of conference junkets".

Thanks are also due to Scot Heckman, Cathy Finley, John Lee, John Knowles, Brent Shaw, Scott Denning, David Mocko, Matt Savoie and Jerry Harrington, who provided endless hours (maybe too many) of insightful discussions and trivial babblings on atmospheric science and other things over the years. Jason Nachamkin, thanks for watching our menagerie whenever we had time to get out of town for a few days. I know that there are many who have not been mentioned by name due to limited space so please forgive me, particularly if you happen to review a manuscript of mine in the future.

Dallas McDonald and Brenda Thompson are owed a tremendous amount of thanks for making sure all the administrative details were taken care of, and that I always managed to arrive in the right city at the right time for a conference.

I also owe deep debts of gratitude to the following professors for helping me get to CSU. The late Dr. Walter Hitschfeld of McGill University who introduced me to atmospheric science. Dr. Roddy Rogers, also of McGill, who in my senior undergraduate year, when I was all set to send out my graduate school applications, said "solid state physics is a dead field, you should continue on in meteorology". Most of all to Dr. Akio Arakawa, of UCLA, who impressed upon me that physical insight is more important than memorizing anything that can be looked up.

I received financial support for my research from National Park Service Contract CA 1268-2-9004, CEGR-R92-0193 and COLR-R92-0204; United States Geological Survey Grant No. 1434-94-A-1275; the Climate System Modeling Program through Subcontract #UCAR S9361; and the Crawfords, my in-laws, for Christmas trips. I would also like to thank Dr. Jim Lenihan for providing the natural vegetation distribution data.

My father for introducing me to computers. I still remember that day he took me into work when I was six and I was typing away on a one line gas-tube display terminal.

Lastly, but most important of all, I would like to thank my wife Cathy. This would not have been possible were it not for her continual support and encouragement over the years.

TABLE OF CONTENTS

LIST OF TABLES

LIST OF FIGURES

LIST OF ABBREVIATIONS

API	Antecedent Precipitation Index
BATS	Biosphere-Atmosphere Transfer Scheme
BMRC	Bureau of Meteorology Research Center
CCC	Canadian Climate Center
CLIMRAMS	Climate version of RAMS
ECMWF	European Center for Medium Range Forecasts
GCM	General Circulation Model
GFDL	Geophysical Fluid Dynamics Laboratory
GISS	Goddard Institute for Space Sciences
GMASS	GISS Mesoscale Atmospheric Simulation System
LAI	Leaf Area Index
NBS	National Biological Survey
NCAR	National Center for Atmospheric Research
NDVI	Normalized Difference Vegetation Index
NMC	National Meteorological Center
NOAA	National Oceanic and Atmospheric Administration
NPS	National Park Service
OSU	Oregon State University
PAR	Photosynthetically Active Radiation
RAMS	Regional Atmospheric Modeling System
RegCM	Regional Climate Model
RISC	Reduced Instruction Set Chip
SST	Sea Surface Temperature
SWP	Soil Water Potential
UKMO	United Kingdom Meteorological Office
USDA	United States Department of Agriculture
USGS	United States Geological Survey
VPD	Vapor Pressure Deficit

LIST OF SYMBOLS

C_p	specific heat of air at constant pressure
C_s	volumetric specific heat of soil
C_w	specific heat of water
d	displacement height
D_η	soil moisture diffusivity
f_v	fractional coverage of vegetation
F	seasonal parameter
k	API regression coefficient
K_η	soil hydraulic conductivity
L	latent heat of evaporation
$\mathcal{P}$	precipitation flux into soil
r_s	stomatal resistance
R_i	API daily precipitation
R_L	net solar longwave radiation
R_S	net solar shortwave radiation
q^*	mixing ratio scale
t	time
T_a	amplitude of annual screen height temperature
T_G	top soil layer temperature
T_m	mean annual screen height temperature
T_{VG}	vegetation temperature
$T_{0.2m}$	soil temperature at 0.2m depth
$\mathcal{T}$	transpiration moisture flux from soil layer
u^*	friction velocity
r_r	root ratio in upper soil layer
r_z	maximum depth of roots
z	depth
Z_{ov}	vegetation roughness length

Δz_G	thickness of top soil layer
ΔZ_c	thickness of pseudo-cloud layer
α_{pc}	pseudo-cloud albedo
α_v	vegetation albedo
ϵ_s	soil emissivity
ϵ_v	vegetation emissivity
ε_p	precipitation efficiency
η	volumetric soil moisture content
η_G	top layer volumetric soil moisture content
Θ_G	top soil layer potential temperature
Θ_S	soil potential temperature
Θ_{VG}	vegetation potential temperature
Θ^*	potential temperature scale
λ	soil thermal conductivity
Π	Exner function
ρ_a	density of air
ρ_w	density of water
σ	Stefan-Boltzmann constant
τ	day of year
τ_v	shortwave transmissivity of vegetation

Chapter 1

INTRODUCTION

General Circulation Models (GCMs) have been used for decades to investigate questions relating to the earth's climate. In recent years they have been used to look at climate change. While the GCMs provide reasonable results on the global scale, Hewitson (1994) states that *GCMs are currently unable to reliably predict the regional climate change resulting from global warming, and it is at the regional scale that predictions are required for understanding human and environmental responses.* Regionally the global models have great difficulty in replicating the current climate, and in climate change scenarios they even disagree on the sign of the changes in atmospheric and surface fields.

To remedy this deficiency various investigators have used different methods to attempt to derive regional information from GCM simulations. These fall into three categories: direct interpolation; statistical interpolation; and dynamic interpolation. Direct interpolation involves making direct comparisons between GCM grid cell results and observations which fall in the area of the grid cell (Stuart and Isaac 1994, Dumenil 1993, Portman et al. 1992, Goodess and Palutikof 1992). Statistical interpolation attempts to relate the sub-grid spatial distribution of parameters which the GCM handles poorly (precipitation, soil moisture, etc.) to large scale parameters which are simulated reasonably well by the GCM (pressure fields, etc.) through statistical regressions (Gao and Sorooshian 1994, Von Storch et al. 1993, Hewitson and Crane 1992). Dynamic interpolation involves taking the output fields from the GCM and using them as initial and boundary conditions for a regional model. The

aim is that the regional model with its much finer resolution (and physics) will be able to spin up appropriate local circulations in response to the large scale forcing Giorgi et al. 1994, Segal et al. 1994, McGregor and Walsh 1993).

Prior to using any numerical model one should know what its capabilities are and be aware of the sensitivities of its parameterizations. This has not been satisfactorily demonstrated with the models currently being used in downscaling experiments. If we are to use the Regional Atmospheric Modeling System (RAMS) developed at Colorado State University to downscale GCM results in order to investigate the potential effects of global climate change at regional scales over the United States, two questions immediately need to be addressed. The first is: what is the capability of RAMS to represent the salient features of the atmosphere and land surface over extended periods of time? In the past RAMS has only been run out from an initialization for up to a couple of days. The second, and most important question is: what is the sensitivity of RAMS over extended time periods to the specification of the landsurface at scales that matter? The "scales that matter" are defined as those which affect the common inhabitants of this planet (animal and vegetable). This means that we are interested in what is happening at or near the surface at regional spatial scales.

This dissertation will explore some of these effects and sensitivities at regional scales over the continental United States for time scales of one month. The method used involves impact assessments using the RAMS model. This was done by running a series of month-long simulations with various surface conditions, and quantifying the impact that changes in land-surface characteristics had on atmospheric properties such as screen height winds, temperature, and humidity; latent and sensible heat fluxes; and precipitation.

The second chapter will discuss some of the work that has been done on the downscaling of GCM simulations to regional scales. A review of sensitivity studies

of atmospheric models (global and mesoscale) to landsurface characterizations will be made. In Chapter 3 the RAMS model will be described. Focus will be on the modifications made to the standard model to run in a climate mode, the limitations of the parameterizations available, and the reasoning for the configuration used in this study. The results of the simulations will be presented in Chapter 4. First, a comparison of the control run, with current landuse distribution, to observations will be made to assess the skill of the regional climate version of RAMS (CLIMRAMS). Then the impact simulations (natural vegetation, homogeneous vegetation, and various soil moisture distributions) will be analyzed statistically to determine the significance of the changes in the results. Finally, in Chapter 5, a summary and conclusions of the results will be presented along with some suggestions for further research.

Chapter 2

BACKGROUND

In recent years there has been heightened awareness in the general public to potential impacts of climate change due to the consequences of human activities. Particular emphasis has been placed on the role of increased greenhouse gases but other important forcings include: deforestation, ozone depletion, and the effects of natural and anthropogenic aerosols. The favored method for studying these forcings and their effects is through the use of GCM simulations. The area where the effects of any climate change will be felt most is at the earth's landsurface. This is intuitive since it is where we live and the majority of our food production depends on the quality of the surface vegetation. In order to assess the impacts of climate change on ecosystems and society one has to look at regional and local scales. A problem with using current GCM scenarios of climate change is that they are unable to accurately simulate even the seasonal cycle of climate at regional scales (Robock et al., 1993).

There are several questions that need to be examined. What atmospheric parameters control plant growth? How might the controls be obtained from model results, either directly or indirectly? How sensitive are the models that we use to the specification of landsurface characteristics? How does the feedback between the atmosphere and the landsurface work?

2.1 Plant Growth Controls and Modeling

The structure and growth rates of vegetation are controlled primarily by atmospheric conditions in time and over space, though soil nutrients can be a limiting

factor (Parton et al., 1987). The CO_2 that plants consume in photosynthesis enters the plants through the stomata in the leaves. Plants control the opening and closing of the stomata to optimize carbon gain while minimizing water loss (Collatz et al., 1991). There are several atmospheric controls on the functioning of the stomata.

The availability of shortwave radiation is the dominant control due to the photochemical reactions in photosynthesis. The stomata will open when light is available and shut when it is not. The intensity and duration of the shortwave radiation are primarily determined by the orbital parameters of the earth and the location of the plant on the earth. The intensity of the solar radiation will be modulated by any cloud cover and other shading effects.

The temperature of the leaf will cause the stomata to open if the temperature exceeds a minimum threshold value but the stomata will close again if the temperature is too high. The leaf temperature is controlled by the net radiation absorbed by the leaf and sensible and latent heat exchanges with the atmosphere.

Water stress will cause the stomata to close to prevent the net loss of moisture by the plant. The water stress is a balance between the supply and demand of water to the plant. The demand is caused by the vapor pressure deficit between the leaves and the atmosphere. The supply is determined by the soil water potential, which is the pressure required to extract water out of the soil by the plant.

The final control is the CO_2 concentration in the atmosphere. Higher CO_2 concentrations will cause the stomatal resistance to decrease. The combination of these four controlling factors is complex in determining the actual openness of the stomata and hence the rate of carbon gain by the plant. This would also have to account for the effect of soil nutrients which act as catalysts in the photosynthetic reactions.

Ecosystem process models such as CENTURY (Parton et al., 1987) and BIOME-BGC (Running and Hunt, 1993) simulate vegetation processes such as:

plant growth; nutrient cycling; and soil organic matter dynamics. The models are run at time steps from one day to one month. For inputs they require accumulated precipitation and average minimum and average maximum temperature valid for the period of the time step. They also require spatial databases of soil texture and vegetation type. The models have been validated spatially from plot to global scales. They have also been validated in equilibrium and transient time modes for a single growing season up to several decades.

Plant growth in the drier regions of the earth is highly sensitive to the seasonal distribution of rainfall. Roughly one-third of the earth's landsurface is covered by arid and semi-arid regions. This also is where the major grain and livestock rangelands occur. These regions may be the first to exhibit signs of any climate change due to their sensitivity to rainfall (Ojima et al., 1992).

Process models provide a good tool to examine the ecosystem vulnerability of the arid and semi-arid regions, along with other areas, to climatic change. This can be accomplished by adjusting the current meteorological inputs to simulate changes in: precipitation amount; precipitation seasonality; mean temperature; and temperature range. Unfortunately policymakers generally want a forecast of conditions at a particular time in the future. This has led to the extraction of grid point data from GCM climate change scenarios for use as inputs for ecosystem process models to make agricultural forecasts (Adams et al., 1990; Parry et al., 1988). The problem with this is that the process models require detailed regional climate inputs, yet the global models do not currently provide accurate regional information (Schimel et al., 1994). This may cause the ecosystem impacts to be determined by the error of extracting grid point data rather than by climate change (Robock et al., 1993).

2.2 Global Models and Downscaling

General circulation models are capable of resolving atmospheric structure at large spatial scales (continental to global) and long time scales (seasonal to annual).

At the important scales for impact studies (local to regional and daily to monthly) GCMs have trouble simulating important parameters such as surface temperature and precipitation (Kiehl, 1992).

Part of the problem is the minimal scale at which any model's results can be interpreted. Pielke (1984) states that the minimal scale of resolved features in a numerical model is at least four times the horizontal grid separation. Grotch and MacCracken (1991) argue for an even larger scale of eight grid intervals. Figure 2.1 shows the horizontal grid structure of several GCMs over the southeastern United States. It is evident from the limits of resolvability that the results of all of these models should not be interpreted at spatial scales of less than the whole area shown. The atmospheric circulations responsible for the distribution of regional scale climate features are the result of systems and gradients that are at the most several hundred kilometers across. This is well below the resolution of current GCMs (1500 to 2000 kilometers).

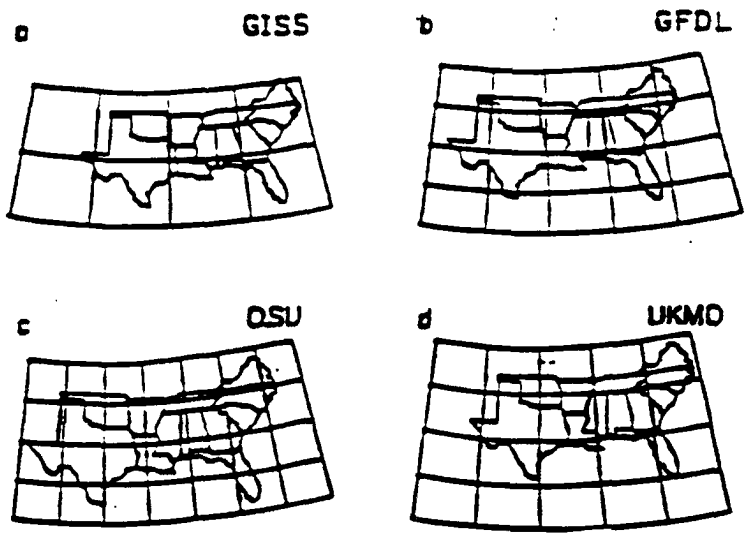

Figure 2.1: Horizontal resolution of four general circulation models across the southern U.S. (from Cooter et al., 1993).

The other part of the problem, and partially related to the spatial resolution of the models, is the lack of appropriate representation of fine-scale effects of terrain,

inland water, land cover, radiation, and cloud processes (Sellers, 1992). The whole problem of resolution and representation of sub-grid physical processes is not limited to the horizontal. Pielke et al. (1992) pose the question, "With coarse vertical resolution, is the flux divergence of longwave radiation properly represented so that accurate estimates of meteorological screen level temperatures can be obtained?".

In order to interpret GCM results at regional and local scales one must use some method of downscaling. The downscaling methods have been classified into three types of interpolation: direct interpolation; statistical interpolation; and dynamic interpolation. The term interpolation is used because in a sense that is what all of the methods do. They obtain a data value at a location from nearby model values. Unlike standard interpolation methods which preserve or filter the scale of information these methods attempt to increase the information content of the original data.

2.2.1 Direct Interpolation

Direct interpolation is either the interpretation of GCM model results at each grid cell as representative of the geographical area they cover or interpreting the model results at the grid nodes and spatially interpolating between them. This method fails because it violates the minimum scale at which one can interpret numerical models described in the previous section. This has not prevented its use.

Dumenil (1993) compared the climatology of Little Rock, Arkansas to that at a nearby grid point from the Max Planck Institute GCM simulations of current climate made at two different resolutions and three different soil moistures (Figure 2.2). Only slight improvement is shown at higher resolution.

Goodess and Palutikof (1992) made inter-model comparisons of $2\times CO_2$ - $1\times CO_2$ equilibrium simulations from the UKMO, GISS, NCAR, GFDL, and OSU GCMs. They made two types of comparisons. The first was comparing the grid points in the area 50°–67.5°N × 11.25°W–10°E. Each model had between six and

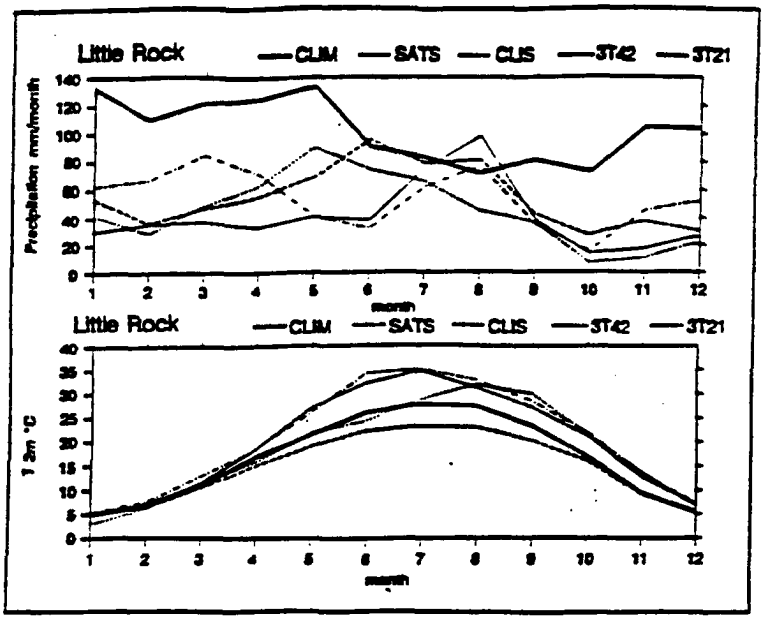

Figure 2.2: Climatology of Little Rock, Arkansas compared with the Max Planck Institute GCM. Little Rock (bold solid), T21 (solid), T42 (dash-dot), CLIS, ideal soil moisture (dot), and SATS, saturated soil (dash) (from Dumenil, 1993).

nine grid points in this region. Scatter plots of seasonal averages of temperature and precipitation changes show the numerical noise associated with individual grid point comparisons. The other comparison was between the GFDL and NCAR GCMs for the grid points along 55.55°N at 7.5°W, 0°, and 7.5°E. Aside from showing the lack of consensus between models the data presented also exhibited short wavelength noise.

Goodess and Palutikof (1992) also presented a comparison between two grid points of the UKMO GCM to climate data for Plymouth, England and Edinburgh, Scotland. They point out that this is not a recommended validation procedure. Their analysis indicated that neither grid point approximated the current climate. The conclusion was that the error in the model was due to inappropriate surface conditions. The grid point near Edinburgh was modeled as an ocean grid while the real surface is a complex mix of highlands, lowlands, and ocean.

Mitchell et al. (1990) produced "best estimates" of changes in temperature, precipitation, and soil moisture for five regions from three GCMS (CCC, GFDL, and

UKMO) (see Table 2.1). The first point to note is that for the regions listed, only SE Asia and Australia come close to being resolved by the GCMs. The estimates show light consensus on the temperature change. There is little or no consensus on the precipitation or soil moisture change, both of which are important controls for plant growth. Mitchell et al. (1990) admit that the confidence in the estimates is low.

Region	Model	Temperature (°C)		Precipitation (%)		Soil moisture (%)	
		DJF	JJA	DJF	JJA	DJF	JJA
Central N. America (35-50N, 80-105W)	CCC	4	2	0	-5	-10	15
	GFDL	2	2	15	-5	15	-15
	UKMO	4	3	10	-10	-10	-20
SE Asia (5-30N, 70-105E)	CCC	1	1	-5	5	0	5
	GFDL	2	1	0	10	-5	10
	UKMO	2	2	-15	15	0	5
Sahel (10-20N, 20W-40E)	CCC	2	3	-10	5	0	-5
	GFDL	2	1	-5	5	5	0
	UKMO	1	2	0	0	10	-10
Southern Europe (35-50N, 10W-45E)	CCC	2	2	5	-15	0	-15
	GFDL	2	2	10	-5	5	-15
	UKMO	2	3	0	-15	-5	-25
Australia (12-45S, 110-155E)	CCC	1	2	15	0	45	5
	GFDL	2	2	5	0	-5	-10
	UKMO	2	2	10	0	5	0

Table 2.1: Areal differences between $1\times CO_2$ and $2\times CO_2$ from several GCMs (from Mitchell et al., 1990).

Similar comparisons of the UKMO GCM over western Europe to local station observations (Reed, 1986; Wilson and Mitchell, 1987) also concluded that the comparisons were inconclusive due to sub-grid variations in topography and landcover not resolved in the model.

Comparisons of GCM current climate scenarios at minimal resolvable scales (greater than 20° × 20° regions) have shown inconsistencies in the simulated cli-

mate in many areas (Grotch and MacCraken, 1991). Robock et al. (1993) showed results from current climate scenarios by the GFDL, OSU, GISS, and UKMO GCMs over China and the GFDL, OSU, and GISS GCMs for equatorial Africa. The results indicate that none of the models were able to simulate the pattern of summer precipitation over China. The GCMs did better with winter temperature over China. All four had the pattern essentially correct but none were close on the magnitudes. For the equatorial Africa simulations the models reproduced the July precipitation pattern fairly well, though all had only about half of the actual precipitation.

All of these studies illustrate the pitfalls involved in making comparisons between grid point data and observations at scales below the resolution limit of the model. This statement applies to all models, not just GCMs. The focus has been on GCMs since it is the results of their altered climate scenarios which are typically used in ecological impact assessments. In all model–observation intercomparisons both the model output and observed data should be interpolated to the same grid and filtered to remove scales which are not resolved by the model.

2.2.2 Statistical Interpolation

Statistical interpolation is the process by which spatial patterns of parameters which are poorly represented by a model are related to fields which the model simulates well. Wigley et al. (1990) used multiple linear regressions to calculate sub-GCM grid patterns of monthly mean surface temperature and precipitation from monthly mean sea-level pressure and 700mb heights. Von Storch et al. (1993) used a canonical correlation analysis to obtain precipitation patterns over the Iberian peninsula from North Atlantic sea-level pressure patterns. Hewitson and Crane (1992) used orthogonal rotated principal component analysis techniques to compare the synoptic scale features present in the GISS GCM with a climatology of NMC analyses. Hewitson (1994) extended the principal component analysis to develop a multivariate index to obtain daily surface temperatures from the daily circulation

pattern. Other techniques which are being used to disaggregate precipitation patterns include wavelets (Foufoula-Georgiou and Perica 1994) and multi-fractals (Over et al. 1994). The major drawback to all of these various statistical methods, in terms of their applicability for impact studies, is their inability to provide information at the required scales. Currently these methods either provide information over time scales that are too long (seasonal as opposed to daily) or have not demonstrated their ability to downscale spatially from a GCM grid cell.

2.2.3 Dynamic Interpolation

In the late 1980's, Giorgi and Bates (1989), Giorgi et al. (1989), and Dickinson et al. (1989) put forth the concept of dynamic interpolation, in which a regional scale model is driven by output fields from a GCM. The assumptions are that the GCM can provide correct large-scale circulations while the regional model can simulate the effect of sub-GCM grid scale forcing due to its finer resolution and better parameterizations (Giorgi 1990). A version of the NCAR - Pennsylvania State University Mesoscale Model (Anthes 1987) has been adapted for use as a regional climate model (RegCM) by Giorgi (1990). A second generation version was developed by Giorgi et al. (1993a, 1993b).

In Giorgi et al. (1993c), the RegCM was validated at a grid separation of 60 km over the United States west of 100° west longitude. The RegCM was forced by European Center for Medium-Range Weather Forecasts (ECMWF) analyses for two periods: from 1 January 1982 through 31 December 1983; and 1 January 1983 through 25 April 1989. The RegCM did a good job of simulating the temperature distribution and trend of both seasonal and monthly surface temperatures. Over the whole of the domain, daily minimum temperatures were about 2° C cooler than observed, except during summer months when a 2° C warm bias was evident. Within various regions of the western U.S., the simulated average daily temperatures were generally within 2° C of observations, though biases as large as ± 4° C were seen.

The pattern of average daily precipitation rate was fairly well represented in the simulations. The daily precipitation rate for the whole domain was best reproduced during fall and worst in summer (about 200% of observed). For the regions in the west, the model consistently produced excess precipitation in the Rocky Mountain regions (130% to 300% of observed) with summer being the worst season. In general the model over-simulated summer precipitation in all regions.

Liu et al. (1994) validated the RegCM with a summer 1990 simulation of the East Asian monsoon, using ECMWF analyses as boundary conditions. Their model domain covered an area roughly bounded by 100°E - 150°E×25°N - 55°N. The RegCM was able to track the progress of the summer monsoon, including the sudden northward transition of the rain belt. In general the RegCM had a cool bias in surface temperatures and under-simulated precipitation. Regionally the RegCM had a cool bias of 2-3° C in southeast China, Korea and Japan, and a warm bias of 1-2° C in Mongolia and northeastern China. Precipitation was under-simulated with the model producing from one-third to one-half of what was observed, except in Mongolia and Manchuria where slightly more was simulated than observed.

Giorgi (1990) applied the output of the NCAR Community Climate Model (CCM1) at R15 (4.5°×7.5°) and T42 (2.89°×2.89°) resolutions to drive the RegCM for six Januarys. The CCM1 January climatologies were compared to ECMWF analysis climatology for 1979-1987 and the RegCM climatology was compared to the 0.5°×0.5° climatological dataset of Legates and Willmott (1990). The CCM1 climatologies reproduce the patterns of the ECMWF climatology with an overall problem of weaker gradients. The RegCM was able to produce the observed average surface temperature structure with a cold bias of 3° C. Overall the precipitation pattern was good, although the RegCM had consistent problems with not being able to reproduce local maxima in precipitation around the Cascades, Wasatch and Teton sub-ranges This was most likely due to the model not properly resolving the topographic forcing.

In Giorgi et al. (1994a, 1994b) the domain of the RegCM was expanded to cover the whole of the continental United States. The model-generated climatologies are from a three-year run of the RegCM, so there is some concern as to the representativeness of the annual averages of the various model fields. The RegCM showed a cold bias in annual average temperature of 1-3° C west of the Mississippi. The precipitation error showed a similar geographical pattern with the model producing approximately twice the observed precipitation in the western U.S., but only about one-half to three-quarters east of the Rocky Mountains.

McGregor and Walsh (1993) have performed a similar experiment by forcing the CSIRO Division of Atmospheric Research Limited Area Model (DARLAM) at grid separations of 125 km and 250 km with output from perpetual January runs of the Bureau of Meteorology Research Center (BMRC) R21 spectral GCM. Their results showed marked improvement in the precipitation pattern over Australia.

These studies demonstrate the capability of a mesoscale model to resolve regional climate features when forced by large-scale information over extended time periods. The errors that are evident in the resulting climatologies are systematic (consistent cold bias, excessive precipitation in the western U.S., too little in the eastern U.S., precipitation error magnitudes larger in summer than in winter) and point to parameterizations that need improvement (convective precipitation, radiation, and land surface). There is also the possibility that finer grid separation may reduce some of these errors through better resolution of terrain and other surface features, but finer resolution may also lead to new problems in the parameterization of physical processes.

2.3 Atmospheric Sensitivity to Landsurface Characteristics

The fluxes of energy, water, momentum and trace gases between the land surface and atmosphere are largely regulated by biological processes (Ojima et al., 1992). Change in vegetative properties such as albedo, roughness, LAI (which are governed

by plant type and growth) can influence local climate patterns through changes in the aforementioned fluxes (Pielke and Avissar 1990). A change in the vegetation type and/or properties of an area may be due to natural climatic variations such as ice ages or seasonal droughts. Changes may also be due to anthropogenic causes such as deforestation or agricultural practices.

Sagan et al. (1979) point out that use of fire, to chase animals during hunts and to clear land for agriculture, over the past 500,000 years had affected the abundance and distribution of vegetation as early as 10,000-20,000 years ago. They went on to estimate the effect of albedo change due to change in vegetation type on the average surface temperature. They estimate that anthropogenic vegetation change over the past several thousand years could be responsible for 1 degree C of cooling and that the vegetation change over the past 25 years (1950-1975) could be responsible for 0.2 degrees C of cooling.

Balling (1988) studied the effect of a Sonoran vegetation discontinuity. There is a sharp contrast in vegetation across the Arizona-Mexico border due to differences in grazing practices over the past 60 years. A result of overgrazing has led to shorter grass, more bare soil, and a higher albedo on the Mexican side. Balling analyzed 25 years of maximum temperature (1969 - 1986) data from stations within 50 km of the border. His results showed a 3.8 degree C difference in average maximum temperature between the U.S. and Mexican stations. This was supported by low-level radiometer overflights which showed a sharp 2-3 degree C temperature discontinuity across the border. These results are counter to the hypothesis of Charney (1975), in which vegetation removal leads to increased albedo and decreased surface temperatures. Instead, Balling's study supports the idea that decreased vegetation reduces evapotranspiration, leading to a net increase in sensible heat flux and surface temperature (Wendler and Eaton 1983). In related studies (Balling 1989, Bryant et al. 1990) it was shown that temperatures were cooler in Mexico for the first few

days following summer convective precipitation due to increased evaporation. The Mexican soils dry out faster than those in the Unites States and in about three days the Mexican temperatures are again higher than in the United States.

It has been shown by Pielke and Avissar (1990), Segal et al. (1988, 1989), and others that discontinuities in landsurface characteristics can generate mesoscale circulations which can modify the regional environment. Anthes (1984) showed, by numerical simulation, how planting bands of vegetation in semiarid areas could lead to increased convective precipitation, more than a homogeneous vegetation coverage would. The mechanisms responsible are: the modification of the environment through decreased albedo, increased net radiation, and increased evapotranspiration; and forcing of vertical motions by mesoscale circulations generated by the vegetation discontinuities.

Chang and Wetzel (1991) examined the effects of spatial variations of soil moisture and vegetation coverage on a prestorm environment using the Goddard mesoscale model (GMASS). They found that the best simulation occurred with a realistic distribution of vegetation and soil moisture. It was shown that the structure of a stationary front was enhanced by the differential heating due to the vegetation and soil moisture gradients.

Clark and Arritt (1994) used a single-column model to investigate the effects of vegetation cover and soil moisture on the latent and sensible heat fluxes and convective precipitation. Their results indicate that increasing soil moisture increases latent heat fluxes while decreasing sensible heat flux, thus leading to an increase in precipitation. Increasing the vegetation coverage increased the latent heat flux for dry soils and increased the sensible heat flux for all soil moistures. Increased vegetation coverage also increased convective precipitation.

An excellent review of landsurface parameterizations and the sensitivity of climate scenarios on the global scale was written by Garrat (1993). In his review he

points out some of the results of sensitivity scenarios on deforestation in the Amazon basin; the most enlightening being the inability in several of the GCMs to reproduce the annual trends of precipitation, evaporation, and net radiation. In a couple of studies focusing on the sensitivity of the Asian monsoon, Fennessy et al. (1994) and Meehl (1994) show that a stronger summer monsoon, in terms of precipitation amount, is related to lower albedo (less snow cover) and greater soil moisture (more snowmelt).

To summarize, it has been shown that the vegetated landsurface is sensitive to the atmosphere on long time scales in terms of species distribution and on shorter time scales in terms of carbon assimilation and photosynthetic rate. The atmosphere is sensitive on short time scales to changes in transpiration rates and on longer time scales to changes in vegetative properties over a growing season or over decades due to species changes. To properly assess these interactions requires a two-way coupling of ecosystem and atmospheric models much like the coupling that has taken place with the atmosphere and ocean.

Chapter 3

MODEL DESCRIPTION

RAMS has traditionally been used for simulations of short time scales. The model has only been run for more than a day from an initial state in an operational mode (Thompson 1993, Stocker et al. 1994) but still for no longer than several days. Because of this, various assumptions and simplifications have been made in the construction of RAMS. Some of these are inappropriate for extended time period runs. Another consideration is that some of the physical parameterizations used in shorter runs must be replaced with simpler ones for overall computational efficiency. In this chapter I will describe the modifications and limitations to the physical parameterizations that I used, the various data sources used to initialize and drive the model, and the particular configuration of RAMS used in the climate simulations. For a general description of RAMS the reader is referred to Tripoli and Cotton (1989), Tremback (1990), and Pielke et al. (1992).

The dominating concern in constructing the RAMS climate model (CLIMRAMS) was balancing computational speed with resolving power and representation of physical processes. It was decided to limit the time to simulate one day, on an IBM RISC workstation, to 3 hours. This would ideally allow the eventual multi-year simulations to be run at the rate of one year per six weeks of computer time. To accomplish this, constraints were placed on the grid configuration and the detail of the precipitation and radiation physics used. The important configuration features of the CLIMRAMS are as follows:

- 60 kilometer horizontal grid separation

- 85 east-west by 55 north-south horizontal grid points
- vertical grid separation from 250 to 2000 meters, stretched by a factor of 1.2
- 20 vertical levels, lowest at 120 meters, highest at 23 kilometers
- 120 second time step
- Mahrer-Pielke (1977) radiation scheme with pseudo-clouds
- Kuo convective parameterization as implemented by Tremback (1990)
- prognostic warm rain species (Tripoli and Cotton 1980)

3.1 Data Sources

RAMS requires various spatial databases for forcing the lower boundary condition. These include topography, sea surface temperature (SST), land percentage, vegetation distribution, and soil type. Some of the databases exist in the current RAMS framework (topography, SST, and vegetation), while some are derived from other databases (land percentage from vegetation), some needed improvement (SST), and others needed to be created (soils).

3.1.1 Topography

Figure 3.1 shows the spatial extent of the modeling domain. The domain encompasses the contiguous United States. The topography data come from the NCAR 10 minute Topographical Data Set. These data have been interpolated to the model grid and then passed through a filter to remove all features of twice the horizontal grid separation to prevent spurious orographic forcing.

The 60 kilometer grid separation resolves many of the important topographical features at the regional scale (Figure 3.2). The Ozarks and Black Hills are present along with many of the intermountain ridge systems and basins in the Rocky Mountains. A 30 kilometer separation would have allowed the resolution of the park

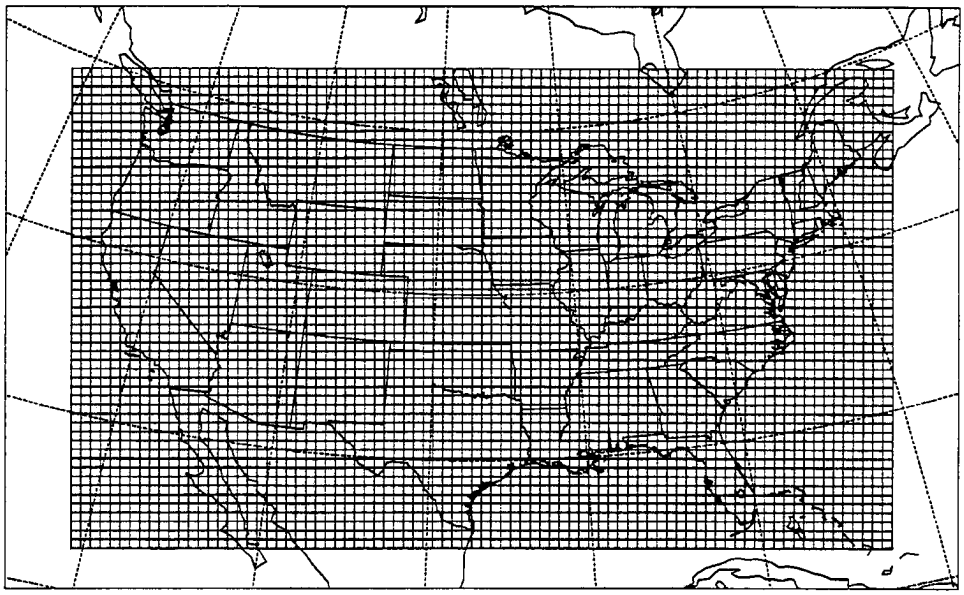

Figure 3.1: The modeling grid domain for the climate simulations on an oblique stereographic projection centered at 97°W 39°N. A 60 kilometer mesh is shown with 85 grid points in the east-west direction and 55 grid points in the north-south direction.

systems in the Rocky Mountains and valley structure in the Appalachians which play an important role in determining the local climatology, but at a cost of a five-fold increase in computer time.

3.1.2 Sea Surface Temperature

A long term climatological sea surface temperature dataset was originally used, but from several preliminary simulations it was found that the convergence along the Southeast Atlantic coastal region was too strong, leading to excessive convective precipitation. This was due in part to the lack of a warm SST anomaly in the original dataset which was present in the observations. To circumvent this problem the weekly observed SST dataset from NOAA (Reynolds and Smith 1994) was used instead.

3.1.3 Soils

In previous studies, RAMS has typically been run with a homogeneous soil distribution. This is generally satisfactory for limited areas where the soil properties

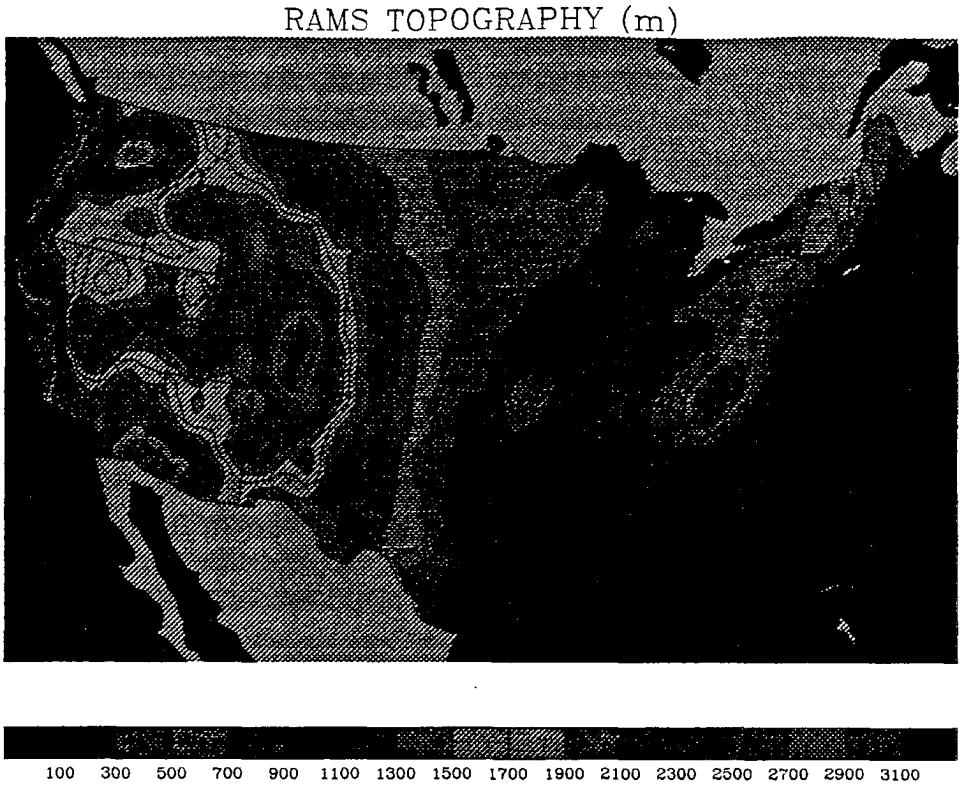

Figure 3.2: The 10 minute topography resolved on the 60 kilometer grid.

are fairly homogeneous across the modeling domain. For the domain of the simulations it was necessary to obtain an accurate representation of the soils distribution across the United States. The soils data were obtained from the VEMAP integrated database (Kittel et al. 1994) and derived from work by Kern (1994a, 1994b).

The original format of the soils data is a set of files indicating the percentage of clay, silt, and sand in the first 50 cm below the surface on a half degree grid across the continental United States. RAMS uses lookup tables to determine soil properties based on the USDA soil textural class for a given grid cell. To incorporate the soils data the percentage of clay, silt, and sand were first interpolated to each model surface grid cell. Then using a decision tree based on the USDA soil triangle (Figure 3.3) a soil textural class was assigned to each grid cell. Figure 3.4 shows the resulting soils distribution used in this study. Soil classes in Canada and Mexico were extrapolated from U.S. border values.

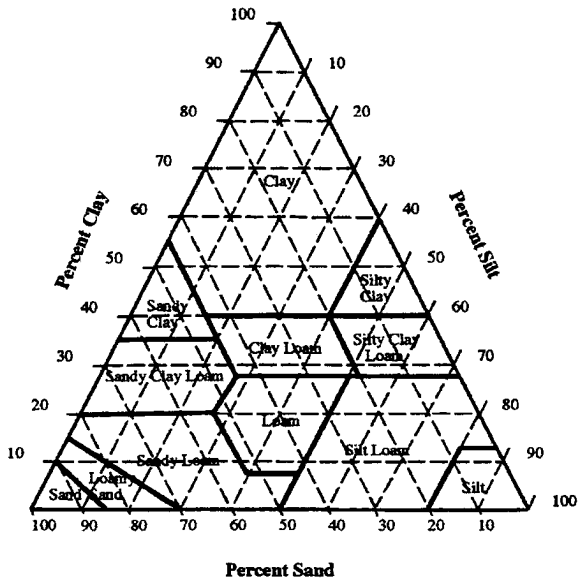

Figure 3.3: The USDA soil triangle (from Kohnke 1968).

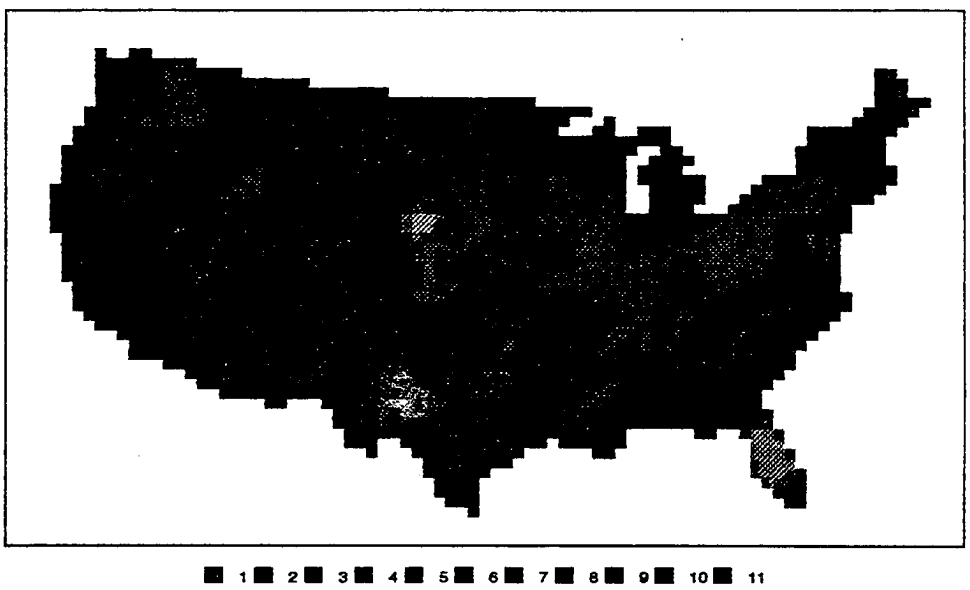

Figure 3.4: The representation of the soil textural class on the model grid. Data are only shown for the conterminous United States. 1 – sand; 2 – loamy sand; 3 – sandy loam; 4 – silt loam; 5 – loam; 6 – sandy clay loam; 7 – silty clay loam; 8 – clay loam; 9 – sandy clay; 10 – silty clay; 11 – clay

3.1.4 Vegetation

The vegetation data used in this study came from two sources, the USGS Land-cover Database (Loveland et al. 1990), and a potential natural vegetation dataset (Kuchler 1964). The USGS database is derived from satellite observations of the normalized difference vegetation index (NDVI). The vegetation type is obtained from relationships based on the amplitude and seasonal phase of the NDVI signal. The USGS database contains 159 vegetation categories which have been reclassified into the 18 categories of the Biosphere Atmosphere Transfer Scheme (BATS) which RAMS uses in lookup tables of vegetation properties. Figure 3.5 shows the resulting current landuse distribution on the model domain.

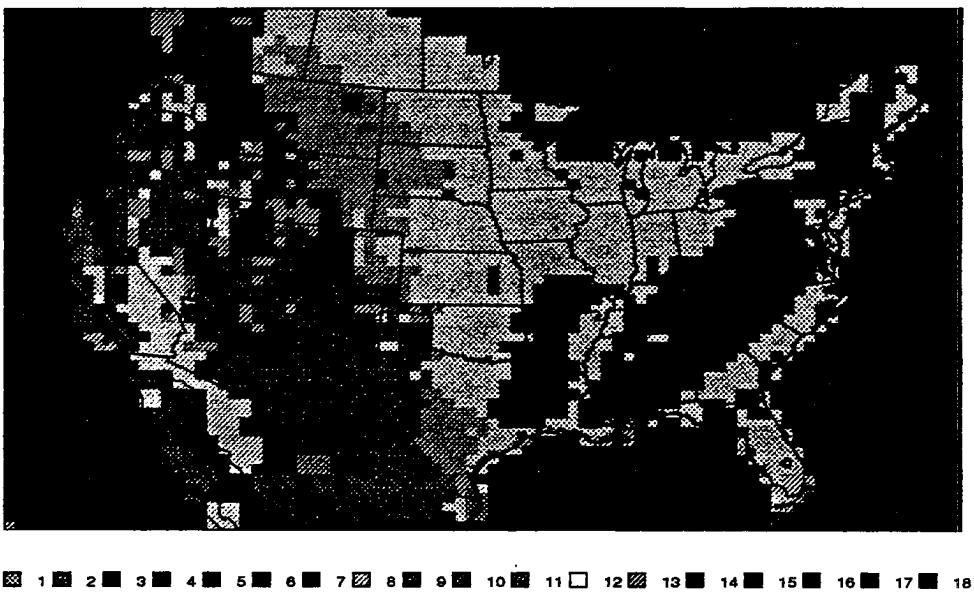

Figure 3.5: Result of the reclassification of the USGS current landuse database to BATS categories. 1 – Crop/mixed farming; 2 – Short grass; 3 – Evergreen needleleaf tree; 4 – Deciduous needleleaf tree; 5 – Deciduous broadleaf tree; 6 – Evergreen broadleaf tree; 7 – Tall grass; 8 – Desert; 9 – Tundra; 10 – Irrigated crop; 11 – Semi-desert; 12 – Ice cap/glacier; 13 – Bog/marsh; 14 – Inland water; 15 – Ocean; 16 – Evergreen shrub; 17 – Deciduous shrub; 18 – Mixed woodland

The natural vegetation dataset, used in one of the sensitivity studies, is based on an interpretation by vegetation ecologists and land managers of the vegetation that would naturally occur in a region in the absence of human activities (Kuchler,

1964). The original vegetation map has been digitized by the Environmental Protection Agency (Kuchler, 1993) which was then reclassified to the BATS categories. Figure 3.6 shows the resulting natural vegetation distribution on the model domain.

Figure 3.6: Result of the reclassification of the natural vegetation database to BATS categories. 1 – Crop/mixed farming; 2 – Short grass; 3 – Evergreen needleleaf tree; 4 – Deciduous needleleaf tree; 5 – Deciduous broadleaf tree; 6 – Evergreen broadleaf tree; 7 – Tall grass; 8 – Desert; 9 – Tundra; 10 – Irrigated crop; 11 – Semi-desert; 12 – Ice cap/glacier; 13 – Bog/marsh; 14 – Inland water; 15 – Ocean; 16 – Evergreen shrub; 17 – Deciduous shrub; 18 – Mixed woodland

One of the main problems with the BATS classification is its lack of spatial heterogeneity within a given vegetation category. For example, there is no differentiation among coniferous trees from the Pacific Northwest to the Colorado Rockies to the Southeast. Each region will have the same LAI and vegetation density as the others, when even the casual observer will notice distinct differences. This problem will be further addressed in the section dealing with the RAMS vegetation parameterization on page 30.

3.2 Parameterizations

Numerical models need to parameterize sub-grid scale processes due to the truncation of resolved scales resulting from the choice of horizontal and vertical grid sepa-

rations. Modifications have had to be made to some parameterizations because they lacked processes that are important at longer time scales. Other parameterizations were chosen due to their computational efficiency but lacked processes important even at short time scales, so simplified additions were introduced to approximate the more complete parameterizations. Finally there are some parameterizations which have inherent limitations which should be explained in order to better understand the extent to which the model results can be interpreted. There are three parameterizations that will be discussed: the surface; radiation; and precipitation schemes.

3.2.1 Surface Schemes

In order to compute the turbulent fluxes of heat, moisture and momentum between the earth's surface and the lowest atmospheric level, RAMS uses the Louis (1979) surface layer scheme to calculate the characteristic velocity, temperature, and humidity scales (u^*,Θ^*,q^*). A soil model (Tremback and Kessler, 1985; McCumber and Pielke, 1981) and vegetation model (McCumber and Pielke, 1981; Avissar and Mahrer, 1988) are used to calculate the necessary quantities of surface temperature and mixing ratio. In order to understand the controls on the fluxes between the surface and atmosphere it is necessary to examine the soil and vegetation submodels.

The soil model contains prognostic equations for the vertical diffusion of heat and moisture. The equation for heat diffusion is given by

$$\frac{\partial \Theta_S}{\partial t} = \frac{\partial}{\partial z}\left[\lambda \frac{\partial \Theta_S}{\partial z}\right] \tag{3.1}$$

and at the surface by

$$C_s \Delta z_G \frac{\partial \Theta_G}{\partial t} = R_S + R_L - \epsilon_s \sigma T_G^4 + \rho_a C_p u^* \Theta^* + \rho_a L u^* q^* - C_s \lambda \left.\frac{\partial \Theta_S}{\partial z}\right|_G \tag{3.2}$$

where Θ_S and Θ_G are the soil potential temperature below and at the surface respectively, λ is the thermal conductivity, and C_s is the volumetric specific heat. The

terms in Equation 3.2 from left to right are: the shortwave longwave radiative fluxes these include the effects of soil and vegetation albedo, the shortwave transmission through the canopy, and the longwave emission by the canopy; the emission of longwave radiation by the soil; the sensible and latent heat fluxes; and the soil heat flux.

The only remaining boundary condition is the potential temperature of the deepest soil level. Traditionally, in RAMS simulations, this is specified and held constant for the duration of the simulation. For extended runs the deepest soil potential temperature can change significantly over the year, unless that level is more than 6 meters below the surface (Deacon, 1969). Fortunately, deep soil potential temperature has a simple sinusoidal form with decreasing amplitude and increasing lag with depth (after Arya 1988)

$$\Theta_S = \frac{T_m + 0.25 T_a \sin\left(\frac{2\pi}{356}(\tau - 150)\right)}{C_p \Pi} \tag{3.3}$$

where T_m is the mean annual screen height temperature, T_a is the amplitude of the annual screen height temperature cycle, τ is the day of the year, and Π is the surface Exner function. The depth coefficient (0.25) and the lag coefficient (150) are both appropriate for a depth of 2.5 meters. This equation was used to force the bottom boundary of the soil model at a depth of 2.5 meters. The initial soil temperature profile was set to an exponential function between the bottom soil potential temperature and the screen height potential temperature at the surface. The choice of a 2.5 meter soil model depth was based on the simple behavior of soil temperature at this depth and that soil moisture would be determined by the gravitational sedimentation of moisture from above. This would not be the case, in regards to soil moisture, if there is a very shallow water table which would maintain saturation or in the case of large inhomogeneities in soil properties with depth.

The equation for moisture diffusion is given by

$$\frac{\partial \eta_S}{\partial t} = \frac{\partial}{\partial z}\left[D_\eta \frac{\partial \eta}{\partial z} + K_\eta\right] - \mathcal{T} \tag{3.4}$$

and at the surface by

$$\frac{\partial \eta_G}{\partial t} = \frac{\rho_a L u^* q^* - D_\eta \frac{\partial \eta}{\partial z} - K_\eta}{\Delta z_G} - \mathcal{T} + \mathcal{P} \tag{3.5}$$

where η_S and η_G are the volumetric soil moisture content below and at the surface respectively, D_η is the moisture diffusivity, K_η is the hydraulic conductivity, $\mathcal{T}$ is the moisture removed by the roots for transpiration, and $\mathcal{P}$ is the source due to precipitation. The precipitation moisture flux can only saturate the top soil layer; any excess not infiltrating the soil in one time step is lost as runoff. The deep soil moisture boundary condition is constant and remained unchanged for the climate scenarios.

The traditional soil moisture initialization in RAMS (Tremback 1990) is a profile based on a prescribed moisture content at depth and a moisture content based on the atmospheric humidity at the surface. This causes an improper initialization if a moist(dry) air mass is over a dry(moist) soil. To better specify the initial soil moisture content of the soil an antecedent precipitation index (API) was used. The API is calculated with a simple regression relation

$$API_i = R_i + k \times API_{i-1} \tag{3.6}$$

where R_i is the 24 hour rainfall for day i and k is a coefficient with a value of 0.75 for the top soil layer and 0.975 for the remaining soil layers (Chang and Wetzel 1991). Three months of daily precipitation data from NCAR archives were used to obtain the soil moisture initializations valid on July 1, 1989 shown in Figure 3.7. The resulting spatial patterns compare well with proxy patterns such as the previous week's precipitation for the top layer moisture (Figure 4.1) and crop moisture measurements for the deep layer moisture (Figure 4.2).

There are several limitations with Equation 3.6. One is that the coefficient k does not vary with soil type and therefore does not account for heterogeneities in soil water infiltration and soil water holding capacity properties. Another drawback is

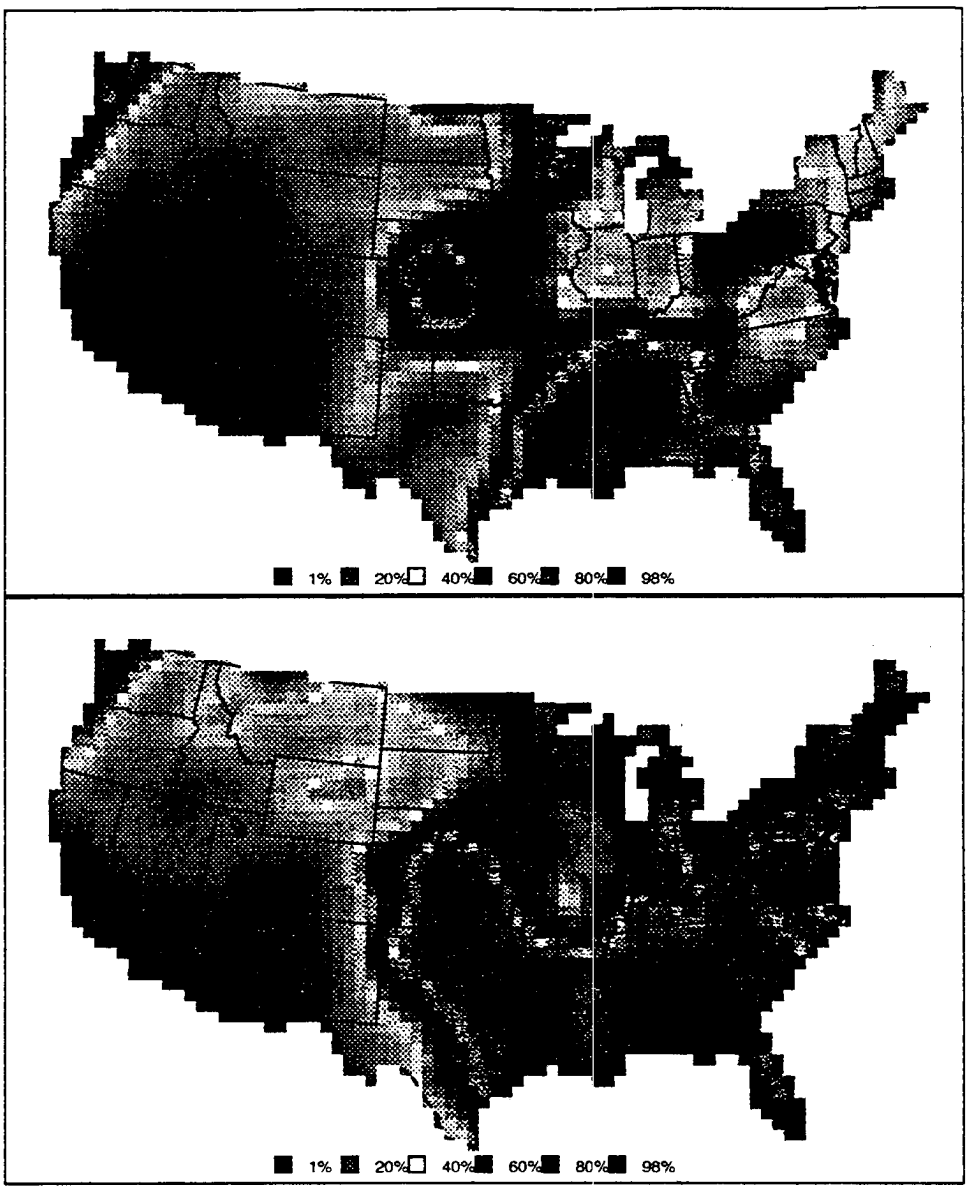

Figure 3.7: The soil moisture initialization for 1 July 1989 from the API method. What is shown is the percent of saturation in the top soil layer (top) and in the deep soil layers (bottom). Data are only shown for the conterminous United States.

that the loss of soil moisture due to transpiration by vegetation is neglected. Finally, atmospheric conditions leading to either enhanced or reduced evapotranspiration are also neglected. On a positive note, this method does represent the spatial patterns and relative magnitudes of soil moisture better than other initialization methods used in the past.

The vegetation model has equations to calculate the potential temperature and mixing ratio of the vegetation. The potential temperature equation is

$$0.6C_w\rho_w\frac{\partial\Theta_{VG}}{\partial t} = \frac{R_S + R_L + \epsilon_s\sigma T_G^4 + 2LAI\rho_a C_p u^*\Theta^* + LAI\rho_a L u^* q^* - 2\epsilon_v\sigma T_{VG}^4}{0.1LAI} \tag{3.7}$$

where Θ_{VG} is the potential temperature of the vegetation and LAI is the leaf area index for the particular vegetation type.

The moisture transpired by the vegetation is inversely proportional to the stomatal resistance, r_s. According to Lee (1992) the stomatal resistance is a function of several environmental controls: photosynthetically active radiation (PAR); leaf temperature; vapor pressure deficit between the atmosphere and leaf; soil water potential; and CO_2 concentration. Figure 3.8 shows how transpiration reacts relative to changes in the control variables. The transpired moisture is removed from the soil column based on the fraction of total roots in each soil layer. The roots are distributed exponentially with depth.

Three important vegetation parameters that are used in the computation of the latent and sensible heat fluxes and various radiation quantities are the LAI, vegetated fraction, and vegetation shortwave transmissivity. In BATS (Biosphere-Atmosphere Transfer Scheme; Dickinson et al., 1993), upon which the RAMS formulation of seasonality in LAI and vegetation fraction is based, these parameters vary with the season through the following equations

$$LAI = LAI^{max} - F \times \delta LAI \tag{3.8}$$

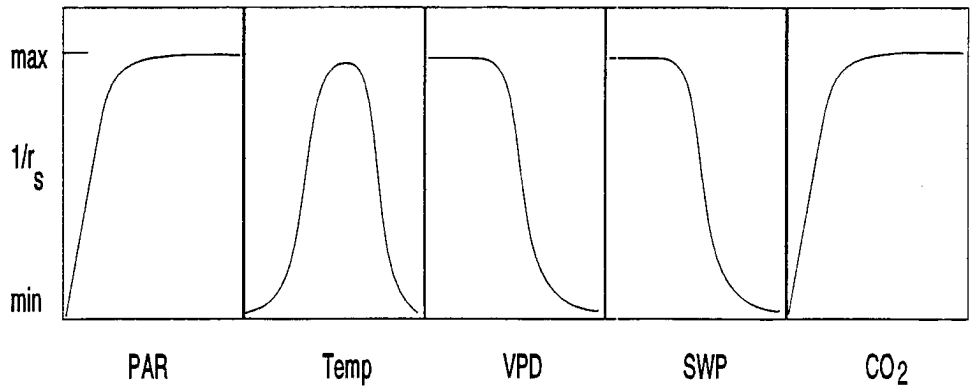

Figure 3.8: The response of stomatal resistances, r_s, to environmental variables. PAR is photosynthetically active radiation, Temp is leaf temperature, VPD is vapor pressure deficit, SWP is soil water potential, and CO_2 is is the carbon dioxide concentration (from Lee, 1992).

$$f_v = f_v^{max} - F \times \delta f_v \tag{3.9}$$

$$F = 0.0016K^{-2}(298 - T_{0.2m})^2 \tag{3.10}$$

where f_v is the fractional coverage of vegetation, f_v^{max} is its maximum value, and δf_v is its seasonal change. F is a seasonal coefficient that varies with the soil temperature at a depth of 0.2 meters ($T_{0.2m}$). The current version of RAMS specifies $T_{0.2m}$ as a fixed constant for the duration of the model simulation, which is appropriate for model runs on the order of one day long. In CLIMRAMS the seasonal coefficient in Equation 3.10 is updated daily with the 00Z 0.2m soil temperature obtained from the prognostic soil model, allowing the fractional coverage of vegetation and LAI to vary with soil temperature. The vegetation shortwave transmissivity is related to LAI through the equation

$$\tau_v = 2\,(0.5)^{LAI+1} \tag{3.11}$$

where the truncated integer value of LAI is used. One of the problems with the BATS classification scheme is the lack of variation in its vegetation parameters. Table 3.1 shows the values of the vegetation parameters that are used in RAMS. These values are approximations to real vegetation. Observations made in the Pawnee National Grasslands of eastern Colorado (Lapitan and Parton, 1994) show for short-

grass prairie a minimum LAI of 0.0 and a maximum of 0.46. For roughness length a minimum of 0.0009m and a maximum of 0.0302m with an annual mean of 0.015 was observed. Only the mean roughness length approximates the value given in Table 3.1. Seasonal changes in roughness length are neglected in the parameterization. According to Table 3.1 and Equation 3.8, in July the vegetation will be at maximum leaf area. If one were to view satellite images of peak greenness, large spatial inhomogeneities would be apparent. Another problem is that differences in the same type of vegetation across different climatic regions is not accounted for. Finally, and the most problematic, is that all vegetation types have the same seasonal function of LAI. Satellite composites of the time of onset of greenness, length of greenness period, and the time of peak greenness all show the large temporal, spatial, and species variability in vegetation properties (Loveland et al., 1990). In fact it is this variability which allows us to determine the vegetation type from satellite data.

Another area which has been modified in the soil-vegetation model is in the transpiration path. Root mass decreases exponentially with depth in the standard version of RAMS. This allows for the the transpired water to be pulled from available soil moisture closest to the surface. This does not allow for the shutdown of transpiration if the soil dries out to sufficient depth. What has been done is to set the root mass to zero below a certain depth. Table 3.1 shows the maximum root depths which were used for the various BATS vegetation categories. For the tree categories there was no limitation placed on their root depth since the soil model used only went down 2.5 meters below the surface. For the shrub, crop, and grass categories the maximum root depth determination was a bit more difficult since there can be wide variation between species in the same category. As an example, Figure 3.9 illustrates the root depths for various prairie species. *Koeleria cristata, Festuca ovina ingrata,* and *Poa sandbergii* are common to the short grass prairie. If we take BATS category 2, short grass, to be a combination of these species,

Type	α_v	ϵ_v	L	δL	f_v	δf_v	Z_{ov} m	d m	r_r	r_z m
Crop/Mixed Farming	.20	.95	6	5.5	.85	.6	0.06	.75	3	1.0
Short Grass	.26	.96	2	1.5	.80	.1	0.02	.00	8	0.5
Evergreen Needleleaf Tree	.10	.97	6	1.0	.80	.1	1.00	15.	10	10.0
Deciduous Needleleaf Tree	.10	.95	6	5.0	.80	.3	1.00	20.	10	10.0
Deciduous Broadleaf Tree	.20	.95	6	5.0	.80	.3	0.80	15.	10	10.0
Evergreen Broadleaf Tree	.15	.95	6	1.0	.90	.5	2.00	20.	12	10.0
Tall Grass	.16	.96	6	5.5	.80	.3	0.10	.00	8	0.5
Desert	.30	.86	0	0.0	.00	.0	0.05	.00	0	0.0
Tundra	.20	.95	6	5.5	.60	.2	0.04	.00	4	0.5
Irrigated Crop	.18	.95	6	5.5	.80	.6	0.06	.00	3	1.0
Semi Desert	.25	.96	6	5.5	.10	.1	0.10	.00	8	0.5
Ice Cap/Glacier	.40	.82	0	0.0	.00	.0	0.01	.00	0	0.0
Bog/Marsh	.12	.98	6	5.5	.80	.4	0.03	.00	5	0.5
Inland Water	.14	.99	0	0.0	.00	.0	0.0024	.00	0	0.0
Ocean	.14	.99	0	0.0	.00	.0	0.0024	.00	0	0.0
Evergreen Shrub	.10	.97	6	1.0	.80	.2	0.10	.00	5	2.0
Deciduous Shrub	.20	.97	6	5.0	.80	.3	0.10	.00	5	2.0
Mixed Woodland	.18	.96	6	3.0	.80	.2	0.80	.20	10	10.0

Table 3.1: The vegetation parameters that correspond to the 18 BATS categories. The columns from left to right are: vegetation type; shortwave albedo; longwave emissivity; max LAI; seasonal change in LAI; max fractional coverage; seasonal change in fractional coverage; roughness length; displacement height; ratio of upper to lower roots; max depth of roots.

then a reasonable estimate for the maximum root depth for BATS category 2 is approximately 0.5 meters.

Figure 3.9: Differences in root structure of various species of prairie plants growing in deep, well aerated soil: *h, Hieracium scouleri; k, Koeleria cristata; b, Balsamina sagittata; f, Festuca ovina ingrata; g, Geranium viscosissimum; p, Poa sandbergii; ho, Hoorebekia racemosa; po, Potentilla blaschkeana* (Kramer, 1983).

3.2.2 Radiative Transfer Scheme

The radiative transfer scheme used for these climate simulations is the Mahrer-Pielke (1977) clear-sky scheme as modified by Thompson (1993). The reason for choosing this scheme over the Chen-Cotton (1983), which includes cloud effects, was for computational efficiency. The Chen-Cotton scheme also underestimates the clear-sky downward fluxes to a greater extent than the Mahrer-Pielke scheme (Zhong and Doran, 1994).

The modified Mahrer-Pielke scheme approximates cloud effects with a relative humidity threshold (94% for a 60km grid separation) as in Thompson (1993). The downward flux of shortwave radiation is reduced by an albedo based on cloud depth

(Neiburger, 1947)

$$\alpha_{pc} = \begin{cases} -C_0 + C_1 \Delta Z_c - C_2 (\Delta Z_c)^2 + C_3 (\Delta Z_c)^3 - C_4 \ln (\Delta Z_c) & \Delta Z_c < 1000\text{m} \\ 0.7 & \Delta Z_c \geq 1000\text{m} \end{cases} \tag{3.12}$$

where the cloud depth, ΔZ_c is determined by the depth for which the relative humidity threshold is exceeded. The coefficients C_1 through C_5 are from the regression fit of observations (C_0=-0.100895, C_1=0.00346179, C_2=-4.34832E-6, C_3=1.78721E-9, C_4=-0.0146811). The downward flux of longwave radiation is then set to the equivalent black body emission flux at the temperature of the bottom of the layer exceeding the 94% relative humidity threshold.

The choice of relative humidity threshold may have been lower than optimal. Results from the control run indicated a slight cool bias in screen height temperatures. This was most evident in coastal regions and areas of high precipitation where the high humidities resulted in too large of a pseudo-cloud shortwave albedo.

3.2.3 Convective Parameterization Scheme

Convective precipitation plays an important role in the hydrologic cycle during the month of July, which this study covers. The resolved scale of the model configuration used requires the use of a convective parameterization.

The convective parameterization used for this study is a modified Kuo (1974) scheme (Tremback 1990). The Kuo scheme works by calculating a columnar water budget and is driven by the surface moisture convergence. One of the important (sensitive) parameters of the parameterization is $b-1$ which Tremback equated to the precipitation efficiency. In the RAMS implementation of the Kuo convective scheme the precipitation efficiency is modeled after Fritsch and Chappell (1980), where a third order polynomial of vertical wind shear is used to calculate the precipitation efficiency as follows:

$$\varepsilon_p = \begin{cases} 1.6 - 0.64 \frac{\partial \overline{V}}{\partial z} + 0.095 \left(\frac{\partial \overline{V}}{\partial z} \right)^2 - 0.005 \left(\frac{\partial \overline{V}}{\partial z} \right)^3 & \frac{\partial \overline{V}}{\partial z} \geq 1.35 \\ 0.9 & \frac{\partial \overline{V}}{\partial z} < 1.35 \end{cases} \tag{3.13}$$

where ε_p is the precipitation efficiency and $\frac{\partial \overline{V}}{\partial z}$ is the vertical wind shear. This allows b to be diagnosed from time varying quantities in the model rather than being specified as in the original form of the Kuo parameterization.

The problem with this formulation is that this polynomial was derived from observations of 14 High-Plains convective storms (see Figure 3.10) and its application to other regions must be seriously scrutinized. In Florida much of the convection occurs under low shear conditions due to the influence of the Bermuda High. Braham (1952) estimated the precipitation efficiency of low-shear cumulus storms over Ohio and Florida to be about 10% (attributing the low efficiencies to entrainment losses of moisture), while the efficiency given by Equation 3.13 would indicate a much higher value of 90%. This could causes excessive precipitation in regions of low vertical wind shear outside of the High Plains. It should be noted that this does not effect the validity of the sensitivity simulations since it is the differences between the simulations which is important , and any errors in the control run would serve as guidance for improvements to the model in the future.

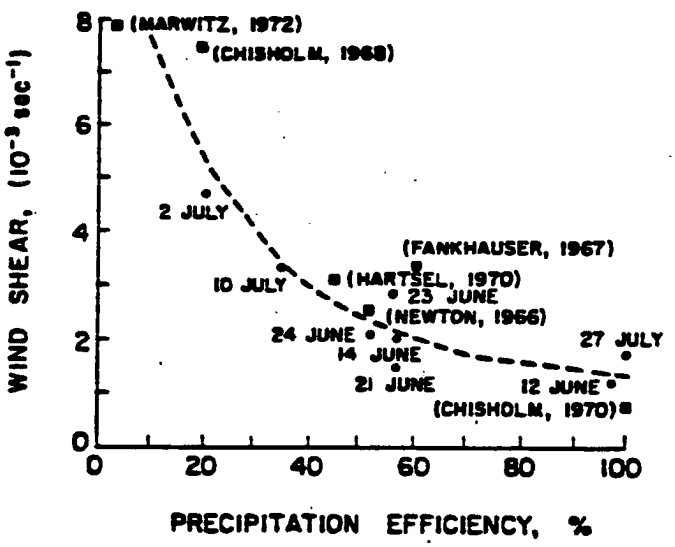

Figure 3.10: Relationship of wind shear versus precipitation efficiency showing observations and third order polynomial regression function (from Marwitz, 1972).

Chapter 4

MONTHLY SENSITIVITIES

4.1 Climatological Description of July 1989

July 1989 was chosen for several reasons. It was desired that the simulation month be recent enough that good initial condition and observational datasets existed. A summertime scenario was desired since the model lacks a snow-cover scheme and therefore would not be able to properly handle a wintertime or transitional season scenario. It was also preferred that the simulation month be fairly average in terms of precipitation. Initial tests of the model for the wet months of July 1992 and 1993 showed that while the precipitation pattern was well replicated the total amount of rainfall was under-simulated by almost an order of magnitude. On the other hand, a drought year would minimize the importance of simulating quantitative precipitation correctly. July 1989 fit these criteria.

The soil moisture distribution at the beginning of July is to a large extent determined by the precipitation distribution for the month of June. This is particularly true for the top layer soil moisture which is almost exclusively determined by the previous week's precipitation. The deep soil moisture can show structures that are the result of the precipitation patterns over the past several months. The month of June 1989 saw the southern and eastern portions of the United States receiving above average precipitation, with large regions getting more than double and even some local areas receiving in excess of four times the average precipitation. The western and north central United States on the other hand were below average,

with much of that area receiving one-half to one-quarter of the average precipitation. Much of the rainfall in the lower Mississippi River Valley and Delta region was due to Tropical Storm Allison, a remnant of Pacific Hurricane Cosme, during the last few days of June. As mentioned in the section on the API soil moisture initialization on page 27, the initial patterns of the deep and top layer soil moisture (Figure 3.7 should correlate with the 1 July crop moisture index pattern (Figure 4.2) and last week of June rainfall pattern (Figure 4.1) respectively. The agreement is quite good.

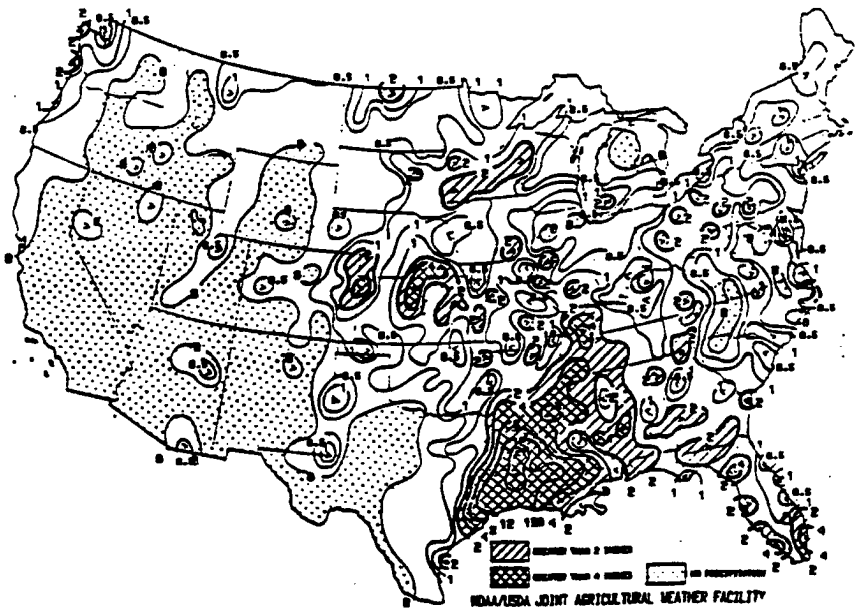

Figure 4.1: The precipitation pattern for the week of 25 June 1989 through 1 July 1989 (from NOAA/USDA 1989).

Figure 4.3 shows the observed mean daily temperature for the month of July 1989. The data were obtained from the Summary of the Day CD (EarthInfo 1993) which contained temperature data for just over 5100 stations across the United States. The observations were adjusted to sea level using the U.S. Standard Lapse Rate, interpolated to the CLIMRAMS grid, and then re-adjusted to the elevations of the CLIMRAMS topography. This was done to minimize elevation errors due to interpolating stations of different altitudes.

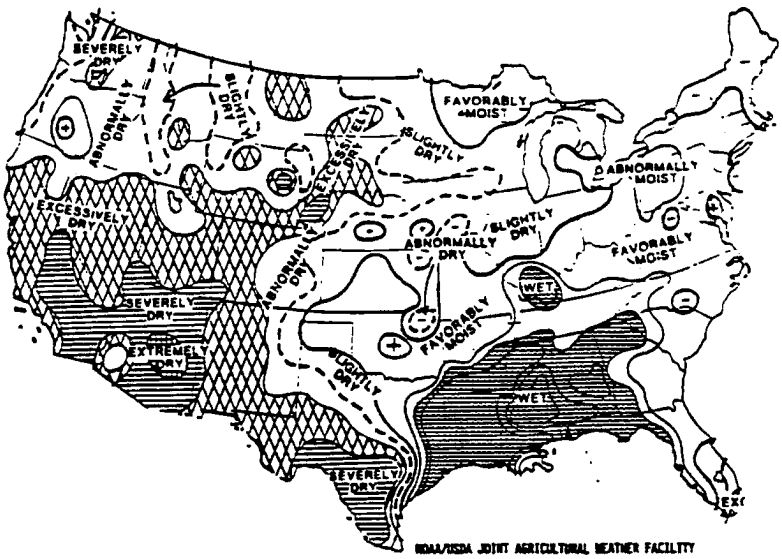

Figure 4.2: The crop moisture index valid 1 July 1989 (from NOAA/USDA 1989).

July 1989 had positive average temperature anomalies of 2-4°C across much of New England, the Northern Plains, Rocky Mountains, and the Southwestern Deserts (Figure 4.3). This was primarily a result of a fairly persistent upper level ridge over the Rocky Mountains. The major negative average temperature anomaly of 2-3°C was centered in the Oklahoma-Arkansas region extending along the Gulf Coast and north along the eastern foothills of the Appalachian Mountains.

Large amounts of precipitation fell across much of the south (Figure 4.4) with the highest amounts in excess of 200mm occurring in southern Arkansas and along the Gulf Coast. Parts of Montana, Arizona, and much of New Mexico received more than 50mm. West Texas, California, and parts of the Intermountain Basins received less than 25mm of rainfall. Much of the United States had precipitation that was close, within 75% to 150%, to average (Figure 4.4). The major areas that were significantly above average (150% or more) were: from Arkansas east and north along the Appalachian Mountains; New Mexico; Pacific Northwest Coast; and along the Missouri River from Montana to Missouri.

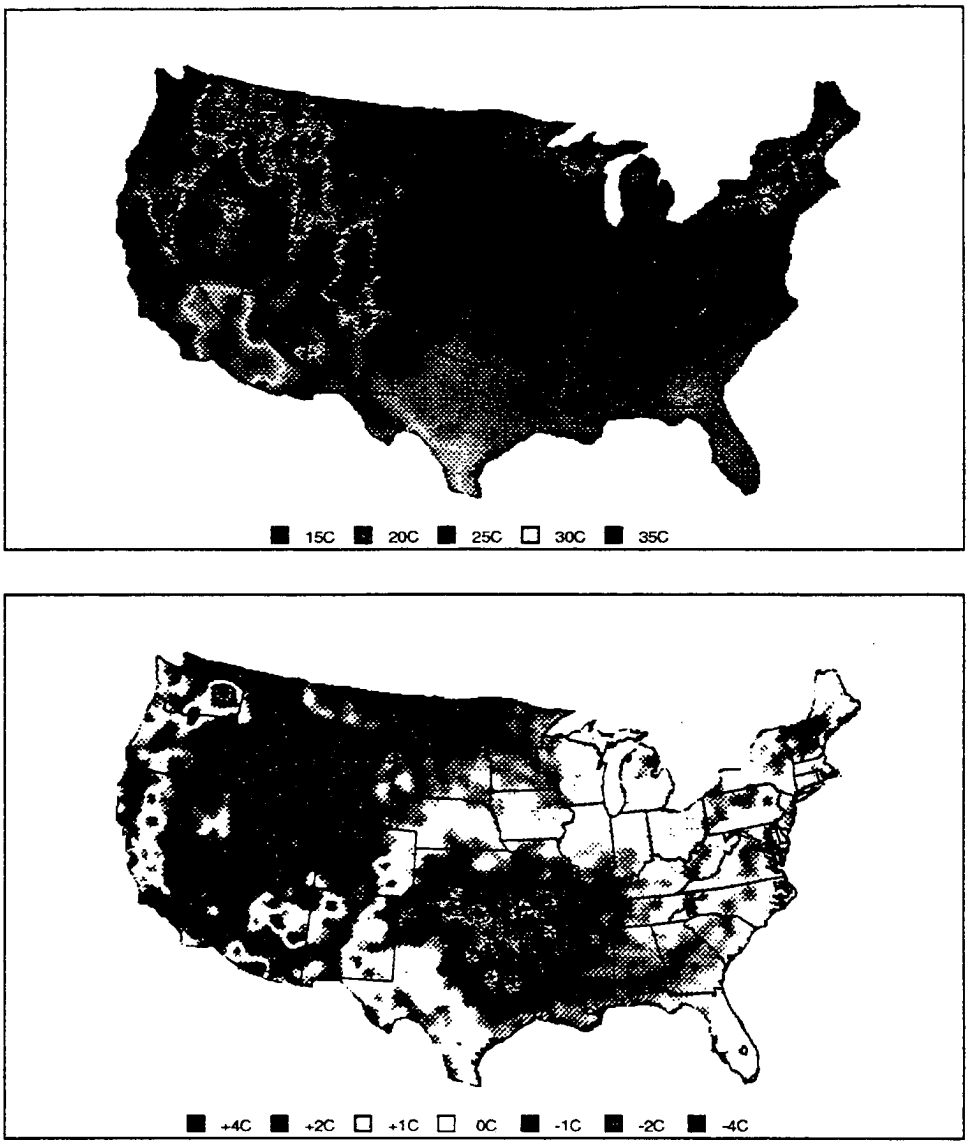

Figure 4.3: The observed mean daily temperature for July 1989 (top panel); units are degrees Celsius. The departure of observed mean daily temperature from climatology; (bottom panel) units are also degrees Celsius.

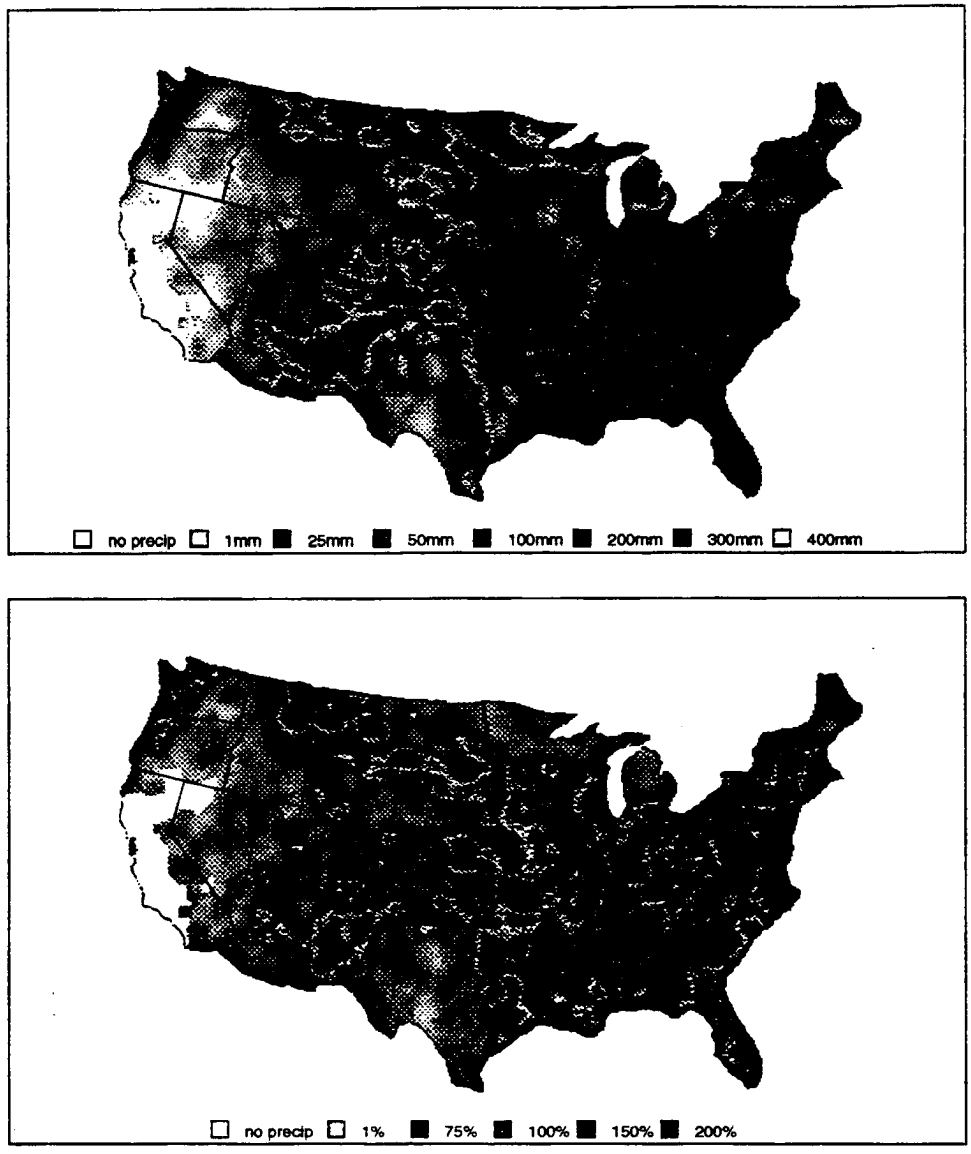

Figure 4.4: The observed accumulated precipitation for July 1989 (top panel); units are millimeters of rainfall. The percentage of average precipitation that fell during July 1989 (bottom panel).

4.2 Current Landscape Simulation

The purpose of the control climate scenario (CNTL) is to test the ability of CLIMRAMS to replicate a month-long climatology and to serve as a baseline for the other sensitivity scenarios to compare with. The vegetation distribution used is the current landuse as shown in Figure 3.5 and the soil moisture initialization is the API distribution shown in Figure 3.7. The model was started at 0000UTC on 1 July 1989 and run through 0000UTC, 1 August 1989. The model was initialized with NMC (National Meteorological Center) analyses and the boundary conditions throughout the period of simulation were interpolated from consecutive 0000UTC and 1200UTC NMC analyses. The atmospheric initial and boundary conditions were the same for all of the sensitivity studies. Quantitative analyses will be made for 21 regions in the United States. These include: the contiguous 48 states; an eastern and western region divided along 97 west longitude; and the 18 regions of Figure 4.5 which represent areas of common climate and ecosystem properties.

The comparisons will be made between model accumulated precipitation and screen height temperature for the control scenario. The sensitivity scenarios will compare surface energy fluxes, daily convective precipitation rate, and screen height quantities of temperature, mixing ratio, and wind speed between model runs. The screen height quantities are obtained from the ground surface and first atmospheric level (120m) values using the Louis (1979) similarity relations for each surface type (bare soil, shaded soil, vegetation, and water) in the grid cell. These are then combined by an areal weighted average to get the screen height value used in the comparisons. The surface fluxes are combined in a similar fashion.

Figure 4.6 shows the modeled mean daily temperature departure from observations. The temperature departures are quite small; 70% of the area is within 1°C of observations and 50% of the area is within 0.5°C. Over the contiguous United States as a whole there is a cold bias of 1.35°C (Table 4.1). Regionally there are

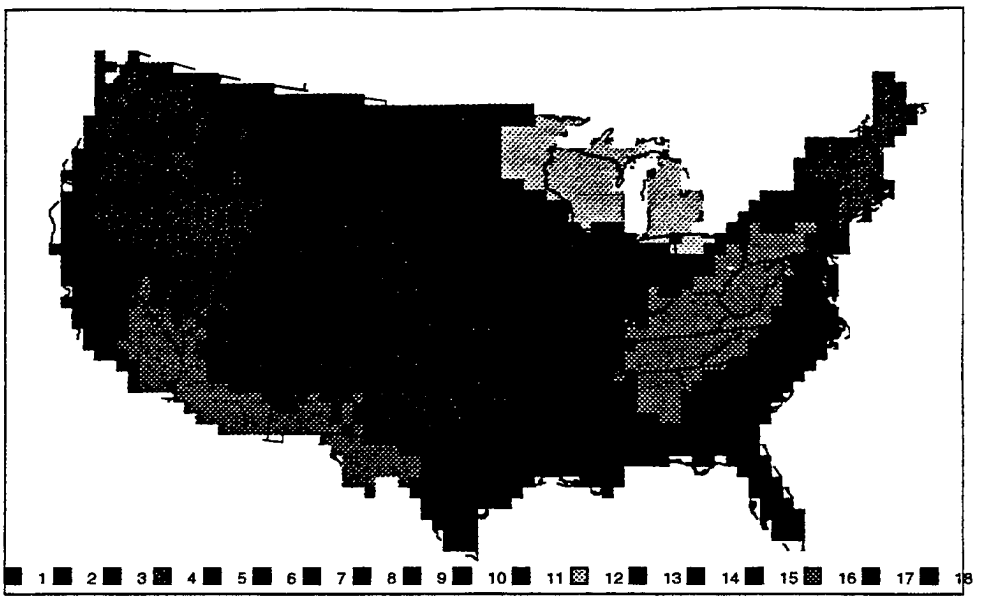

Figure 4.5: The regional analysis areas. These are derived from the Environmental Protection Agency's 74 ecoregions-regions. 1–Cascades, 2–California, 3–Intermountain Basin, 4–Southwestern Deserts, 5–Northern Rockies, 6–Southern Rockies, 7–Northern Plains, 8–Central Plains, 9–Southern Plains, 10–Ozark Highlands, 11–Prairie Peninsula, 12–Great Lakes Forests, 13–Mississippi Valley, 14–Florida, 15–Southeast Coastal, 16–Appalachia, 17–Mid Atlantic, 18–New England.

cold biases in excess of 2°C in coastal regions and the South and Central Plains. These biases can be attributed to a couple of causes. The regions of large cold bias appear to be due to the pseudo-cloud albedo in the modified radiation scheme. The coastal areas have consistently high enough humidity to cause excessive reduction in the downward solar radiation flux. This also occurs in regions of anomalously high precipitation, South and Central Plains and Southwestern Deserts, where the Kuo convective precipitation scheme has sufficiently moistened the vertical column to lead to excessive pseudo-cloudiness. A re-comparison of the NMC analyses with surface observations has shown a cold bias of 1°C for July 1989 in the original NMC surface analyses (John Roads, personal communication) which were used as the initial and boundary conditions for the model simulation.

The precipitation ratio (Figure 4.6) shows a striking pattern of too much simulated precipitation in the west and too little in the east. The regional analysis

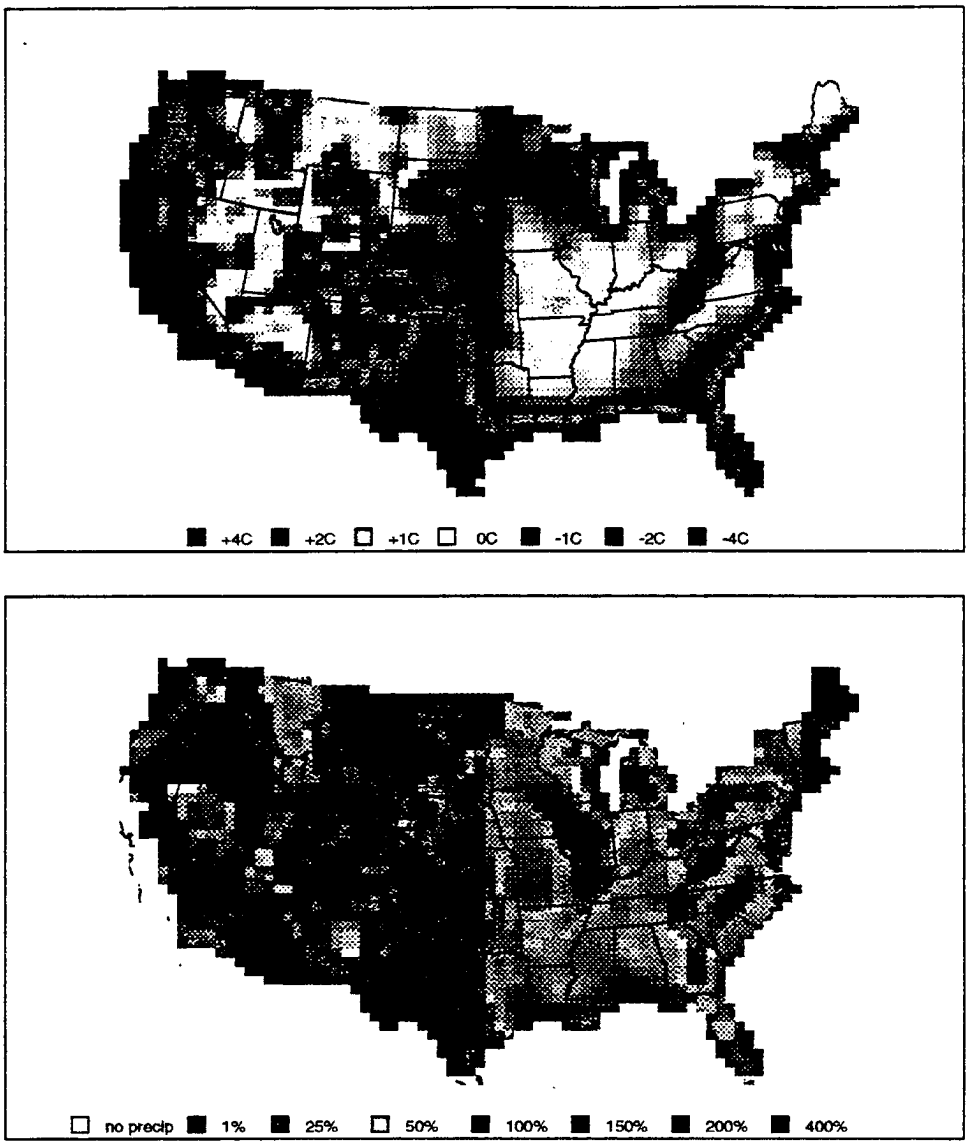

Figure 4.6: The departure of simulated mean daily temperature from observations in degrees Celsius (top panel). Ratio of model precipitation to observations as a percentage (bottom panel).

from Table 4.1 indicates that while the simulated precipitation was 87% of observed for the contiguous United States, this is actually a result of 220% in the western region and 45% in the eastern region. This error structure of a sharp north-south demarcation line separating the regions of high and low precipitation ratios near 97° west longitude was also seen in the RegCM (Giorgi et al. 1994a, 1994b).

The Kuo scheme is activated when a cloud base vertical velocity threshold is exceeded in the presence of instability. This threshold is constant across the whole domain and the probability of it being exceeded is higher in regions where there is orographic forcing of vertical velocities such as the western United States. One problem with the precipitation results is the presence of numerical point storms where very high precipitation occurs in a short time in highly localized areas. For example, in western Texas and the Arizona Monsoon region, 15% of the modeled monthly precipitation would fall in a single day, an amount equivalent to the observed monthly precipitation. These numerical point storms have been seen in MM4 (Giorgi 1991) and GMASS (Koch et al. 1985). Giorgi (1991) explains the mechanism responsible for the anomalously high precipitation as a local circulation response to the latent heat release in the Kuo scheme leading to increased low-level moisture convergence further fueling the convective precipitation parameterization.

The Kuo scheme also does not account for various forcing mechanisms other than surface heated convective instability. One of the results of this was a problem of the convection ceasing at sundown. This would lead to lower precipitation accumulations in areas where nocturnal convective systems are the dominant producers of rainfall.

To summarize the results of the control scenario, CLIMRAMS did an excellent job of simulating the surface temperature structure for the month. Comparisons of daily and weekly extrema and hourly values with observations (not shown) also exhibited small biases. This further demonstrates the capability of CLIMRAMS to

Region	Temperature			Precipitation		
	OBS	CNTL	Δ	OBS	CNTL	ratio
Contiguous U.S.	296.96	295.61	-1.35	72.10	62.40	0.87
Eastern U.S	297.24	296.37	-0.87	124.45	56.19	0.45
Western U.S	296.73	295.00	-1.73	30.63	67.31	2.20
Cascades	289.83	286.93	-2.90	25.36	6.15	0.24
California	295.39	290.80	-4.59	1.51	6.16	4.08
Intermountain Basin	294.54	293.18	-1.36	6.14	15.61	2.54
Southwestern Deserts	302.58	299.59	-2.99	24.71	83.04	3.36
Northern Rockies	293.16	292.67	-0.49	26.39	33.44	1.27
Southern Rockies	295.87	295.12	-0.75	40.81	72.76	1.78
Northern Plains	296.56	296.17	-0.39	45.11	79.94	1.77
Central Plains	298.18	296.15	-2.03	51.36	119.03	2.32
Southern Plains	300.85	298.48	-2.37	91.54	81.30	0.89
Ozark Highlands	297.72	298.05	0.33	110.63	52.53	0.47
Prairie Peninsula	297.29	296.74	-0.55	96.90	53.90	0.56
Great Lakes Forests	294.76	293.41	-1.35	57.43	30.69	0.53
Mississippi Valley	299.01	298.63	-0.38	158.25	64.83	0.41
Florida	300.61	298.52	-2.09	165.68	52.90	0.32
Southeast Coastal	298.87	298.10	-0.77	184.51	83.70	0.45
Appalachia	296.74	296.37	-0.37	139.60	74.42	0.53
Mid Atlantic	294.45	293.94	-0.51	93.27	49.66	0.53
New England	292.67	292.16	-0.51	82.90	17.26	0.21

Table 4.1: Regional averages of mean daily temperature and precipitation for the observations (OBS) and control scenario (CNTL). Units are degree Kelvin for the temperatures and millimeters for precipitation.

provide high resolution, in space and time, high quality screen height temperature information for ecosystem models. Summertime precipitation on the other hand still leaves a lot to be desired. The Kuo parameterization does a much better job of simulating the pattern of precipitation than the actual amount. Comparisons of hourly precipitation rate for one week during an earlier simulation of July 1993 with the radar summary maps produced by NMC (not shown) showed that during daylight hours the two almost always coincided. The precipitation amounts were generally within a factor of two of observations though this is probably not accurate enough for ecosystem modeling needs. Though for the United States as a whole the simulated precipitation rate of 1.91mm·day^{-1} is close to the rate of 2.3mm·day^{-1} as analyzed by Roads et al. (1994).

4.3 Half Soil Moisture Simulation

Initialization of soil moisture is a problem for mesoscale models due mainly to the lack of sufficient quantitative measurements. Qualitatively it is possible to obtain a description of the soil moisture pattern from precipitation data. The purpose of the half soil moisture (HALF) scenario is to investigate the effects of underestimating the initial columnar soil moisture content but maintaining the same patterns as in the CNTL scenario. This situation arises in downscaling GCM scenarios since there are large differences in both the pattern and amount of soil moisture between various models (Kellogg and Zhao 1988). The only difference between the HALF and CNTL scenarios is that the initial soil moisture has been reduced by 50% of the original value.

4.3.1 Screen Height Analysis

The effect of decreased initial soil moisture on mean daily screen height temperature is shown in Figure 4.7. There is a general increase in temperature of 0.1-0.2°C in the Southeast and a slightly larger increase of 0.3-0.5°C in the Great Lakes and

Northeast. This is due to a decrease in the heat capacity of the soil allowing for a greater increase in temperature per unit net radiation. In the Western United States the soil moisture was so low originally that decreasing it had little effect on the heat capacity. Figure 4.8 shows the spatial patterns of a Student's t-test for significance in the temperature difference between the CNTL and HALF scenarios. The test statistic t is given by

$$t = \frac{|\mu_1 - \mu_2|}{\left(\frac{\sigma_1^2+\sigma_2^2}{n}\right)^{1/2}} \tag{4.1}$$

where: μ_1 and μ_2 are the means of the two scenarios that are being compared; σ_1^2 and σ_2^2 are the respective variances; and n is the degrees of freedom. In the case of Figure 4.8 the degrees of freedom is equal to the number of days in the month. The test statistic is essentially the ratio of the difference to the combined variance. The significance levels 20%, 50%, 80%, and 90% correspond to the test statistic values 0.253, 0.674, 1.282, and 1.645 respectively. The significance pattern shows that for the areas which had an increase in mean daily temperature of more than 0.1°C there was a small, less than 80%, statistical significance associated with the change. A difficulty with applying this type of analysis to atmospheric data is that the variances of all of the scenarios are correlated. This is because all of the scenarios are forced by the same atmospheric boundary condition, and are subject to the same pattern of variations on a daily basis. The result of the correlation is an overestimation of the combined variance, so the calculated significance test score should be considered as a lower limit.

The change in monthly mean screen height mixing ratio (Figure 4.7) is concentrated in a region of decrease (0.2-0.3 $g \cdot kg^{-1}$) along the western and southern boundaries of the Central Plains region and an increase (0.1-0.2 $g \cdot kg^{-1}$) in Nebraska and Minnesota. Only the western Central Plains shows any coherent area of significance test score (Figure 4.8). There are several possible mechanisms for the

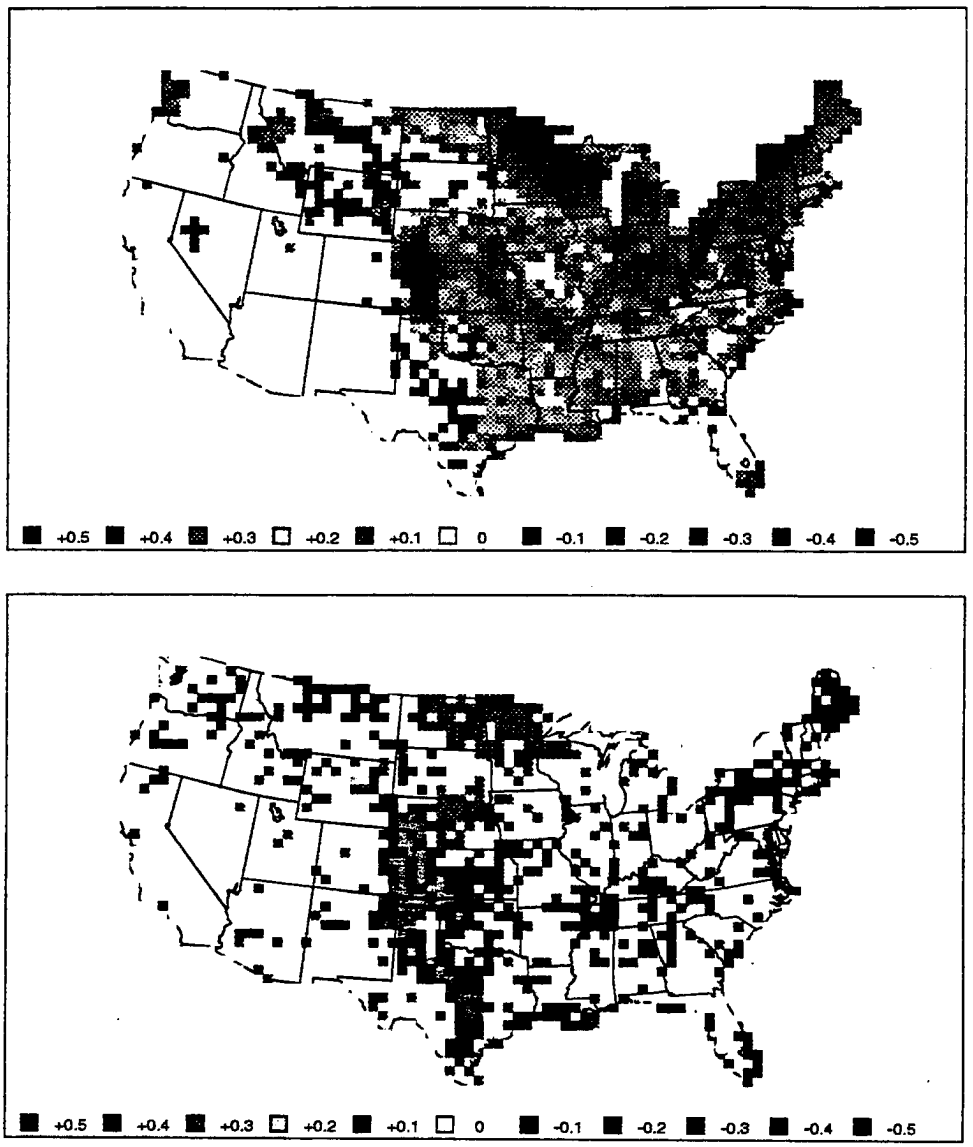

Figure 4.7: The departure of mean daily temperature for the HALF scenario from the CNTL scenario in degrees Celsius (top panel). The departure of mean daily mixing ratio for the HALF scenario from the CNTL scenario in $g \cdot kg^{-1}$ (bottom panel).

change in mixing ratio: a change in precipitation providing more or less soil moisture for evapotranspiration; increase in surface temperature increases the boundary layer depth thus diluting moisture through mixing; increase in temperature increases moisture flux to the atmosphere; decrease in soil moisture decreases soil water potential thus shutting down transpiration.

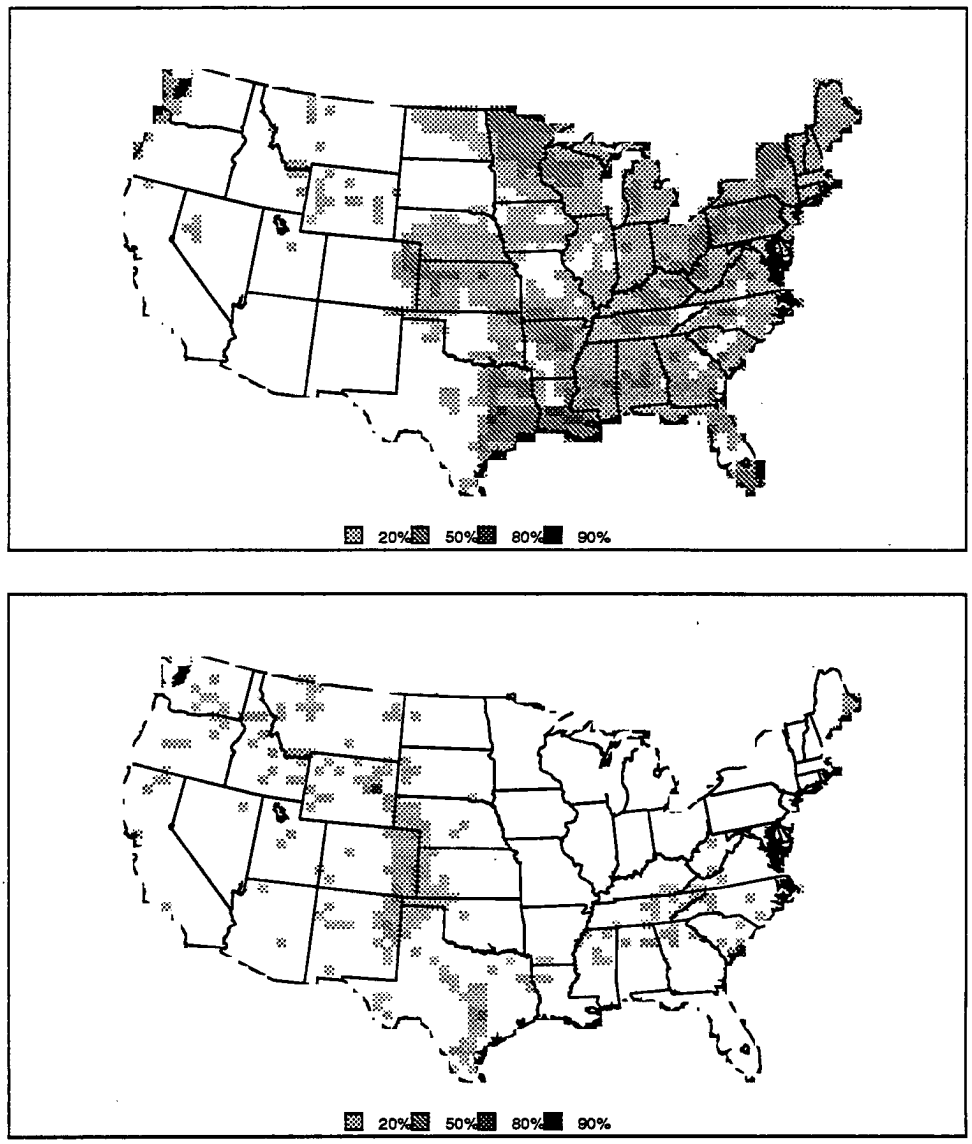

Figure 4.8: Significance test score levels for the departure of mean daily temperature (top panel) and the departure of mean daily mixing ratio (bottom panel).

The change in screen height wind speed (Figure 4.9) shows a decrease of wind speed of 4-10$cm \cdot s^{-1}$ in the Great Lakes region extending southwest towards Ne-

braska. The significance test score map (Figure 4.10) has a low, less that 50%, significance level associated with the greatest decrease in wind speed. The wind speed decrease is also collocated with the temperature increase indicating that a possible reduction in baroclinicity has led to a decrease in surface wind speed through reduced winds speeds at the first atmospheric model level. The temperature gradient from the Gulf of Mexico to the Great Lakes was reduced by about 15% due to the decrease in soil moisture.

The mean daily convective precipitation rate (Figure 4.9) shows decreases of about $0.3mm \cdot day^{-1}$ for south Texas and south Georgia and an increase of the same magnitude along the Appalachian ridge. These daily rates are equivalent to 1cm differences in total monthly accumulation. The significance test shows no coherent pattern (Figure 4.10). A rain-rate of $1mm \cdot day^{-1}$ is equivalent to 3cm accumulated precipitation in a month or about what Denver receives in a year.

For the regional analyses the significance test statistic was computed in a slightly different manner than what was used in the previous section. Instead of computing the variance over time, as was done in the spatial maps of significance level, the variance is computing over the spatial domain of the region being analyzed. This reduces correlations due to synoptic variability but correlations still exist since neighboring grid cells are generally under the influence of a common air mass.

Table 4.2 shows the regional means of screen height temperature and daily convective precipitation rate for the CNTL and HALF scenarios, their differences, and the significance level of the test statistic. The results show the overall increase in temperature due to the decrease in initial soil moisture. The eastern region had an increase of 0.25°C, about eight times larger than the western region, due to a larger absolute decrease in initial soil moisture. The Great Lakes region had the largest increase, 0.65°C, while the Prairie Peninsula had the highest significance level, 90%. The mixing ratio and wind speed summaries are shown in Table 4.3.

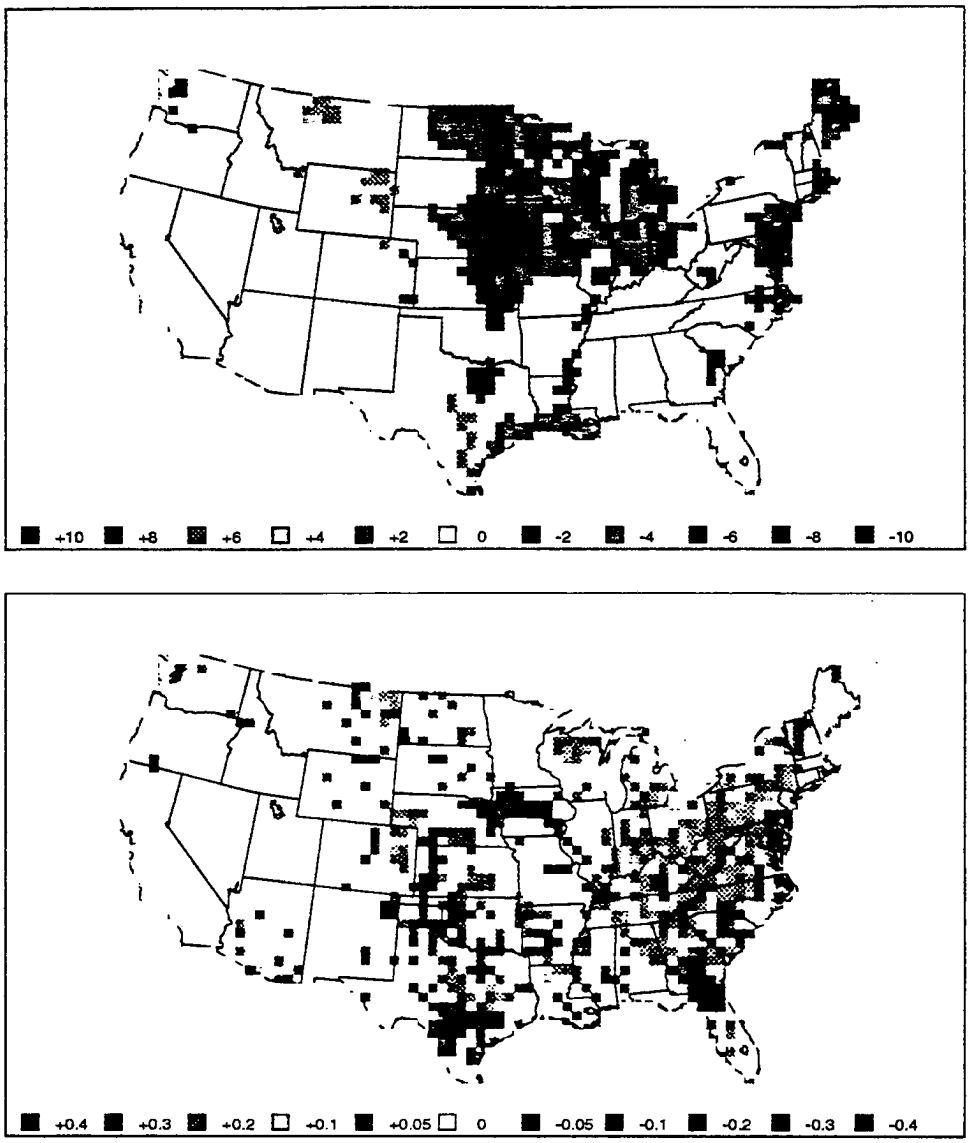

Figure 4.9: The departure of mean wind speed for the HALF scenario from the CNTL scenario in $cm \cdot s^{-1}$ (top panel). The departure of mean daily convective precipitation rate for the HALF scenario from the CNTL scenario in $mm \cdot day^{-1}$ (bottom panel).

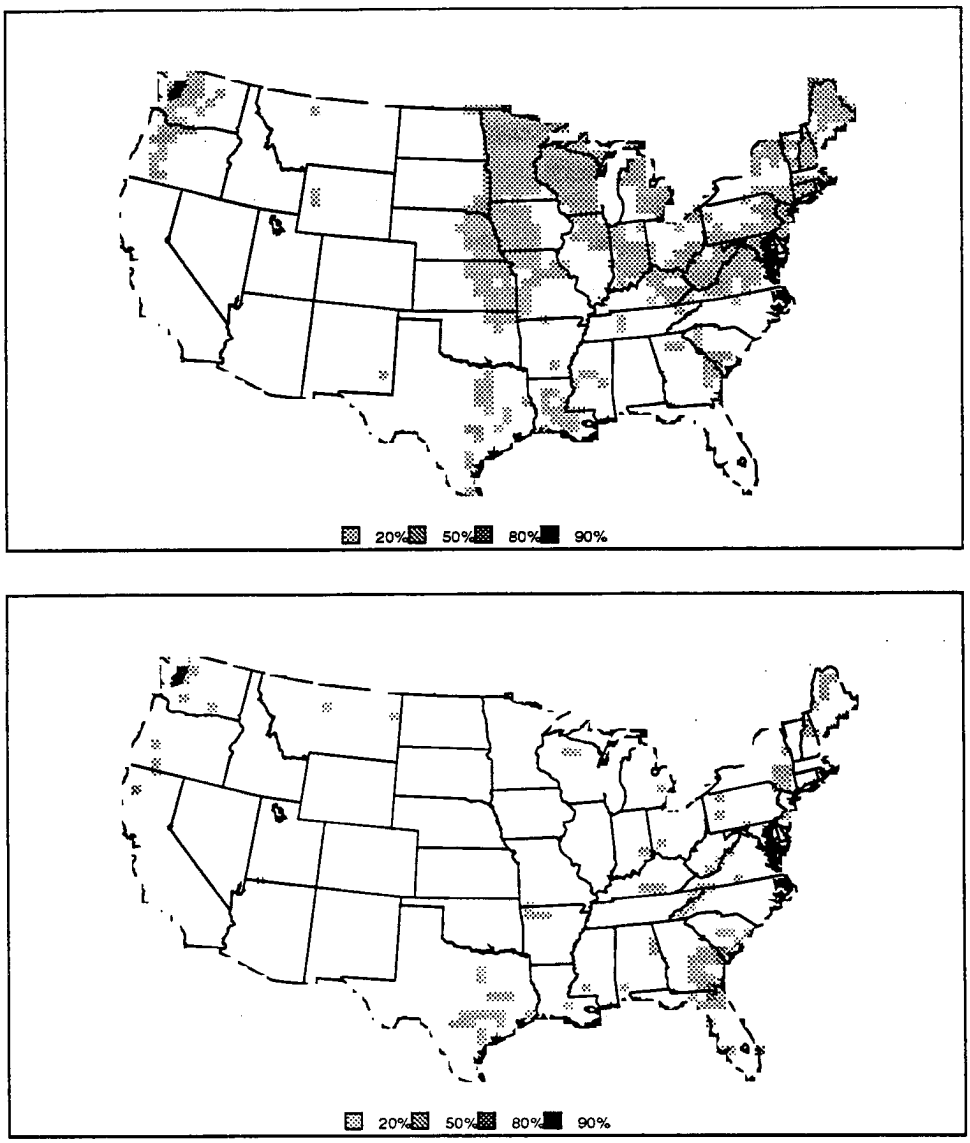

Figure 4.10: The significance levels of differences between mean wind speed for the HALF scenario from the CNTL scenario top panel) and mean daily convective precipitation rate (bottom panel).

The mixing ratio and wind speed both show small but consistent decreases for most regions. This is consistent with an increase in boundary layer depth providing a larger volume for the dilution of moisture.

Region	Temperature (K)				Precipitation ($mm \cdot day^{-1}$)			
	CNTL	HALF	Δ	sig	CNTL	HALF	Δ	sig
Contiguous U.S.	295.61	295.73	0.12	50	1.91	1.91	0.00	
Eastern U.S.	296.37	296.62	0.25	95	1.65	1.67	0.02	20
Western U.S.	295.00	295.03	0.03		2.11	2.10	-0.01	
Cascades	286.79	287.01	0.22		0.05	0.05	0.00	
California	290.76	290.79	0.03		0.17	0.17	0.00	
Intermountain Basin	293.18	293.17	-0.01		0.49	0.49	0.00	
Southwestern Deserts	299.55	299.59	0.04		2.71	2.71	0.00	
Northern Rockies	292.67	292.63	-0.04		1.02	1.02	0.00	
Southern Rockies	295.12	295.12	0.00		2.32	2.32	0.00	
Northern Plains	296.12	296.21	0.09		2.34	2.35	0.01	
Central Plains	296.15	296.29	0.14	50	3.83	3.82	-0.01	
Southern Plains	298.48	298.57	0.09	50	2.49	2.46	-0.03	
Ozark Highlands	298.05	298.29	0.24	80	1.70	1.72	0.02	
Prairie Peninsula	296.74	296.99	0.25	90	1.73	1.73	0.00	
Great Lakes Forests	293.14	293.79	0.65	20	0.93	0.96	0.03	20
Mississippi Valley	298.59	298.85	0.26	20	1.85	1.85	0.00	
Florida	298.52	298.59	0.07	20	1.72	1.66	-0.06	
Southeast Coastal	298.10	298.27	0.17	50	2.57	2.59	0.02	
Appalachia	296.37	296.55	0.18	20	2.29	2.38	0.09	20
Mid Atlantic	293.80	294.29	0.49	20	1.42	1.48	0.06	20
New England	292.17	292.49	0.32	50	0.49	0.53	0.04	20

Table 4.2: Regional averages, differences and significance levels for mean daily temperature and daily convective precipitation rate for the half soil moisture (HALF) and control scenario (CNTL). Units are degree Kelvin for the temperatures and $mm \cdot day^{-1}$ for precipitation.

4.3.2 Surface Energy Budget Analysis

In the surface energy budget analyses the sign convention where a downward flux is positive and an upward flux is negative is used. It should also be noted that the sum of the fluxes is not necessarily zero. This is because what is shown are averages over space and time and not instantaneous point values.

Region	Mixing Ratio ($g \cdot kg^{-1}$)				Wind Speed ($m \cdot s^{-1}$)			
	CNTL	HALF	Δ	sig	CNTL	HALF	Δ	sig
Contiguous U.S.	15.46	15.44	-0.02		1.94	1.93	-0.01	20
Eastern U.S.	17.47	17.45	-0.02		1.57	1.55	-0.02	50
Western U.S.	13.87	13.85	-0.02		2.23	2.23	0.00	
Cascades	9.31	9.25	-0.06		1.09	1.07	-0.02	
California	12.07	12.07	0.00		1.72	1.72	0.00	
Intermountain Basin	10.42	10.41	-0.01		1.72	1.72	0.00	
Southwestern Deserts	13.36	13.36	0.00		2.51	2.51	0.00	
Northern Rockies	11.67	11.67	0.00		1.40	1.41	0.01	
Southern Rockies	13.25	13.25	0.00		1.55	1.55	0.00	
Northern Plains	15.60	15.62	0.02		3.05	3.04	-0.01	
Central Plains	17.62	17.54	-0.08	20	2.84	2.83	-0.01	
Southern Plains	19.45	19.42	-0.03		2.19	2.19	0.00	
Ozark Highlands	19.35	19.33	-0.02		1.04	1.02	-0.02	20
Prairie Peninsula	17.35	17.34	-0.01		2.26	2.21	-0.05	50
Great Lakes Forests	14.36	14.40	0.04		1.69	1.65	-0.04	20
Mississippi Valley	19.59	19.55	-0.04		1.67	1.65	-0.02	20
Florida	19.48	19.46	-0.02		1.51	1.52	0.01	
Southeast Coastal	19.38	19.36	-0.02		1.40	1.38	-0.02	20
Appalachia	17.97	17.94	-0.03		0.99	0.97	-0.02	20
Mid Atlantic	15.27	15.22	-0.05		1.19	1.17	-0.02	20
New England	13.46	13.41	-0.05		1.28	1.25	-0.03	20

Table 4.3: Regional averages, differences and significance levels for mean mixing ratio and wind speed for the half soil moisture (HALF) and control scenario (CNTL). Units are $g \cdot kg^{-1}$for mixing ratio and $m \cdot s^{-1}$ for wind speed.

The net radiation (Table 4.4) shows several interesting results. The peak nocturnal flux shows an increase in magnitude, which is a result of the higher surface temperatures. The peak daylight flux also increased. At first this seemed counter-intuitive since a dry soil has a higher albedo than a wet soil and would increase the reflected shortwave component, decreasing the net radiation flux and the increased upward longwave emission would also serve to decrease the net radiation. What is occurring is that with the higher temperatures and lower mixing ratios there is a decrease in relative humidity. This reduces the shortwave albedo of pseudo-clouds allowing more downward shortwave to reach the surface and overcome the albedo and longwave emission effects. The mean net radiation shows a general decrease of a net downward flux on the order of $1W \cdot m^{-2}$. This is a result of the change in the nocturnal flux dominating the diurnal cycle. The changes in the peak fluxes is larger than the changes in the mean flux leading to an increase in the diurnal range with only a slight change in the mean. The increase in diurnal range for the contiguous United States was $8.38W \cdot m^{-2}$ while the mean decreased by only $0.66W \cdot m^{-2}$.

Region	Peak Nocturnal			Peak Daylight			Mean		
	CNTL	HALF	Δ	CNTL	HALF	Δ	CNTL	HALF	Δ
Contiguous U.S.	-74.67	-79.59	-4.92	539.90	543.29	3.39	160.69	160.03	-0.66
Eastern U.S.	-56.40	-58.89	-2.49	455.80	462.10	6.30	145.83	145.53	-0.30
Western U.S.	-92.08	-97.22	-5.14	612.33	614.08	1.75	172.47	171.92	-0.55
Cascades	-16.13	-29.31	-13.18	453.69	457.33	3.64	167.10	165.50	-1.60
California	-53.94	-54.35	-0.41	621.15	622.12	0.97	192.86	192.90	0.04
Intermountain Basin	-93.30	-93.63	-0.33	712.35	715.96	3.61	205.73	206.03	0.30
Southwestern Deserts	-113.60	-130.39	-16.79	665.00	665.54	0.54	170.21	169.02	-1.19
Northern Rockies	-99.28	-98.88	0.40	648.71	646.13	-2.58	189.17	187.98	-1.19
Southern Rockies	-100.74	-100.79	-0.05	703.04	700.65	-2.39	197.21	196.97	-0.24
Northern Plains	-97.62	-104.27	-6.65	508.33	513.55	5.22	142.03	141.91	-0.12
Central Plains	-107.89	-110.83	-2.94	565.23	573.95	8.72	144.91	145.22	0.31
Southern Plains	-64.27	-66.75	-2.48	487.15	501.16	14.01	141.48	143.39	1.91
Ozark Highlands	-68.39	-72.35	-3.96	462.12	464.64	2.52	145.25	144.66	-0.59
Prairie Peninsula	-84.55	-86.01	-1.46	546.77	555.34	8.57	158.91	159.88	0.97
Great Lakes Forests	-61.02	-70.34	-9.32	511.55	524.03	12.48	165.28	165.05	-0.23
Mississippi Valley	-54.25	-56.98	-2.73	418.13	423.00	4.87	134.62	133.83	-0.79
Florida	-22.45	-22.14	0.31	398.35	399.18	0.83	133.92	133.61	-0.31
Southeast Coastal	-47.40	-49.55	-2.15	397.14	404.74	7.60	129.82	131.75	1.93
Appalachia	-63.85	-68.55	-4.70	429.01	429.17	0.16	135.64	135.28	-0.36
Mid Atlantic	-52.73	-55.02	-2.29	469.56	472.03	2.47	151.09	151.15	0.06
New England	-52.30	-56.18	-3.88	463.81	461.25	-2.56	151.92	150.73	-1.19

Table 4.4: Regional averages and differences and significance levels for net radiation for the control (CNTL) and half soil moisture (HALF) scenarios. Units are $W \cdot m^{-2}$.

In almost all regions the latent heat flux (Table 4.5) increased in magnitude. Looking at the stomatal response functions (Figure 3.8) would suggest that a decrease in soil moisture would increase the magnitude of the soil water potential and thus decrease transpiration. This is opposite to what the model results show. The explanation is that because of the tight gradients in the soil moisture initialization, which remained through the simulation period, the dry regions are to the right of the step in the soil water potential curve in Figure 3.8 and the wet regions are so far to the left of the curve that even after reducing the soil moisture by half they are still at the top of the step. This means that the change in soil water potential has little effect on the stomatal conductance and the dominant control is temperature, indicating that those regions are to the left of the peak of the temperature curve. The big exception to this is the Cascades region, which saw a decrease in the magnitude of the latent heat flux. The Cascades crossed the step in the soil water potential curve with the decrease in soil moisture so water limitation became an important control of transpiration.

The sensible heat flux (Table 4.6) shows the effect of increased surface temperatures with increased flux to the atmosphere during daylight and decreased flux to the surface during the night. The changes are greater in the eastern United States where the temperature changes were greater. The overall trend in the mean is an increase in the upward flux of sensible heat. Regions where the mean was upward in the CNTL scenario saw an increase in the mean magnitude with drier soils. Regions where the mean was originally downward saw decreases in the magnitude of the mean sensible heat flux. Two regions, Great Lakes and Mid Atlantic, had a change in direction of the mean daily sensible heat flux from downward to upward.

The soil heat flux (Table 4.7) shows a decrease in the downward flux during daytime and in the mean. This is a result of the decrease in the thermal conductivity due to lower soil moisture content. The upward soil heat flux during the night follows

Region	Peak Daylight			Peak Nocturnal			Mean		
	CNTL	HALF	Δ	CNTL	HALF	Δ	CNTL	HALF	Δ
Contiguous U.S.	-462.98	-470.61	-7.63	-20.71	-20.74	-0.03	-189.86	-192.49	-2.63
Eastern U.S.	-406.96	-418.11	-11.15	-16.95	-18.44	-1.49	-167.37	-171.59	-4.22
Western U.S.	-508.10	-514.64	-6.54	-20.94	-20.01	0.93	-207.67	-209.05	-1.38
Cascades	-284.58	-273.18	11.40	-12.93	-5.53	7.40	-122.77	-113.73	9.04
California	-514.95	-515.66	-0.71	-9.59	-8.90	0.69	-201.85	-201.59	0.26
Intermountain Basin	-579.06	-588.55	-9.49	-11.05	-10.32	0.73	-226.88	-227.38	-0.50
Southwestern Deserts	-473.30	-473.48	-0.18	-17.73	-17.61	0.12	-183.29	-183.05	0.24
Northern Rockies	-555.33	-559.32	-3.99	-16.47	-16.63	-0.16	-227.33	-228.49	-1.16
Southern Rockies	-630.18	-624.73	5.45	-18.47	-18.45	0.02	-244.77	-244.51	0.26
Northern Plains	-394.04	-409.74	-15.70	-25.39	-24.82	0.57	-171.84	-175.16	-3.32
Central Plains	-522.04	-540.32	-18.28	-29.52	-28.77	0.75	-213.62	-218.69	-5.07
Southern Plains	-446.42	-464.38	-17.96	-18.42	-17.28	1.14	-179.88	-182.13	-2.25
Ozark Highlands	-454.24	-463.22	-8.98	-14.28	-16.41	-2.13	-180.28	-184.69	-4.41
Prairie Peninsula	-502.58	-520.42	-17.84	-12.09	-15.01	-2.92	-192.59	-201.03	-8.44
Great Lakes Forests	-406.07	-426.72	-20.65	-13.11	-15.12	-2.01	-167.78	-174.00	-6.22
Mississippi Valley	-380.56	-396.15	-15.59	-13.78	-15.31	-1.53	-154.26	-158.77	-4.51
Florida	-341.86	-340.35	1.51	-15.95	-15.11	0.84	-139.64	-138.20	1.44
Southeast Coastal	-380.16	-390.43	-10.27	-15.26	-17.02	-1.76	-158.34	-162.55	-4.21
Appalachia	-415.63	-416.84	-1.21	-9.67	-11.08	-1.41	-168.39	-172.47	-4.08
Mid Atlantic	-397.00	-401.98	-4.98	-10.49	-11.91	-1.42	-156.21	-159.26	-3.05
New England	-403.08	-399.63	3.45	-14.79	-14.98	-0.19	-165.36	-167.59	-2.23

Table 4.5: Regional averages and differences and significance levels for latent heat flux for the control (CNTL) and half soil moisture (HALF) scenarios. Units are $W \cdot m^{-2}$.

Region	Peak Daylight			Peak Nocturnal			Mean		
	CNTL	HALF	Δ	CNTL	HALF	Δ	CNTL	HALF	Δ
Contiguous U.S.	-58.65	-65.86	-7.21	53.87	52.58	-1.29	10.66	7.00	-3.66
Eastern U.S.	-27.48	-37.10	-9.62	48.18	44.51	-3.67	16.59	10.89	-5.70
Western U.S.	-91.88	-96.69	-4.81	67.18	66.34	-0.84	5.96	3.92	-2.04
Cascades	-151.22	-179.07	-27.85	24.16	17.89	-6.27	-50.08	-62.27	-12.19
California	-108.20	-109.35	-1.15	58.53	58.04	-0.49	-9.77	-10.36	-0.59
Intermountain Basin	-129.03	-130.49	-1.46	64.89	64.52	-0.37	-11.77	-12.45	-0.68
Southwestern Deserts	-188.77	-188.92	-0.15	76.18	76.15	-0.03	-22.46	-22.55	-0.09
Northern Rockies	-102.03	-107.50	-5.47	55.31	54.07	-1.24	-2.24	-4.29	-2.05
Southern Rockies	-105.00	-104.77	0.23	58.74	58.77	0.03	-2.18	-2.19	-0.01
Northern Plains	-76.98	-84.26	-7.28	69.29	66.14	-3.15	12.14	8.86	-3.28
Central Plains	-22.07	-29.10	-7.03	109.55	107.87	-1.68	51.39	47.50	-3.89
Southern Plains	-27.77	-38.82	-11.05	84.07	80.74	-3.33	24.51	19.83	-4.68
Ozark Highlands	-11.74	-20.63	-8.89	59.26	55.72	-3.54	24.36	20.21	-4.15
Prairie Peninsula	-28.09	-36.01	-7.92	59.11	54.44	-4.67	26.02	20.86	-5.16
Great Lakes Forests	-72.89	-88.66	-15.77	52.41	45.63	-6.78	1.46	-7.52	-8.98
Mississippi Valley	-19.57	-25.13	-5.56	47.41	44.38	-3.03	14.41	10.18	-4.23
Florida	-43.16	-45.81	-2.65	28.59	27.51	-1.08	-4.01	-5.24	-1.23
Southeast Coastal	-4.10	-11.34	-7.24	61.38	57.79	-3.59	23.83	19.28	-4.55
Appalachia	-3.64	-12.81	-9.17	52.21	49.94	-2.27	27.13	22.08	-5.05
Mid Atlantic	-46.42	-59.81	-13.39	38.51	32.95	-5.56	3.97	-3.83	-7.80
New England	-36.76	-49.22	-12.46	63.06	56.24	-6.82	15.64	7.85	-7.79

Table 4.6: Regional averages and differences and significance levels for sensible heat flux for the control (CNTL) and half soil moisture (HALF) scenarios. Units are $W \cdot m^{-2}$.

the same logic for the western regions but there is an increase in the magnitude of the flux for most of the eastern regions and the United States as a whole. The decrease in the heat capacity of the eastern region soils was largest due to the large absolute reductions in soil moisture content. This allows the top soil layer to experience a larger drop in temperature for a given loss of radiational energy during the night. In the eastern regions the larger nocturnal vertical soil temperature gradient offsets the effects of reduced thermal conductivity.

Region	Peak Nocturnal			Peak Daylight			Mean		
	CNTL	HALF	Δ	CNTL	HALF	Δ	CNTL	HALF	Δ
Contiguous U.S.	-15.29	-16.06	-0.77	36.00	25.31	-10.69	7.25	2.05	-5.20
Eastern U.S.	-8.26	-12.36	-4.10	38.94	25.40	-13.54	12.99	4.56	-8.43
Western U.S.	-21.10	-19.19	1.91	33.66	25.23	-8.43	2.70	0.06	-2.64
Cascades	-16.47	-9.24	7.23	32.93	15.40	-17.53	4.04	0.88	-3.16
California	-9.48	-8.72	0.76	14.22	12.63	-1.59	0.61	0.42	-0.19
Intermountain Basin	-18.38	-16.79	1.59	23.64	20.85	-2.79	1.34	0.89	-0.45
Southwestern Deserts	-23.71	-23.58	0.13	30.85	30.77	-0.08	-1.40	-1.37	0.03
Northern Rockies	-23.94	-18.84	5.10	36.44	22.96	-13.48	4.00	0.65	-3.35
Southern Rockies	-19.98	-19.82	0.16	22.24	22.16	-0.08	-1.03	-1.01	0.02
Northern Plains	-25.00	-22.72	2.28	42.27	27.71	-14.56	5.29	-0.02	-5.31
Central Plains	-23.31	-23.89	-0.58	51.21	35.76	-15.45	8.14	1.19	-6.95
Southern Plains	-16.77	-14.68	2.09	37.88	24.27	-13.61	5.49	1.48	-4.01
Ozark Highlands	-10.17	-13.91	-3.74	38.04	24.54	-13.50	12.33	4.25	-8.08
Prairie Peninsula	-14.39	-16.03	-1.64	43.97	22.82	-21.15	13.43	2.34	-11.09
Great Lakes Forests	-11.14	-17.70	-6.56	50.08	29.70	-20.38	17.22	4.12	-13.10
Mississippi Valley	-7.82	-11.37	-3.55	32.84	19.78	-13.06	10.85	3.06	-7.79
Florida	-10.57	-10.22	0.35	24.24	23.22	-1.02	3.83	3.51	-0.32
Southeast Coastal	-5.99	-10.46	-4.47	33.81	26.28	-7.53	11.43	5.80	-5.63
Appalachia	-6.55	-12.51	-5.96	38.94	27.04	-11.90	14.44	5.60	-8.84
Mid Atlantic	-6.81	-12.74	-5.93	45.42	31.40	-14.02	16.87	7.27	-9.60
New England	-4.27	-9.97	-5.70	46.60	30.56	-16.04	19.30	8.79	-10.51

Table 4.7: Regional averages and differences and significance levels for soil heat flux for the control (CNTL) and half soil moisture (HALF) scenarios. Units are $W \cdot m^{-2}$.

4.3.3 Summary

The decrease in the soil moisture throughout the column led to a decreased soil heat capacity and increased soil temperatures. This in turn led to an increase in mean daily temperature through increased heat flux to the atmosphere. The decrease in soil moisture was not sufficient to limit transpiration, except in the Cascades, so the increase in temperature increased the stomatal conductance leading to greater latent heat flux. The increased moisture flux to the boundary layer did not show up as an increase in the screen height mixing ratio. The higher temperatures

led to greater boundary layer growth and the additional moisture was able to mix through a larger volume of atmosphere. The surface wind speed decreased due to lower wind speeds at the first atmospheric level in the model. The warmer boundary layer in the north reduced the temperature gradient from the Great Lakes to the Gulf Coast. This reduces the westerly wind speed at the first atmospheric level through the weaker north–south geopotential gradient.

4.4 Half Deep Soil Moisture Simulation

This scenario (HBOT) investigates the effect of leaving the moisture content in the top soil layer the same as in the CNTL scenario but reducing the soil moisture in the remaining 10 layers in the same manner as the HALF scenario. The initial hypothesis was that over the period of a month the model should be fairly insensitive to the the moisture content of the top soil layer since it is only 5cm thick and thus can respond very quickly to inputs of heat and moisture. The results of the HBOT scenario should be fairly similar to the HALF scenario.

4.4.1 Screen Height Analysis

The temperature anomaly of mean daily temperature for the HBOT scenario (Figure 4.11) shows the same pattern as in the HALF scenario (Figure 4.7). The major difference is a slightly cooler mean temperature in the HBOT scenario which is closer to that of the CNTL run. This shows up as a reduction in both the magnitude (0.5°C for HBOT verses 0.6°C for HALF) and areal coverage of the positive anomalies located in eastern Colorado and western Kansas. There was also an increase in negative anomalies (0.2°C for HBOT verses 0.1°C for HALF) in Wyoming and Montana. There was no difference in the significance maps (Figures 4.12 and 4.8) other than a slight reduction in significance of temperature difference in the Mississippi Delta area.

Screen height mixing ratio shows that the lowest portion of the boundary layer is more moist with a wetter topsoil layer (Figure 4.11). This shows up as the reduced negative anomaly in western Kansas eastern Colorado ($0.3g \cdot kg^{-1}$ in HBOT verses $0.4g \cdot kg^{-1}$ in HALF). The region of positive mixing ratio anomaly in eastern Nebraska and Minnesota increased from $0.1g \cdot kg^{-1}$ in the HALF scenario to $0.2g \cdot kg^{-1}$ in the HBOT scenario. The significance pattern for mixing ratio (Figure 4.12) shows a decrease in overall significance, almost no grid cells exceed the 50% threshold. There was an slight reduction in the areal coverage in eastern Colorado and central Texas.

The wind speed shows the same pattern of reduced velocity at screen height (Figure 4.13) in the HBOT run as in the HALF scenario. The difference between the two is that the HBOT scenario has slightly stronger wind speeds as shown in the difference field (-$7cm \cdot s^{-1}$ for HBOT verses -$10cm \cdot s^{-1}$ for HALF). The pattern of significance (Figure 4.14) is greatly reduced in area. The region of significance in Kansas, Missouri, and Indiana that is evident in the HALF scenario (Figure 4.10) is almost non-existent in the HBOT case. The only areas showing any significant difference in wind speed between the HBOT and CNTL scenarios is in Minnesota, Wisconsin, and along the northern half of the Atlantic coast.

The HBOT scenario had more convective precipitation (Figure 4.13) than the HALF scenario, though still less than the CNTL run, in Iowa, south Texas, and south Georgia. The magnitude of the negative anomalies in those regions decreased from $0.4mm \cdot day^{-1}$ in the HALF scenario (Figure 4.9) to $0.3mm \cdot day^{-1}$ in the HBOT case. The region of positive precipitation anomaly along the ridge of the Appalachians decreased in the HBOT case ($0.2mm \cdot day^{-1}$) from $0.3mm \cdot day^{-1}$ in the HALF scenario. With very little area showing any significance in the HALF scenario (Figure 4.10) there was not much difference in the significance map for the HBOT scenario (Figure 4.14). The only change was the absence in south Georgia of the 20% significance area.

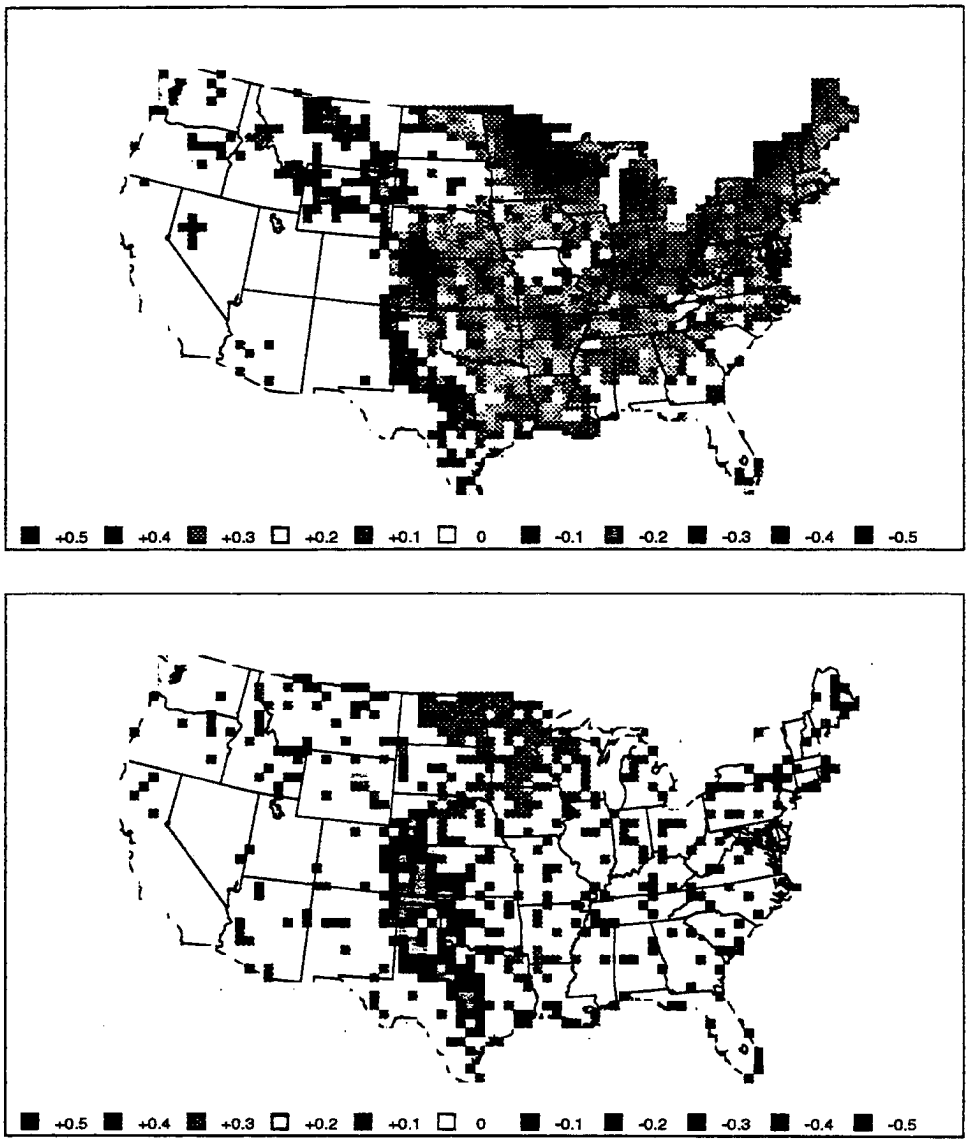

Figure 4.11: The departure of mean daily temperature for the HBOT scenario from the CNTL scenario in degrees Celsius (top panel). The departure of mean daily mixing ratio for the HBOT scenario from the CNTL scenario in $g \cdot kg^{-1}$ (bottom panel).

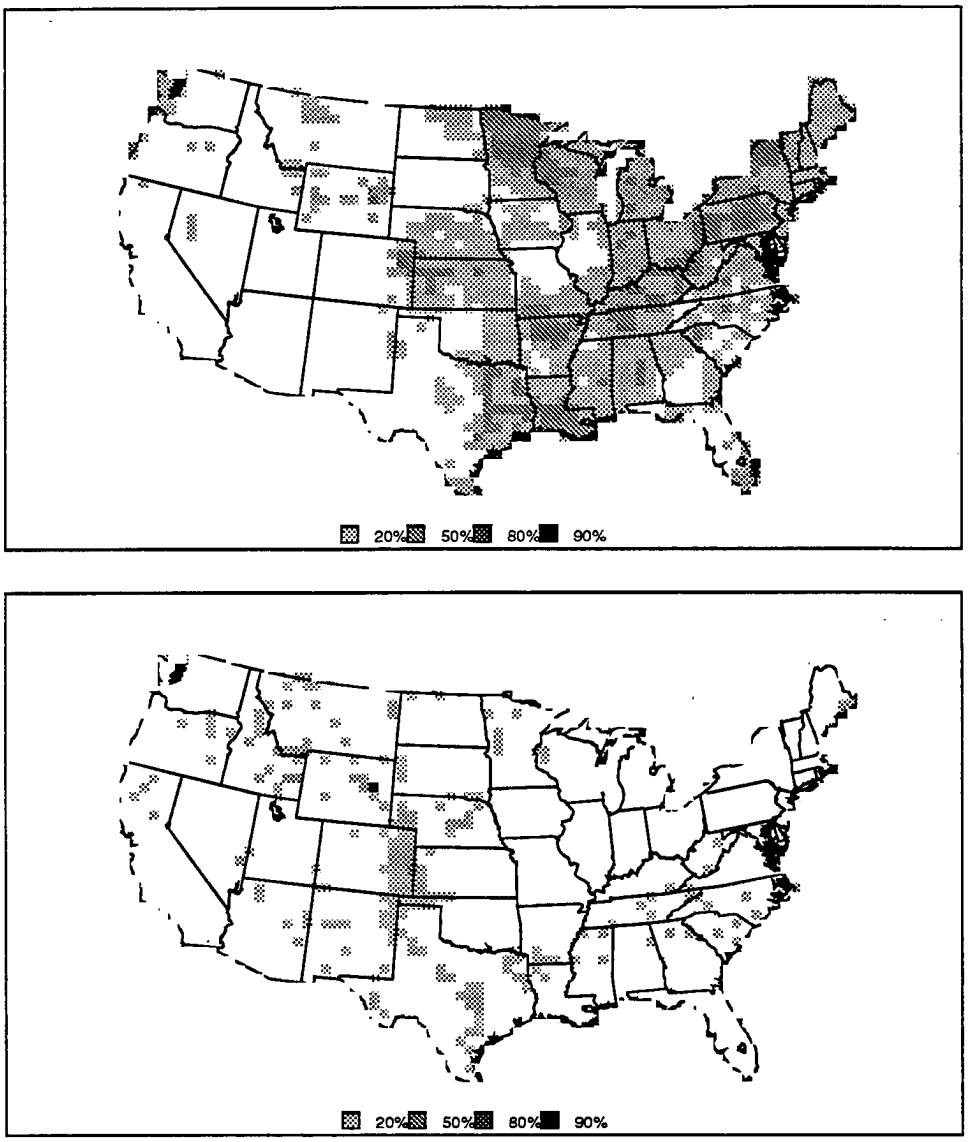

Figure 4.12: Significance test score levels for the departure of mean daily temperature (top panel) and the departure of mean daily mixing ratio (bottom panel).

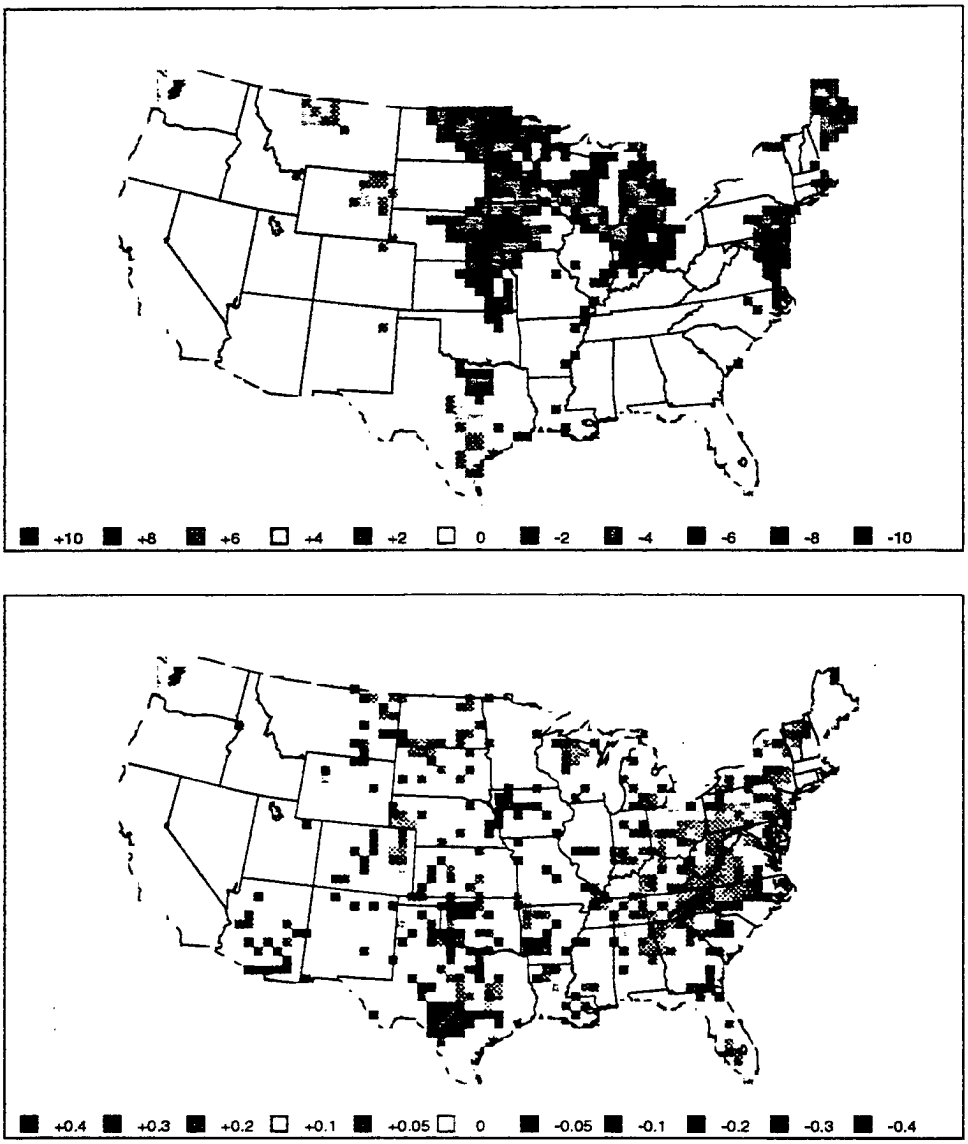

Figure 4.13: The departure of mean wind speed for the HBOT scenario from the CNTL scenario in $cm \cdot s^{-1}$ (top panel). The departure of mean daily convective precipitation rate for the HBOT scenario from the CNTL scenario in $mm \cdot day^{-1}$ (bottom panel).

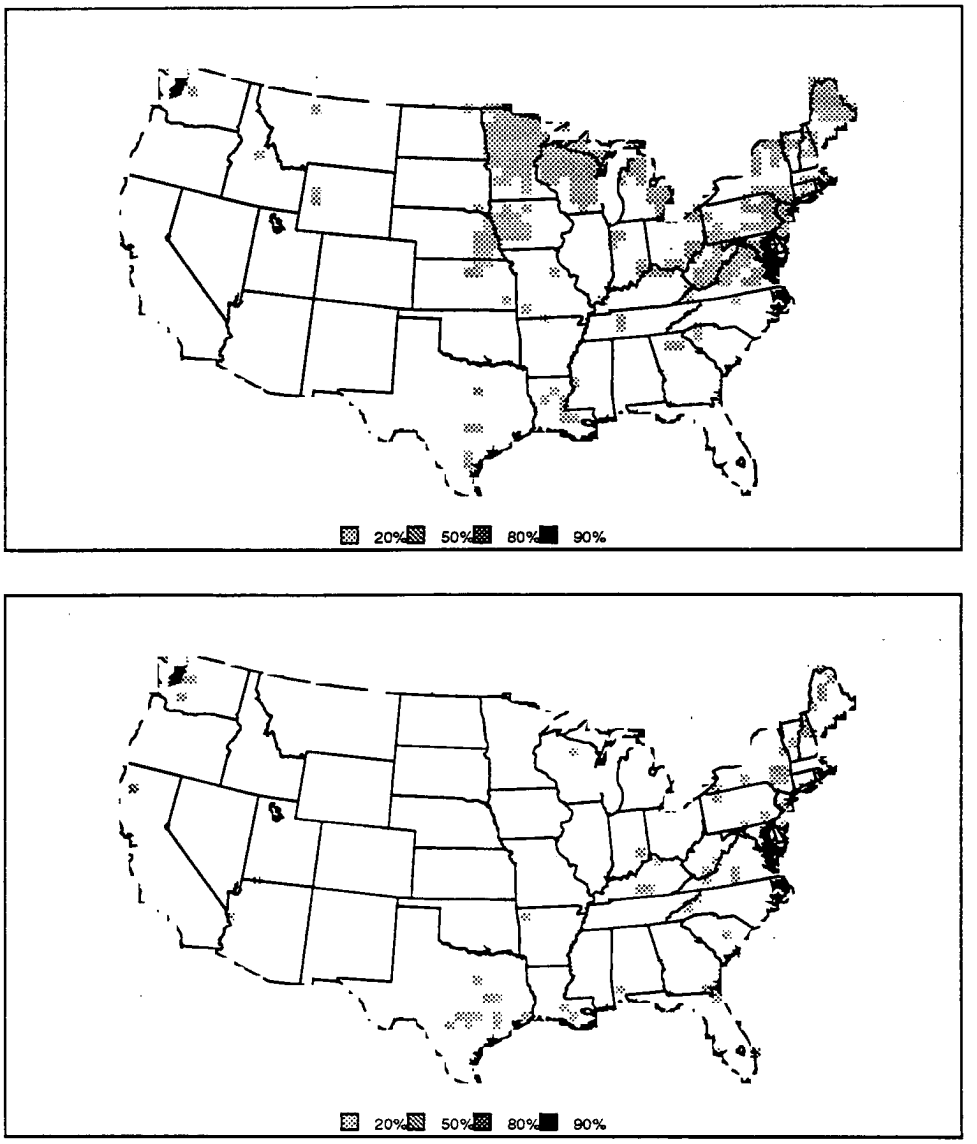

Figure 4.14: The significance levels of differences between mean wind speed for the HBOT scenario from the CNTL scenario top panel) and mean daily convective precipitation rate (bottom panel).

The regional temperature averages of the HBOT scenario (Table 4.8) are very close to those of the HALF scenario. Both runs show similar differences with the CNTL run. The HBOT regional temperatures tend to be slightly cooler than the temperatures from the HALF scenario. This would be consistent with the idea of greater evaporation occurring from a more moist top soil layer. The increase in the heat capacity would also serve to keep the screen height temperature in the HBOT run lower than in the HALF scenario since the top soil would have a greater thermal inertia. The daily convective precipitation rates in the HBOT run (Table 4.8) are about the same as the HALF scenario (Table 4.2). The differences that were evident in the spatial maps have been lost in the averaging process since they were confined to fairly small geographical regions. The mixing ratio summary (Table 4.9) shows that the HBOT scenario while still drier than the CNTL run was a little more moist than the HALF scenario. This can arise from increased evaporation, as compared to the HALF run, from the wetter top soil layer and the cooler screen height temperatures indicate more stability and smaller boundary layer depth than the HALF run would help to concentrate the moisture closer to the surface. The change in wind speeds between the HBOT and CNTL scenarios is consistent with the mechanism of reduced north-south gradient in temperature as in the HALF scenario. The HBOT wind speeds are still slower than the CNTL run (Table 4.9) but are a little stronger than the HALF scenario (Table 4.3) since the temperature gradient is not as small as in the HALF run..

4.4.2 Surface Energy Budget Analysis

The net radiation summary (Table 4.10) shows the same overall pattern as the HALF scenario in comparison with the CNTL run. The nocturnal emission is increased (compared to CNTL) due to warmer surface temperatures and the daylight shortwave increases due to an overall drier boundary layer. The change in the nocturnal flux has a larger impact on the daily mean than the change in

Region	Temperature (K)				Precipitation ($mm \cdot day^{-1}$)			
	CNTL	HBOT	Δ	sig	CNTL	HBOT	Δ	sig
Contiguous U.S.	295.61	295.71	0.10	50.00	1.91	1.92	0.01	
Eastern U.S.	296.37	296.59	0.22	90.00	1.65	1.68	0.03	20.00
Western U.S.	295.00	295.00	0.00		2.11	2.11	0.00	
Cascades	286.79	286.98	0.19		0.05	0.05	0.00	
California	290.76	290.79	0.03		0.17	0.17	0.00	
Intermountain Basin	293.18	293.15	-0.03		0.49	0.49	0.00	
Southwestern Deserts	299.55	299.59	0.04		2.71	2.71	0.00	
Northern Rockies	292.67	292.62	-0.05	20.00	1.02	1.03	0.01	
Southern Rockies	295.12	295.12	0.00		2.32	2.32	0.00	
Northern Plains	296.12	296.18	0.06		2.34	2.36	0.02	
Central Plains	296.15	296.25	0.10	20.00	3.83	3.83	0.00	
Southern Plains	298.48	298.53	0.05	20.00	2.49	2.46	-0.03	
Ozark Highlands	298.05	298.28	0.23	50.00	1.70	1.72	0.02	
Prairie Peninsula	296.74	296.94	0.20	50.00	1.73	1.73	0.00	
Great Lakes Forests	293.14	293.77	0.63	20.00	0.93	0.96	0.03	20.00
Mississippi Valley	298.59	298.83	0.24	20.00	1.85	1.86	0.01	
Florida	298.52	298.56	0.04		1.72	1.73	0.01	
Southeast Coastal	298.10	298.23	0.13	50.00	2.57	2.60	0.03	
Appalachia	296.37	296.63	0.26	50.00	2.29	2.37	0.08	20.00
Mid Atlantic	293.80	294.26	0.46	20.00	1.42	1.48	0.06	20.00
New England	292.17	292.47	0.30	50.00	0.49	0.52	0.03	20.00

Table 4.8: Regional averages, differences and significance levels for mean daily temperature and daily convective precipitation rate for the half deep soil moisture (HBOT) and control scenario (CNTL). Units are degree Kelvin for the temperatures and $mm \cdot day^{-1}$ for precipitation.

Region	Mixing Ratio ($g \cdot kg^{-1}$)				Wind Speed ($m \cdot s^{-1}$)			
	CNTL	HBOT	Δ	sig	CNTL	HBOT	Δ	sig
Contiguous U.S.	15.46	15.46	0.00		1.94	1.92	-0.02	50.00
Eastern U.S.	17.47	17.48	0.01		1.57	1.55	-0.02	50.00
Western U.S.	13.87	13.86	-0.01		2.23	2.23	0.00	
Cascades	9.31	9.29	-0.02		1.09	1.08	-0.01	
California	12.07	12.07	-0.00		1.72	1.72	0.00	
Intermountain Basin	10.42	10.42	0.00		1.72	1.72	0.00	
Southwestern Deserts	13.36	13.37	0.01		2.51	2.51	0.00	
Northern Rockies	11.69	11.69	0.00		1.40	1.41	0.01	
Southern Rockies	13.25	13.25	-0.00		1.55	1.55	0.00	
Northern Plains	15.60	15.63	0.04		3.05	3.05	0.00	
Central Plains	17.62	17.60	-0.02		2.84	2.83	-0.01	
Southern Plains	19.45	19.43	-0.02		2.19	2.19	0.00	
Ozark Highlands	19.35	19.37	0.02		1.04	1.03	-0.01	
Prairie Peninsula	17.35	17.38	0.03	20.00	2.26	2.23	-0.03	50.00
Great Lakes Forests	14.36	14.42	0.06	20.00	1.69	1.65	-0.04	20.00
Mississippi Valley	19.59	19.58	-0.01		1.67	1.65	-0.02	20.00
Florida	19.48	19.48	-0.00		1.51	1.52	0.01	
Southeast Coastal	19.38	19.37	-0.01		1.40	1.38	-0.02	20.00
Appalachia	17.97	17.97	-0.00		0.99	0.98	-0.01	20.00
Mid Atlantic	15.27	15.26	-0.01		1.19	1.17	-0.02	
New England	13.46	13.44	-0.02		1.28	1.26	-0.02	

Table 4.9: Regional averages, differences and significance levels for mean mixing ratio and wind speed for the half deep soil moisture (HBOT) and control scenario (CNTL). Units are $g \cdot kg^{-1}$for mixing ratio and $m \cdot s^{-1}$ for wind speed.

the daylight flux. Comparing the net radiation values of the HBOT run with those from the HALF run (Table 4.4) show a consistent change of lower daytime and nocturnal net flux in the HBOT run due to a more moist boundary layer and lower temperatures than in the HALF scenario.

Region	Peak Nocturnal			Peak Daylight			Mean		
	CNTL	HBOT	Δ	CNTL	HBOT	Δ	CNTL	HBOT	Δ
Contiguous U.S.	-74.67	-79.37	-4.70	539.90	541.81	1.91	160.69	159.66	-1.03
Eastern U.S.	-56.40	-58.45	-2.05	455.80	459.83	4.03	145.83	145.12	-0.71
Western U.S.	-92.08	-97.07	-4.99	612.33	612.66	0.33	172.47	171.59	-0.88
Cascades	-16.13	-28.93	-12.80	453.69	456.25	2.56	167.10	165.58	-1.52
California	-53.94	-53.83	0.11	621.15	621.21	0.06	192.86	192.69	-0.17
Intermountain Basin	-93.30	-93.26	0.04	712.35	712.13	-0.22	205.73	205.45	-0.28
Southwestern Deserts	-113.60	-130.48	-16.88	665.00	665.01	0.01	170.21	168.93	-1.28
Northern Rockies	-99.28	-99.10	0.18	648.71	644.20	-4.51	189.17	188.02	-1.15
Southern Rockies	-100.74	-100.69	0.05	703.04	699.70	-3.34	197.21	196.87	-0.34
Northern Plains	-97.62	-103.71	-6.09	508.33	511.83	3.50	142.03	141.69	-0.34
Central Plains	-107.89	-110.13	-2.24	565.23	571.02	5.79	144.91	144.57	-0.34
Southern Plains	-64.27	-65.62	-1.35	487.15	500.82	13.67	141.48	143.11	1.63
Ozark Highlands	-68.39	-72.35	-3.96	462.12	459.74	-2.38	145.25	144.71	-0.54
Prairie Peninsula	-84.55	-85.93	-1.38	546.77	550.73	3.96	158.91	158.59	-0.32
Great Lakes Forests	-61.02	-69.78	-8.76	511.55	522.86	11.31	165.28	164.89	-0.39
Mississippi Valley	-54.25	-56.60	-2.35	418.13	421.62	3.49	134.62	133.26	-1.36
Florida	-22.45	-22.24	0.21	398.35	402.98	4.63	133.92	134.14	0.22
Southeast Coastal	-47.40	-49.46	-2.06	397.14	401.06	3.92	129.82	130.75	0.93
Appalachia	-63.85	-67.63	-3.78	429.01	429.12	0.11	135.64	135.30	-0.34
Mid Atlantic	-52.73	-54.92	-2.19	469.56	468.99	-0.57	151.09	151.17	0.08
New England	-52.30	-56.04	-3.74	463.81	463.38	-0.43	151.92	151.17	-0.75

Table 4.10: Regional averages and differences and significance levels for net radiation for the control (CNTL) and half deep soil moisture (HBOT) scenarios. Units are $W \cdot m^{-2}$.

The daytime latent heat fluxes for the HBOT run (Table 4.11) show a general increase in almost all regions as compared to the CNTL run due to the higher screen height temperatures. This is similar to the result from the HALF scenario except that the flux is slightly lower. The nocturnal latent heat flux for the HBOT run is larger that for the HALF run (Table 4.5) due to increased evaporation from the more moist top soil layer. The net result for the daily mean flux is a larger flux to the atmosphere. The HBOT mean daily flux compared with the HALF scenario is larger. This is due to the increased nocturnal evaporation from the top soil layer offsetting the decrease in daytime evapotranspiration.

The sensible heat flux summary of the HBOT run (Table 4.6) is consistent with the screen height temperatures. The HBOT temperatures are higher than the

Region	Peak Daylight			Peak Nocturnal			Mean		
	CNTL	HBOT	Δ	CNTL	HBOT	Δ	CNTL	HBOT	Δ
Contiguous U.S.	-462.98	-469.50	-6.52	-20.71	-21.81	-1.10	-189.86	-192.96	-3.10
Eastern U.S.	-406.96	-416.90	-9.94	-16.95	-19.90	-2.95	-167.37	-172.22	-4.85
Western U.S.	-508.10	-512.31	-4.21	-20.94	-20.81	0.13	-207.67	-209.40	-1.73
Cascades	-284.58	-278.98	5.60	-12.93	-9.09	3.84	-122.77	-117.76	5.01
California	-514.95	-515.81	-0.86	-9.59	-9.47	0.12	-201.85	-202.00	-0.15
Intermountain Basin	-579.06	-579.63	-0.57	-11.05	-10.88	0.17	-226.88	-226.75	0.13
Southwestern Deserts	-473.30	-479.88	-6.58	-17.73	-17.76	-0.03	-183.29	-183.01	0.28
Northern Rockies	-555.33	-554.81	0.52	-16.47	-17.45	-0.98	-227.33	-228.92	-1.59
Southern Rockies	-630.18	-620.46	9.72	-18.47	-18.45	0.02	-244.77	-[illegible].94	0.83
Northern Plains	-394.04	-410.54	-16.50	-25.39	-25.81	-0.42	-171.84	-176.43	-4.59
Central Plains	-522.04	-536.84	-14.80	-29.52	-30.10	-0.58	-213.62	-219.24	-5.62
Southern Plains	-446.42	-466.77	-20.35	-18.42	-18.11	0.31	-179.88	-183.26	-3.38
Ozark Highlands	-454.24	-460.04	-5.80	-14.28	-16.96	-2.68	-180.28	-185.13	-4.85
Prairie Peninsula	-502.58	-519.24	-16.66	-12.09	-17.93	-5.84	-192.59	-200.88	-8.29
Great Lakes Forests	-406.07	-425.96	-19.89	-13.11	-16.67	-3.56	-167.78	-174.62	-6.84
Mississippi Valley	-380.56	-391.38	-10.82	-13.78	-16.44	-2.66	-154.26	-158.94	-4.68
Florida	-341.86	-343.92	-2.06	-15.95	-15.57	0.38	-139.64	-139.56	0.08
Southeast Coastal	-380.16	-385.16	-5.00	-15.26	-17.49	-2.23	-158.34	-162.32	-3.98
Appalachia	-415.63	-427.42	-11.79	-9.67	-11.88	-2.21	-168.39	-173.49	-5.10
Mid Atlantic	-397.00	-400.40	-3.40	-10.49	-12.56	-2.07	-156.21	-160.38	-4.17
New England	-403.08	-404.37	-1.29	-14.79	-16.75	-1.96	-165.36	-169.14	-3.78

Table 4.11: Regional averages and differences and significance levels for latent heat flux for the control (CNTL) and half deep soil moisture (HBOT) scenarios. Units are $W \cdot m^{-2}$.

CNTL run but lower than the HALF scenario. The sensible heat fluxes reflect this difference with fluxes to the atmosphere during the day and night that fall between the fluxes in the CNTL and HALF scenarios.

The soil heat fluxes (Table 4.13) show a smaller diurnal range and lower mean value than the CNTL run due to the lower overall soil moisture leading to a lower heat conductivity. The diurnal range in the HBOT scenario is larger than the HALF run but the means are about the same (Table 4.7). The dry subsurface soil layers act to reduce the thermal conductivity but the more moist top soil layer in the HBOT run tends to compensate somewhat for the drier layers below.

4.4.3 Summary

The results from the scenario where the top soil layer retained its original initial moisture content but the moisture content of the lower layers was reduced by 50% were very similar to the results of the HALF scenario. The moist top layer had a moderating effect leading to slightly cooler and more moist screen height conditions

Region	Peak Daylight			Peak Nocturnal			Mean		
	CNTL	HBOT	Δ	CNTL	HBOT	Δ	CNTL	HBOT	Δ
Contiguous U.S.	-58.65	-64.24	-5.59	53.87	53.07	-0.80	10.66	7.88	-2.78
Eastern U.S.	-27.48	-35.18	-7.70	48.18	45.14	-3.04	16.59	11.97	-4.62
Western U.S.	-91.88	-95.31	-3.43	67.18	66.87	-0.31	5.96	4.65	-1.31
Cascades	-151.22	-171.27	-20.05	24.16	20.38	-3.78	-50.08	-58.25	-8.17
California	-108.20	-108.76	-0.56	58.53	58.48	-0.05	-9.77	-9.93	-0.16
Intermountain Basin	-129.03	-129.86	-0.83	64.89	64.95	0.06	-11.77	-12.02	-0.25
Southwestern Deserts	-188.77	-188.77	0.00	76.18	76.05	-0.13	-22.46	-22.51	-0.05
Northern Rockies	-102.03	-106.41	-4.38	55.31	54.57	-0.74	-2.24	-3.77	-1.53
Southern Rockies	-105.00	-104.71	0.29	58.74	58.77	0.03	-2.18	-2.10	0.08
Northern Plains	-76.98	-81.83	-4.85	69.29	67.44	-1.85	12.14	10.14	-2.00
Central Plains	-22.07	-27.68	-5.61	109.55	108.74	-0.81	51.39	48.48	-2.91
Southern Plains	-27.77	-36.63	-8.86	84.07	81.91	-2.16	24.51	21.10	-3.41
Ozark Highlands	-11.74	-19.43	-7.69	59.26	55.85	-3.41	24.36	20.82	-3.54
Prairie Peninsula	-28.09	-34.25	-6.16	59.11	55.46	-3.65	26.02	22.03	-3.99
Great Lakes Forests	-72.89	-86.55	-13.66	52.41	46.55	-5.86	1.46	-6.56	-8.02
Mississippi Valley	-19.57	-23.35	-3.78	47.41	45.09	-2.32	14.41	11.29	-3.12
Florida	-43.16	-44.76	-1.60	28.59	28.14	-0.45	-4.01	-4.76	-0.75
Southeast Coastal	-4.10	-10.11	-6.01	61.38	59.31	-2.07	23.83	20.37	-3.46
Appalachia	-3.64	-9.86	-6.22	52.21	50.32	-1.89	27.13	23.06	-4.07
Mid Atlantic	-46.42	-58.04	-11.62	38.51	33.23	-5.28	3.97	-2.91	-6.88
New England	-36.76	-47.95	-11.19	63.06	57.90	-5.16	15.64	8.80	-6.84

Table 4.12: Regional averages and differences and significance levels for sensible heat flux for the control (CNTL) and half deep soil moisture (HBOT) scenarios. Units are $W \cdot m^{-2}$.

Region	Peak Nocturnal			Peak Daylight			Mean		
	CNTL	HBOT	Δ	CNTL	HBOT	Δ	CNTL	HBOT	Δ
Contiguous U.S.	-15.29	-16.58	-1.29	36.00	26.06	-9.94	7.25	2.06	-5.19
Eastern U.S.	-8.26	-13.16	-4.90	38.94	26.48	-12.46	12.99	4.59	-8.40
Western U.S.	-21.10	-19.50	1.60	33.66	25.73	-7.93	2.70	0.05	-2.65
Cascades	-16.47	-12.76	3.71	32.93	20.00	-12.93	4.04	0.92	-3.12
California	-9.48	-8.89	0.59	14.22	13.03	-1.19	0.61	0.42	-0.19
Intermountain Basin	-18.38	-16.99	1.39	23.64	21.09	-2.55	1.34	0.88	-0.46
Southwestern Deserts	-23.71	-23.60	0.11	30.85	30.76	-0.09	-1.40	-1.38	0.02
Northern Rockies	-23.94	-19.04	4.90	36.44	23.14	-13.30	4.00	0.64	-3.36
Southern Rockies	-19.98	-19.84	0.14	22.24	22.15	-0.09	-1.03	-1.02	0.01
Northern Plains	-25.00	-23.14	1.86	42.27	28.28	-13.99	5.29	-0.03	-5.32
Central Plains	-23.31	-24.66	-1.35	51.21	36.75	-14.46	8.14	1.19	-6.95
Southern Plains	-16.77	-15.21	1.56	37.88	25.15	-12.73	5.49	1.50	-3.99
Ozark Highlands	-10.17	-15.30	-5.13	38.04	26.41	-11.63	12.33	4.38	-7.95
Prairie Peninsula	-14.39	-17.46	-3.07	43.97	24.59	-19.38	13.43	2.31	-11.12
Great Lakes Forests	-11.14	-18.80	-7.66	50.08	31.11	-18.97	17.22	4.14	-13.08
Mississippi Valley	-7.82	-12.37	-4.55	32.84	21.53	-11.31	10.85	3.17	-7.68
Florida	-10.57	-10.62	-0.05	24.24	23.76	-0.48	3.83	3.53	-0.30
Southeast Coastal	-5.99	-10.63	-4.64	33.81	26.78	-7.03	11.43	5.88	-5.55
Appalachia	-6.55	-13.05	-6.50	38.94	27.75	-11.19	14.44	5.67	-8.77
Mid Atlantic	-6.81	-13.09	-6.28	45.42	31.98	-13.44	16.87	7.29	-9.58
New England	-4.27	-10.33	-6.06	46.60	31.13	-15.47	19.30	8.79	-10.51

Table 4.13: Regional averages and differences and significance levels for soil heat flux for the control (CNTL) and half deep soil moisture (HBOT) scenarios. Units are $W \cdot m^{-2}$.

with marginally stronger winds than the HALF scenario. The surface energy fluxes responded in a way consistent with a more moist and cooler surface. The latent heat flux was reduced overall but was higher during the night due to increased evaporation. The sensible heat fluxes during the day (night) were lower (higher) than in the HALF scenario, consistent with the lower (higher) screen height temperatures. The increase in the diurnal range in the soil heat flux was also consistent with the increase in the top soil layer moisture leading to greater thermal conductivity.

4.5 Half Top Soil Moisture Simulation

This scenario (HTOP) is the reverse of the HBOT scenario. In this run the initial top layer soil moisture was reduced by 50% but the remaining lower layers retained their original soil moisture content as in the CNTL run. This scenario also tests the sensitivity to the specification of top layer soil moisture and should be fairly similar to the CNTL run.

4.5.1 Screen Height Analysis

The difference in mean daily temperature is almost non-existent (Figure 4.15). The only areas on the map showing any change are located along the gradient in top soil moisture content where the original content was around 30% (Figure 3.7). There is no significance to these differences as illustrated by Figure 4.16. The mixing ratio differences are small and widely scattered. The only coherent area of change is in eastern Colorado (Figure 4.15). This area shows low significance, greater than 20% (Figure 4.16).

The wind speed differences are as expected, they are all within $2cm \cdot s^{-1}$ of the CNTL scenario (Figure 4.17). The area of low significance along the Northwest Pacific Coast is due to the very low variance in the wind speed in that area (Figure 4.18). The changes in daily convective precipitation rate are small (less than $0.1mm \cdot day^{-1}$) and tend to be concentrated in the areas of greatest horizontal

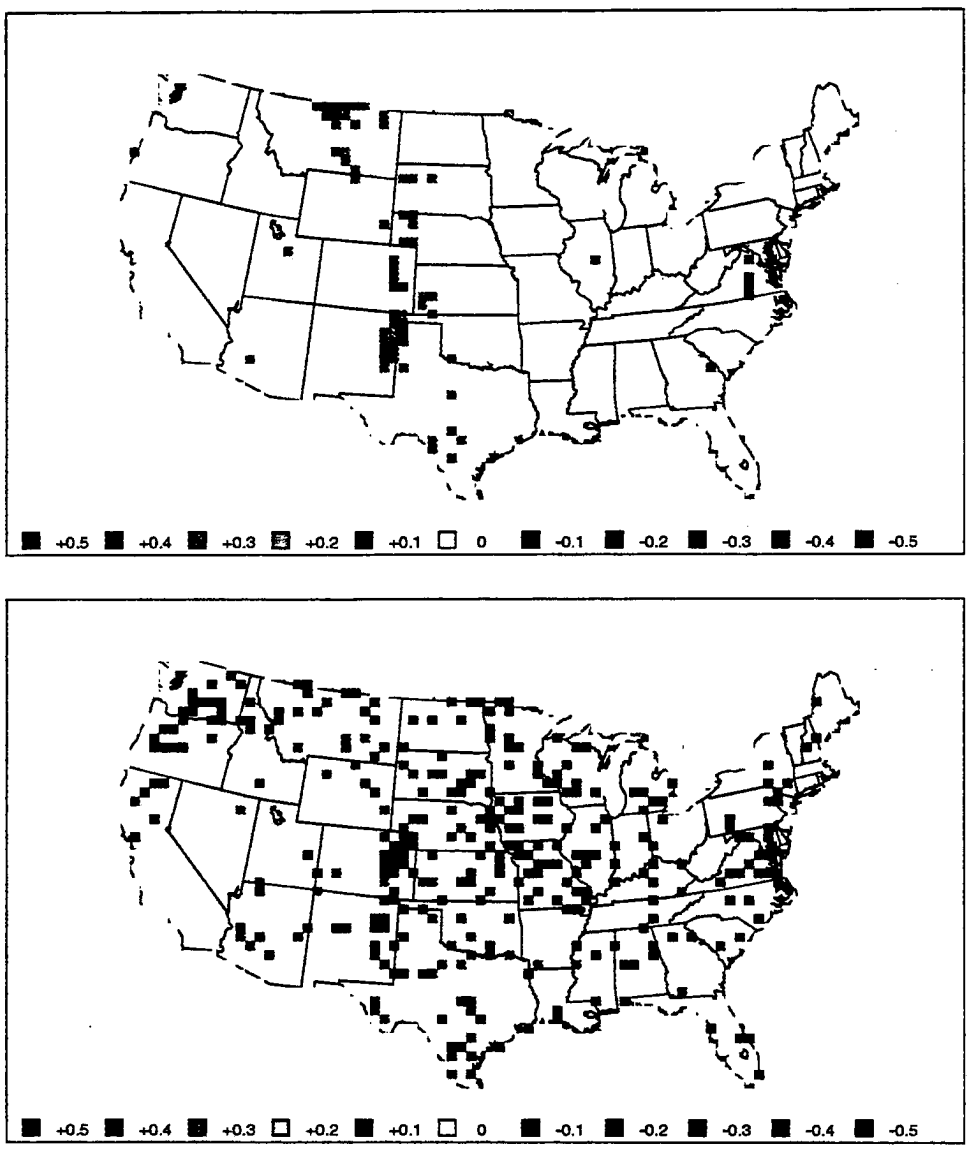

Figure 4.15: The departure of mean daily temperature for the HTOP scenario from the CNTL scenario in degrees Celsius (top panel). The departure of mean daily mixing ratio for the HTOP scenario from the CNTL scenario in $g \cdot kg^{-1}$ (bottom panel).

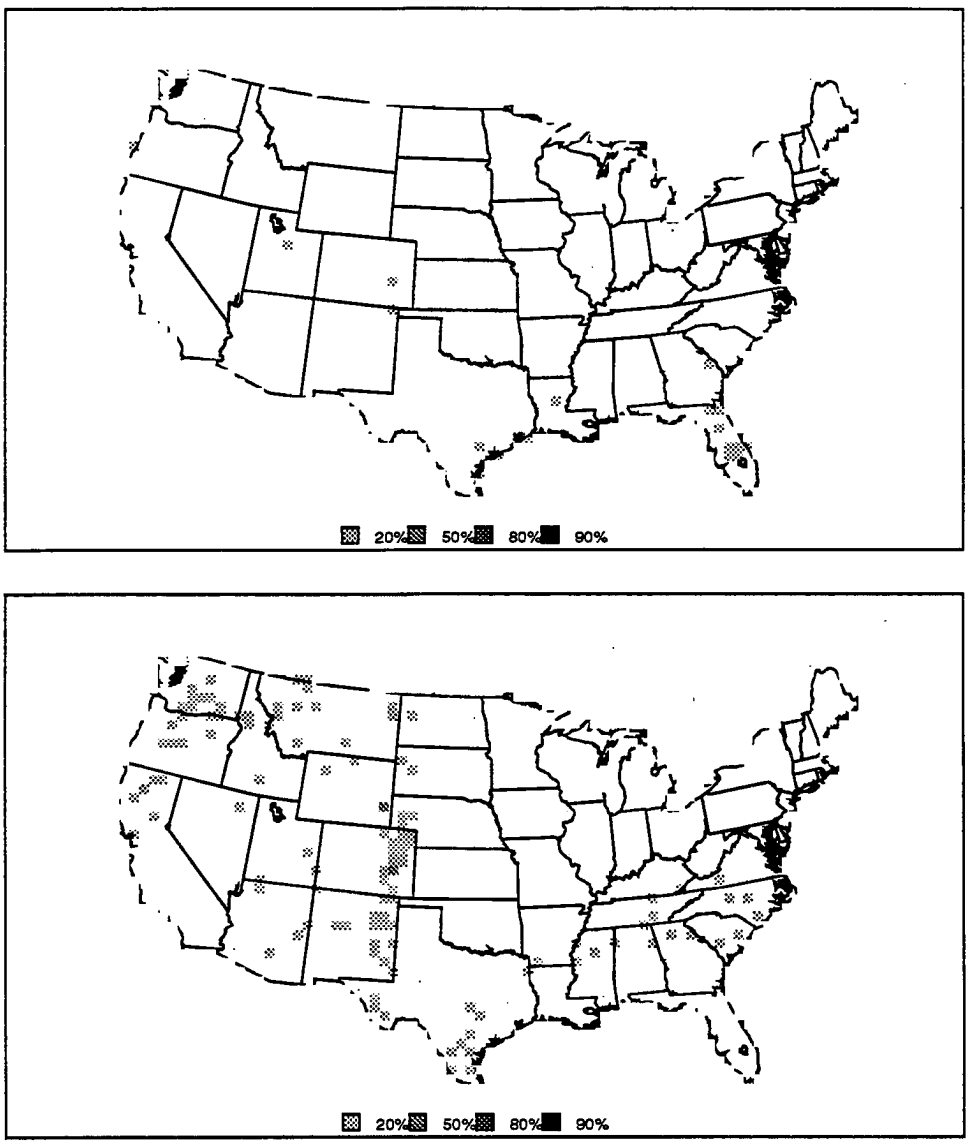

Figure 4.16: Significance test score levels for the departure of mean daily temperature (top panel) and the departure of mean daily mixing ratio (bottom panel).

gradient in top layer soil moisture (Figure 4.17). There is no significance to the precipitation rate differences outside of Florida (Figure 4.18).

The screen height summary tables 4.14 and 4.15 show that there is no regional change in either precipitation rate or wind speed. The screen height temperatures are slightly warmer due to the drier soil, but the differences are not significant. The mixing ratio shows a slight decrease due to reduced evaporation from the soil and increased mixing in the boundary layer due to the slightly higher temperatures.

Region	Temperature (K)				Precipitation ($mm \cdot day^{-1}$)			
	CNTL	HTOP	Δ	sig	CNTL	HTOP	Δ	sig
Contiguous U.S.	295.61	295.63	0.02		1.91	1.91	0.00	
Eastern U.S.	296.37	296.39	0.02		1.65	1.65	0.00	
Western U.S.	295.00	295.02	0.02		2.11	2.11	0.00	
Cascades	286.79	286.96	0.17		0.05	0.05	0.00	
California	290.76	290.80	0.04		0.17	0.17	0.00	
Intermountain Basin	293.18	293.19	0.01		0.49	0.49	0.00	
Southwestern Deserts	299.55	299.60	0.05		2.71	2.71	0.00	
Northern Rockies	292.67	292.69	0.02		1.02	1.02	0.00	
Southern Rockies	295.12	295.13	0.01		2.32	2.32	0.00	
Northern Plains	296.12	296.21	0.09		2.34	2.34	0.00	
Central Plains	296.15	296.18	0.03		3.83	3.83	0.00	
Southern Plains	298.48	298.50	0.02		2.49	2.48	-0.01	
Ozark Highlands	298.05	298.08	0.03		1.70	1.70	0.00	
Prairie Peninsula	296.74	296.77	0.03		1.73	1.73	0.00	
Great Lakes Forests	293.14	293.43	0.29		0.93	0.93	0.00	
Mississippi Valley	298.59	298.65	0.06		1.85	1.85	0.00	
Florida	298.52	298.52	0.00		1.72	1.74	0.02	
Southeast Coastal	298.10	298.10	0.00		2.57	2.58	0.01	
Appalachia	296.37	296.38	0.01		2.29	2.30	0.01	
Mid Atlantic	293.80	293.94	0.14		1.42	1.42	0.00	
New England	292.17	292.16	-0.01		0.49	0.49	0.00	

Table 4.14: Regional averages, differences and significance levels for mean daily temperature and daily convective precipitation rate for the half top soil moisture (HTOP) and control scenario (CNTL). Units are degree Kelvin for the temperatures and $mm \cdot day^{-1}$ for precipitation.

4.5.2 Surface Energy Budget Analysis

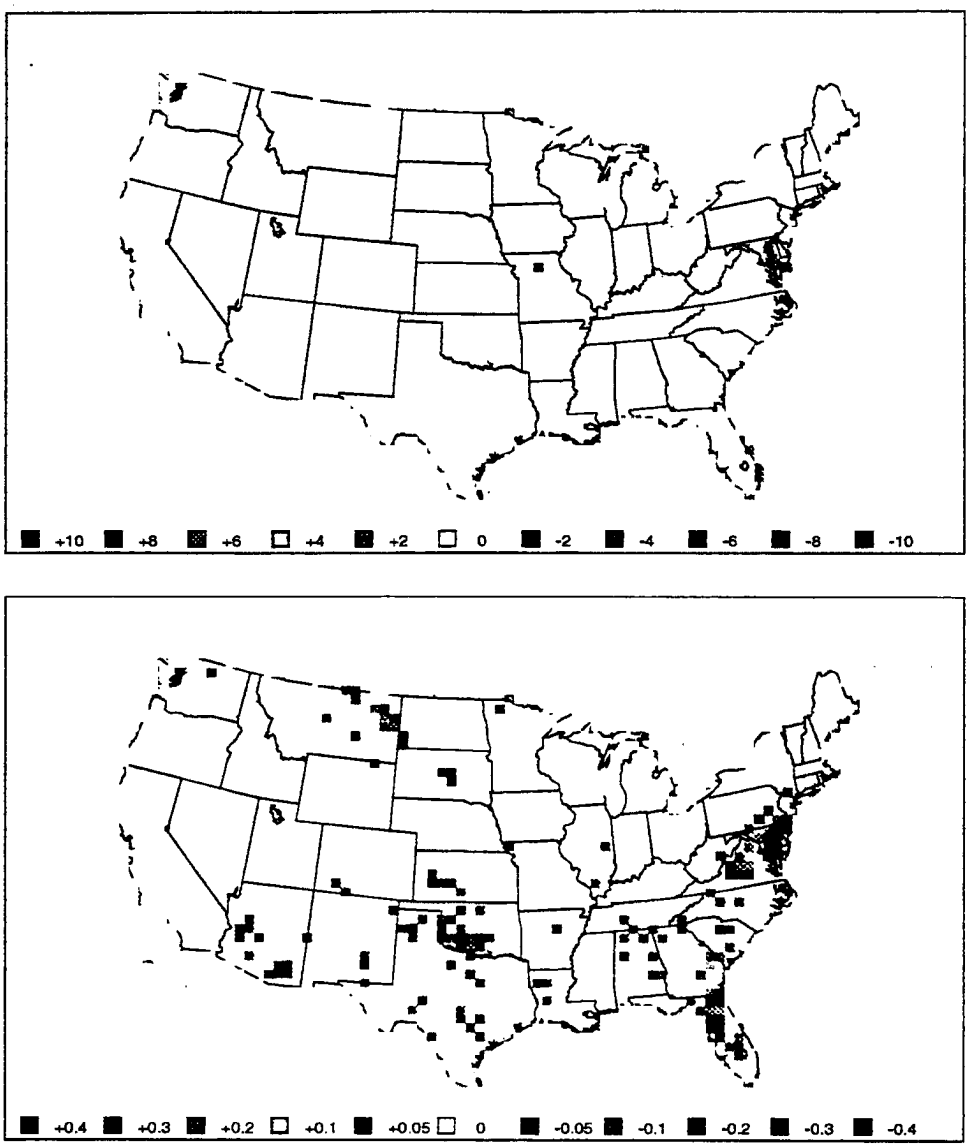

Figure 4.17: The departure of mean wind speed for the HTOP scenario from the CNTL scenario in $cm \cdot s^{-1}$ (top panel). The departure of mean daily convective precipitation rate for the HTOP scenario from the CNTL scenario in $mm \cdot day^{-1}$ (bottom panel).

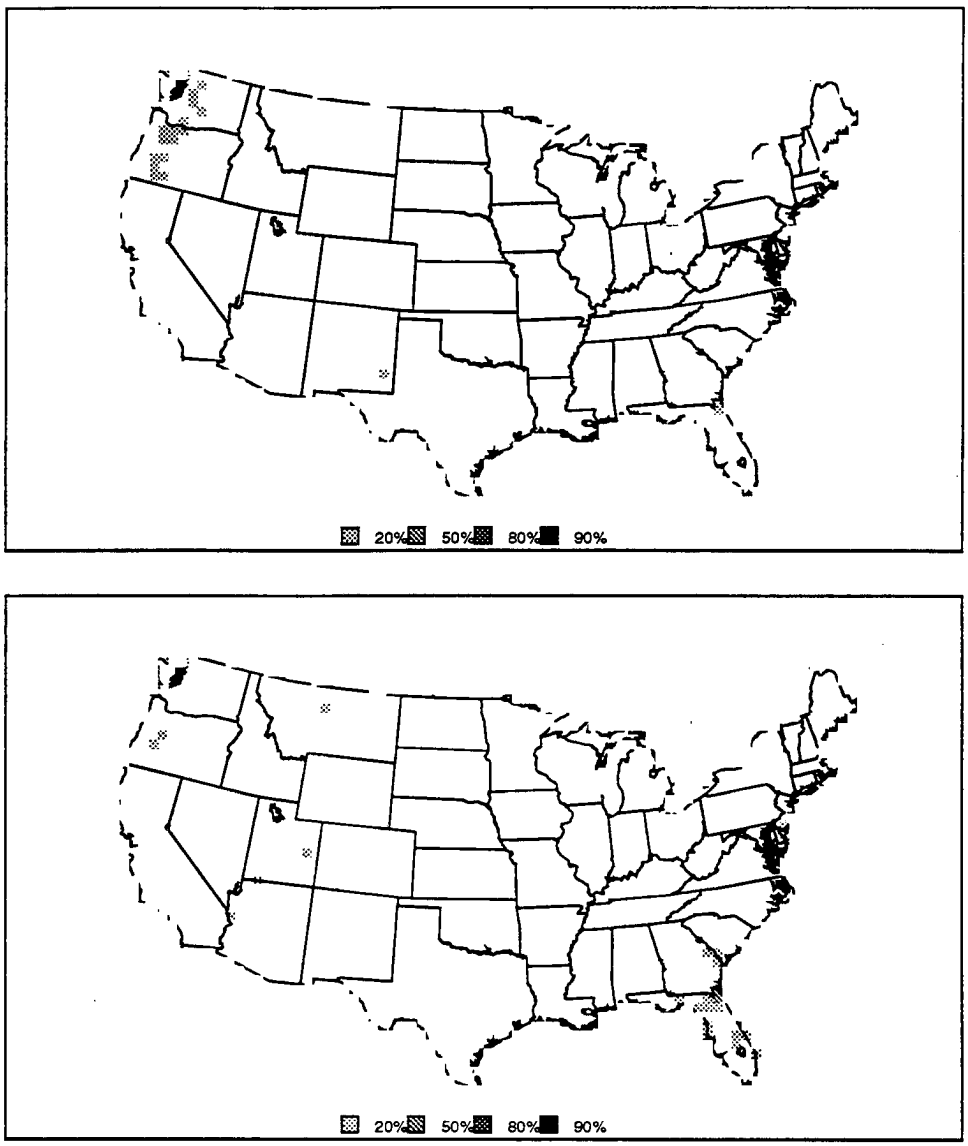

Figure 4.18: The significance levels of differences between mean wind speed for the HTOP scenario from the CNTL scenario top panel) and mean daily convective precipitation rate (bottom panel).

Region	Mixing Ratio ($g \cdot kg^{-1}$)				Wind Speed ($m \cdot s^{-1}$)			
	CNTL	HTOP	Δ	sig	CNTL	HTOP	Δ	sig
Contiguous U.S.	15.46	15.45	-0.01		1.94	1.94	0.00	
Eastern U.S.	17.47	17.46	-0.01		1.57	1.57	0.00	
Western U.S.	13.87	13.86	-0.01		2.23	2.23	0.00	
Cascades	9.31	9.28	-0.03		1.09	1.08	-0.01	
California	12.07	12.07	-0.00		1.72	1.72	0.00	
Intermountain Basin	10.42	10.41	-0.01		1.72	1.72	0.00	
Southwestern Deserts	13.36	13.36	0.00		2.51	2.51	0.00	
Northern Rockies	11.69	11.68	-0.01		1.40	1.40	0.00	
Southern Rockies	13.25	13.25	-0.00		1.55	1.55	0.00	
Northern Plains	15.60	15.58	-0.02		3.05	3.05	0.00	
Central Plains	17.62	17.61	-0.01		2.84	2.84	0.00	
Southern Plains	19.45	19.44	-0.01		2.19	2.19	0.00	
Ozark Highlands	19.35	19.33	-0.02		1.04	1.03	-0.01	
Prairie Peninsula	17.35	17.32	-0.03		2.26	2.26	0.00	
Great Lakes Forests	14.36	14.34	-0.02		1.69	1.69	0.00	
Mississippi Valley	19.59	19.58	-0.01		1.67	1.67	0.00	
Florida	19.48	19.47	-0.01		1.51	1.52	0.01	
Southeast Coastal	19.38	19.37	-0.01		1.40	1.40	0.00	
Appalachia	17.97	17.96	-0.01		0.99	0.99	0.00	
Mid Atlantic	15.27	15.26	-0.01		1.19	1.19	0.00	
New England	13.46	13.45	-0.01		1.28	1.28	0.00	

Table 4.15: Regional averages, differences and significance levels for mean mixing ratio and wind speed for the half top soil moisture (HTOP) and control scenario (CNTL). Units are $g \cdot kg^{-1}$for mixing ratio and $m \cdot s^{-1}$ for wind speed.

Region	Peak Nocturnal			Peak Daylight			Mean		
	CNTL	HTOP	Δ	CNTL	HTOP	Δ	CNTL	HTOP	Δ
Contiguous U.S.	-74.67	-78.82	-4.15	539.90	540.74	0.84	160.69	159.67	-1.02
Eastern U.S.	-56.40	-56.45	-0.05	455.80	456.33	0.53	145.83	145.21	-0.62
Western U.S.	-92.08	-97.41	-5.33	612.33	612.11	-0.22	172.47	171.53	-0.94
Cascades	-16.13	-30.35	-14.22	453.69	456.70	3.01	167.10	166.25	-0.85
California	-53.94	-54.50	-0.56	621.15	622.27	1.12	192.86	192.79	-0.07
Intermountain Basin	-93.30	-93.54	-0.24	712.35	714.39	2.04	205.73	205.69	-0.04
Southwestern Deserts	-113.60	-130.03	-16.43	665.00	663.07	-1.93	170.21	168.64	-1.57
Northern Rockies	-99.28	-99.55	-0.27	648.71	645.82	-2.89	189.17	188.65	-0.52
Southern Rockies	-100.74	-100.69	0.05	703.04	701.12	-1.92	197.21	197.10	-0.11
Northern Plains	-97.62	-103.61	-5.99	508.33	510.52	2.19	142.03	141.77	-0.26
Central Plains	-107.89	-108.33	-0.44	565.23	566.88	1.65	144.91	143.88	-1.03
Southern Plains	-64.27	-64.93	-0.66	487.15	489.13	1.98	141.48	141.63	0.15
Ozark Highlands	-68.39	-68.84	-0.45	462.12	465.08	2.96	145.25	145.09	-0.16
Prairie Peninsula	-84.55	-84.76	-0.21	546.77	548.93	2.16	158.91	159.47	0.56
Great Lakes Forests	-61.02	-67.54	-6.52	511.55	516.62	5.07	165.28	165.12	-0.16
Mississippi Valley	-54.25	-54.78	-0.53	418.13	419.81	1.68	134.62	134.25	-0.37
Florida	-22.45	-21.81	0.64	398.35	402.16	3.81	133.92	134.72	0.80
Southeast Coastal	-47.40	-47.09	0.31	397.14	400.31	3.17	129.82	130.00	0.18
Appalachia	-63.85	-63.88	-0.03	429.01	427.27	-1.74	135.64	135.42	-0.22
Mid Atlantic	-52.73	-52.37	0.36	469.56	468.58	-0.98	151.09	151.04	-0.05
New England	-52.30	-52.35	-0.05	463.81	459.85	-3.96	151.92	151.36	-0.56

Table 4.16: Regional averages and differences and significance levels for net radiation for the control (CNTL) and half top soil moisture (HTOP) scenarios. Units are $W \cdot m^{-2}$.

The net radiation (Figure 4.16) shows a slight increase in the upward flux at night due to the warmer surface temperatures and a slight increase in the daytime flux due to increased solar shortwave.

The latent heat flux (Figure 4.17) increased during the day due to the higher temperatures and increased stomatal conductance. At night the reduced surface soil moisture decreases the evaporation from the top soil layer.

The sensible heat flux (Figure 4.18) shows that the mean surface temperature increased while the diurnal range remained the same. Daytime flux increased and nighttime flux decreased due to higher temperatures.

The soil heat flux (Figure 4.19) shows the effect of reduced thermal conductivity due to reduced soil moisture content. The soil heat flux was generally reduced throughout the day in all regions.

4.5.3 Summary

The effect of reducing the soil moisture content in the top soil layer was very minor as compared with the control scenario. Precipitation rate and wind speed

Region	Peak Daylight			Peak Nocturnal			Mean		
	CNTL	HTOP	Δ	CNTL	HTOP	Δ	CNTL	HTOP	Δ
Contiguous U.S.	-462.98	-463.20	-0.22	-20.71	-20.18	0.53	-189.86	-189.38	0.48
Eastern U.S.	-406.96	-409.15	-2.19	-16.95	-16.52	0.43	-167.37	-167.50	-0.13
Western U.S.	-508.10	-507.16	0.94	-20.94	-20.25	0.69	-207.67	-206.71	0.96
Cascades	-284.58	-278.07	6.51	-12.93	-9.62	3.31	-122.77	-119.84	2.93
California	-514.95	-515.15	-0.20	-9.59	-8.99	0.60	-201.85	-201.34	0.51
Intermountain Basin	-579.06	-581.64	-2.58	-11.05	-10.39	0.66	-226.88	-226.31	0.57
Southwestern Deserts	-473.30	-469.01	4.29	-17.73	-17.64	0.09	-183.29	-182.39	0.90
Northern Rockies	-555.33	-548.55	6.78	-16.47	-15.74	0.73	-227.33	-226.31	1.02
Southern Rockies	-630.18	-619.37	10.81	-18.47	-18.41	0.06	-244.77	-244.34	0.43
Northern Plains	-394.04	-396.18	-2.14	-25.39	-24.54	0.85	-171.84	-170.68	1.16
Central Plains	-522.04	-523.26	-1.22	-29.52	-28.94	0.58	-213.62	-212.66	0.96
Southern Plains	-446.42	-448.32	-1.90	-18.42	-18.12	0.30	-179.88	-179.70	0.18
Ozark Highlands	-454.24	-464.24	-10.00	-14.28	-14.00	0.28	-180.28	-179.96	0.32
Prairie Peninsula	-502.58	-505.03	-2.45	-12.09	-11.07	1.02	-192.59	-192.89	-0.30
Great Lakes Forests	-406.07	-412.09	-6.02	-13.11	-12.54	0.57	-167.78	-168.15	-0.37
Mississippi Valley	-380.56	-384.51	-3.95	-13.78	-13.41	0.37	-154.26	-154.58	-0.32
Florida	-341.86	-341.32	0.54	-15.95	-15.89	0.06	-139.64	-139.61	0.03
Southeast Coastal	-380.16	-383.35	-3.19	-15.26	-15.18	0.08	-158.34	-159.10	-0.76
Appalachia	-415.63	-418.37	-2.74	-9.67	-9.51	0.16	-168.39	-167.97	0.42
Mid Atlantic	-397.00	-400.51	-3.51	-10.49	-10.28	0.21	-156.21	-156.71	-0.50
New England	-403.08	-395.30	7.78	-14.79	-14.71	0.08	-165.36	-164.57	0.79

Table 4.17: Regional averages and differences and significance levels for latent heat flux for the control (CNTL) and half top soil moisture (HTOP) scenarios. Units are $W \cdot m^{-2}$.

Region	Peak Daylight			Peak Nocturnal			Mean		
	CNTL	HTOP	Δ	CNTL	HTOP	Δ	CNTL	HTOP	Δ
Contiguous U.S.	-58.65	-59.41	-0.76	53.87	53.58	-0.29	10.66	10.19	-0.47
Eastern U.S.	-27.48	-27.88	-0.40	48.18	48.03	-0.15	16.59	16.35	-0.24
Western U.S.	-91.88	-92.95	-1.07	67.18	66.68	-0.50	5.96	5.31	-0.65
Cascades	-151.22	-156.29	-5.07	24.16	21.09	-3.07	-50.08	-53.02	-2.94
California	-108.20	-108.84	-0.64	58.53	57.91	-0.62	-9.77	-10.27	-0.50
Intermountain Basin	-129.03	-129.43	-0.40	64.89	64.54	-0.35	-11.77	-12.16	-0.39
Southwestern Deserts	-188.77	-188.96	-0.19	76.18	76.04	-0.14	-22.46	-22.56	-0.10
Northern Rockies	-102.03	-102.93	-0.90	55.31	54.99	-0.32	-2.24	-2.74	-0.50
Southern Rockies	-105.00	-104.94	0.06	58.74	58.74	0.00	-2.18	-2.23	-0.05
Northern Plains	-76.98	-79.36	-2.38	69.29	67.87	-1.42	12.14	10.90	-1.24
Central Plains	-22.07	-22.83	-0.76	109.55	108.69	-0.86	51.39	50.66	-0.73
Southern Plains	-27.77	-29.02	-1.25	84.07	83.79	-0.28	24.51	23.91	-0.60
Ozark Highlands	-11.74	-12.57	-0.83	59.26	58.65	-0.61	24.36	23.89	-0.47
Prairie Peninsula	-28.09	-29.14	-1.05	59.11	58.55	-0.56	26.02	25.40	-0.62
Great Lakes Forests	-72.89	-73.83	-0.94	52.41	52.01	-0.40	1.46	0.97	-0.49
Mississippi Valley	-19.57	-20.15	-0.58	47.41	47.46	0.05	14.41	14.16	-0.25
Florida	-43.16	-44.14	-0.98	28.59	28.51	-0.08	-4.01	-4.43	-0.42
Southeast Coastal	-4.10	-3.67	0.43	61.38	62.48	1.10	23.83	23.84	0.01
Appalachia	-3.64	-4.60	-0.96	52.21	52.57	0.36	27.13	27.04	-0.09
Mid Atlantic	-46.42	-46.19	0.23	38.51	38.81	0.30	3.97	3.79	-0.18
New England	-36.76	-36.71	0.05	63.06	63.14	0.08	15.64	15.75	0.11

Table 4.18: Regional averages and differences and significance levels for sensible heat flux for the control (CNTL) and half top soil moisture (HTOP) scenarios. Units are $W \cdot m^{-2}$.

Region	Peak Nocturnal			Peak Daylight			Mean		
	CNTL	HTOP	Δ	CNTL	HTOP	Δ	CNTL	HTOP	Δ
Contiguous U.S.	-15.29	-15.15	0.14	36.00	35.77	-0.23	7.25	7.23	-0.02
Eastern U.S.	-8.26	-8.16	0.10	38.94	38.70	-0.24	12.99	12.92	-0.07
Western U.S.	-21.10	-20.95	0.15	33.66	33.45	-0.21	2.70	2.71	0.01
Cascades	-16.47	-14.76	1.71	32.93	31.33	-1.60	4.04	4.14	0.10
California	-9.48	-9.34	0.14	14.22	13.92	-0.30	0.61	0.62	0.01
Intermountain Basin	-18.38	-18.25	0.13	23.64	23.48	-0.16	1.34	1.36	0.02
Southwestern Deserts	-23.71	-23.67	0.04	30.85	30.79	-0.06	-1.40	-1.40	0.00
Northern Rockies	-23.94	-23.67	0.27	36.44	36.29	-0.15	4.00	4.04	0.04
Southern Rockies	-19.98	-19.99	-0.01	22.24	22.27	0.03	-1.03	-1.04	-0.01
Northern Plains	-25.00	-24.76	0.24	42.27	41.89	-0.38	5.29	5.29	0.00
Central Plains	-23.31	-23.29	0.02	51.21	51.02	-0.19	8.14	8.13	-0.01
Southern Plains	-16.77	-16.73	0.04	37.88	37.95	0.07	5.49	5.52	0.03
Ozark Highlands	-10.17	-10.09	0.08	38.04	37.76	-0.28	12.33	12.20	-0.13
Prairie Peninsula	-14.39	-13.81	0.58	43.97	43.30	-0.67	13.43	13.34	-0.09
Great Lakes Forests	-11.14	-11.16	-0.02	50.08	49.89	-0.19	17.22	17.12	-0.10
Mississippi Valley	-7.82	-7.69	0.13	32.84	32.44	-0.40	10.85	10.77	-0.08
Florida	-10.57	-10.65	-0.08	24.24	24.57	0.33	3.83	3.83	0.00
Southeast Coastal	-5.99	-5.95	0.04	33.81	33.73	-0.08	11.43	11.39	-0.04
Appalachia	-6.55	-6.53	0.02	38.94	38.89	-0.05	14.44	14.36	-0.08
Mid Atlantic	-6.81	-6.81	0.00	45.42	45.26	-0.16	16.87	16.80	-0.07
New England	-4.27	-4.37	-0.10	46.60	46.29	-0.31	19.30	19.21	-0.09

Table 4.19: Regional averages and differences and significance levels for soil heat flux for the control (CNTL) and half top soil moisture (HTOP) scenarios. Units are $W \cdot m^{-2}$.

showed no difference. The temperature and mixing ratio differences were small with a slight increase in temperature and decrease in mixing ratio. The sign of the differences is consistent with the sign of the differences for the HALF scenario.

4.6 Homogeneous Landscape Simulation

The homogeneous landscape simulation (GRAS) is a dramatic investigation into the combined effects of roughness length, albedo, and leaf area index. The scenario is set up the same as the CNTL run but with a homogeneous short grass prairie (BATS category 2) over the whole domain. Short grass has the highest albedo, smallest roughness length, and smallest leaf area index of the vegetation types in the BATS categories (Table 3.1) not counting desert, ice, and water.

4.6.1 Screen Height Analysis

The largest changes in mean screen height temperature are west of the Mississippi River (Figure 4.19). The changes in the eastern half of the country are

generally a cooling by less than half a degree. In the west there is an arc of warming extending north from central California to northern Idaho and western Montana, with a maximum in excess of 2°C. There is also a smaller region of positive temperature anomaly in southern Texas of about the magnitude. Both of these areas of warming occur along boundaries between different vegetation types in the current landuse. There are three main and two lesser areas of cooling. The largest, both in area and magnitude, is associated with the Rocky Mountain region south of Montana. The maximum cooling was in excess of 6°C with much of the area cooling by more than 4°C. The other main areas of cooling, as defined by a difference of more than 2°C, were in western Oklahoma and extreme northern Minnesota. The minor regions of cooling, between 1-2°C, were in a band from Texas to Minnesota, and scattered along the eastern seaboard.

Mixing ratio overall saw a very large decrease due to the vegetation change (Figure 4.19). There was a small region of increase in mixing ratio by up to $1g \cdot kg^{-1}$ in the desert region of southern Nevada, California, and Arizona. The sign of the mixing ratio change followed the sign of the change in LAI. This is intuitive since the latent heat flux scales with LAI. The regions of nearly zero change in mixing ratio in Texas and Montana were areas which were originally short grass in the CNTL scenario. The eastern United States saw a small decrease of mixing ratio, typically less than $1g \cdot kg^{-1}$. The higher elevations in the west had the largest decreases in mixing ratio, in excess of $4.5g \cdot kg^{-1}$.

The screen height wind speeds showed an increase in all regions except for the Arizona–California border where replacement of the desert by short grass resulted in a decrease in the wind speed by up to $0.5m \cdot s^{-1}$ (Figure 4.21). The largest increase in wind speeds (up to $3m \cdot s^{-1}$) occurred along the Pacific Coast where originally there were evergreen needle leaf trees (1.0m roughness length) to slow down the strong onshore winds of the Pacific. The other areas of large increase in wind speed

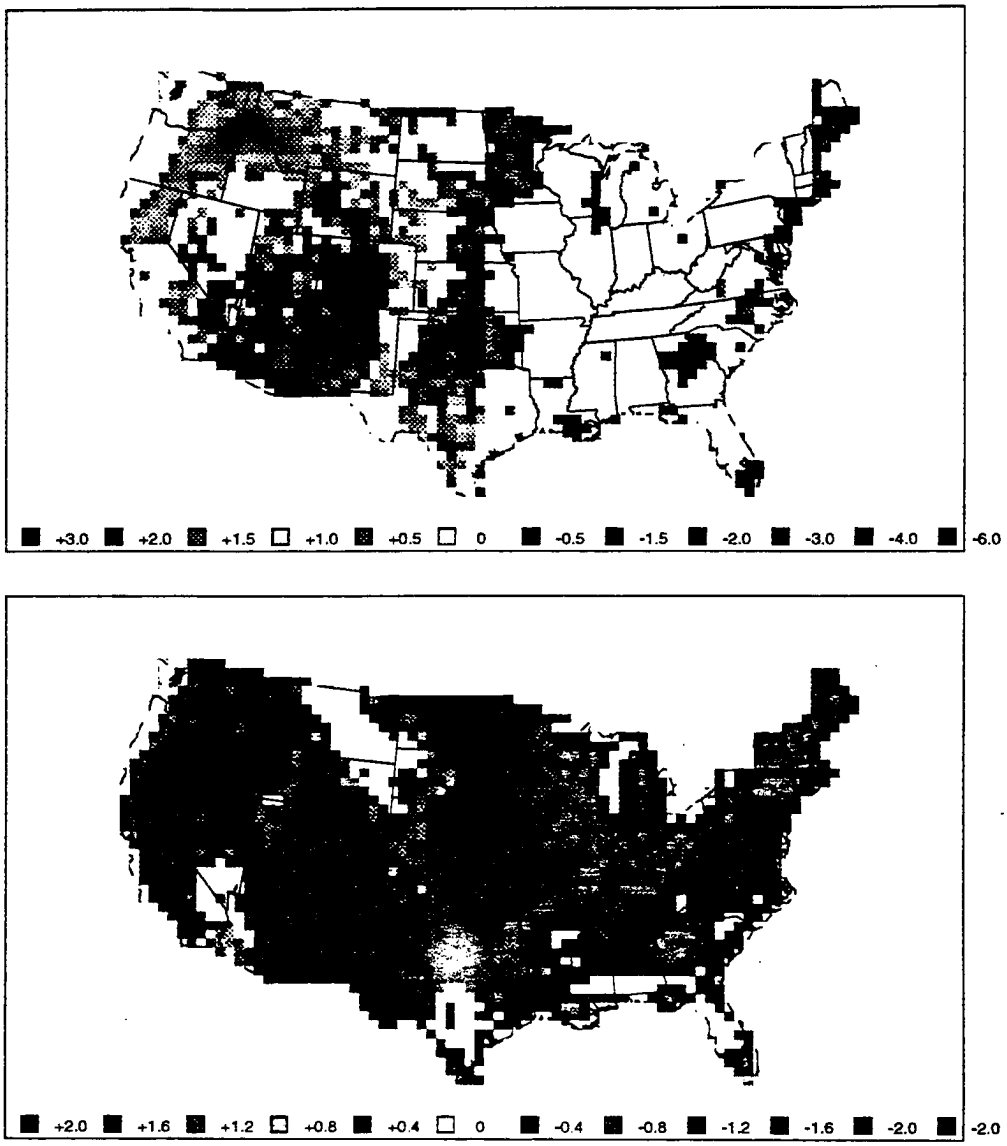

Figure 4.19: The departure of mean daily temperature for the GRAS scenario from the CNTL scenario in degrees Celsius (top panel). The departure of mean daily mixing ratio for the GRAS scenario from the CNTL scenario in $g \cdot kg^{-1}$ (bottom panel).

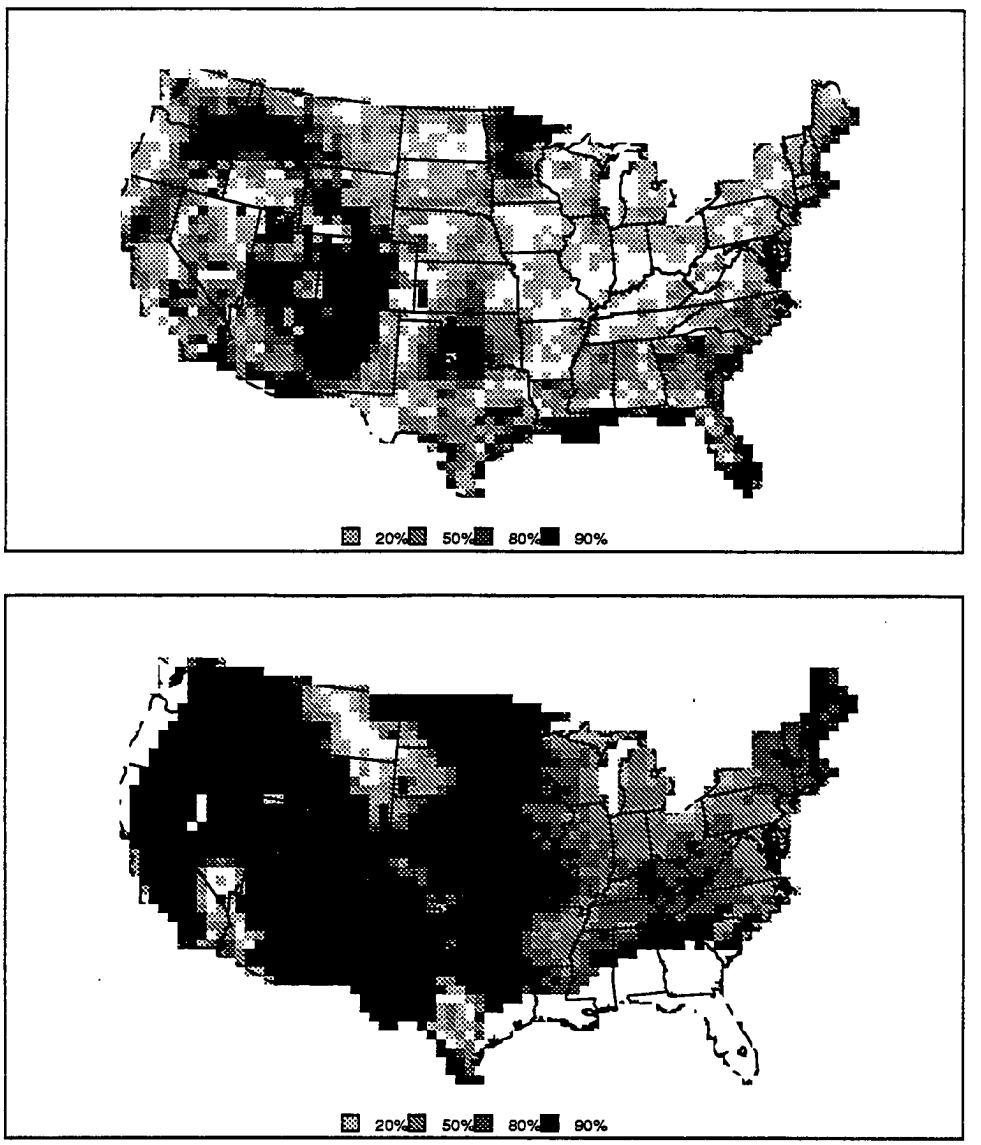

Figure 4.20: Significance test score levels for the departure of mean daily temperature (top panel) and the departure of mean daily mixing ratio (bottom panel).

(around $1.5m \cdot s^{-1}$) occurred in areas which originally had trees. Most of the area of the United States showed significance in the wind speed difference above the 90% threshold (Figure 4.22). Convective precipitation rate tended to decrease in the west and was mixed in the east (Figure 4.21). The areas of largest decrease (more than $1mm \cdot day^{-1}$) were in Florida, Texas, and scattered throughout the region from the Rocky Mountains on west. The areas of largest increase in precipitation rate (more than $0.8mm \cdot day^{-1}$) were located in a line from eastern Texas, through Mississippi, Alabama, Georgia, and north along the ridge of the Appalachian Mountains. The areas showing the greatest significance to the daily precipitation rate differences were located west of the Continental Divide around Oregon Idaho and Nevada, in Florida, and small areas scattered across the South (Figure 4.22).

Table 4.20 shows the temperature summary for the GRAS scenario. Most of the regions of the United States exhibited a decrease in mean daily temperature. The typical decrease was in the range of 0.2-0.3°C with many exceeding the 90% significance threshold. Several regions in the west had an increase in mean temperature, indicating the possibility of increased sensible heat flux offsetting the reduced net radiation due to lower albedo. The magnitude of the temperature increases was generally small with none exceeding 0.38°C. The precipitation rate (Table 4.20) , overall, showed large decreases between 10-20% of the CNTL value; almost half of these were above the 90% significance threshold. The few regions that showed an increase in precipitation were in the east with small magnitudes (less than $0.2mm \cdot day^{-1}$) and low significance test scores.

The mixing ratio (Table 4.21) dramatically showed the effect of decreasing LAI with a decrease in all regions of the model domain. The decrease in mixing ratio ranged from 0.4-3.5$g \cdot kg^{-1}$ and all regions showed significance in excess of 90%. The magnitude of the decrease was largest in the Northern and Southern Rockies subregions of the western U.S. Most of the mixing ratio differences were 5-10%

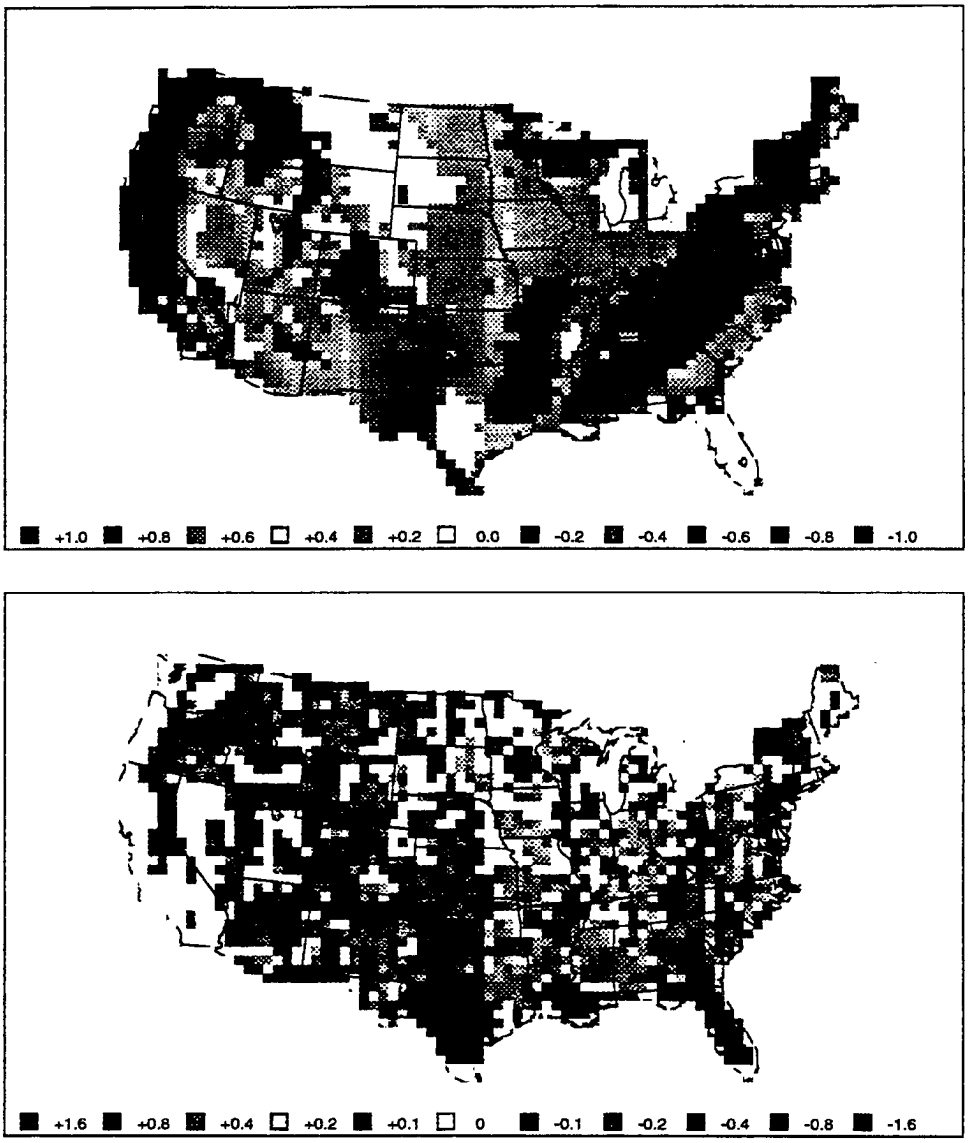

Figure 4.21: The departure of mean wind speed for the GRAS scenario from the CNTL scenario in $cm \cdot s^{-1}$ (top panel). The departure of mean daily convective precipitation rate for the GRAS scenario from the CNTL scenario in $mm \cdot day^{-1}$ (bottom panel).

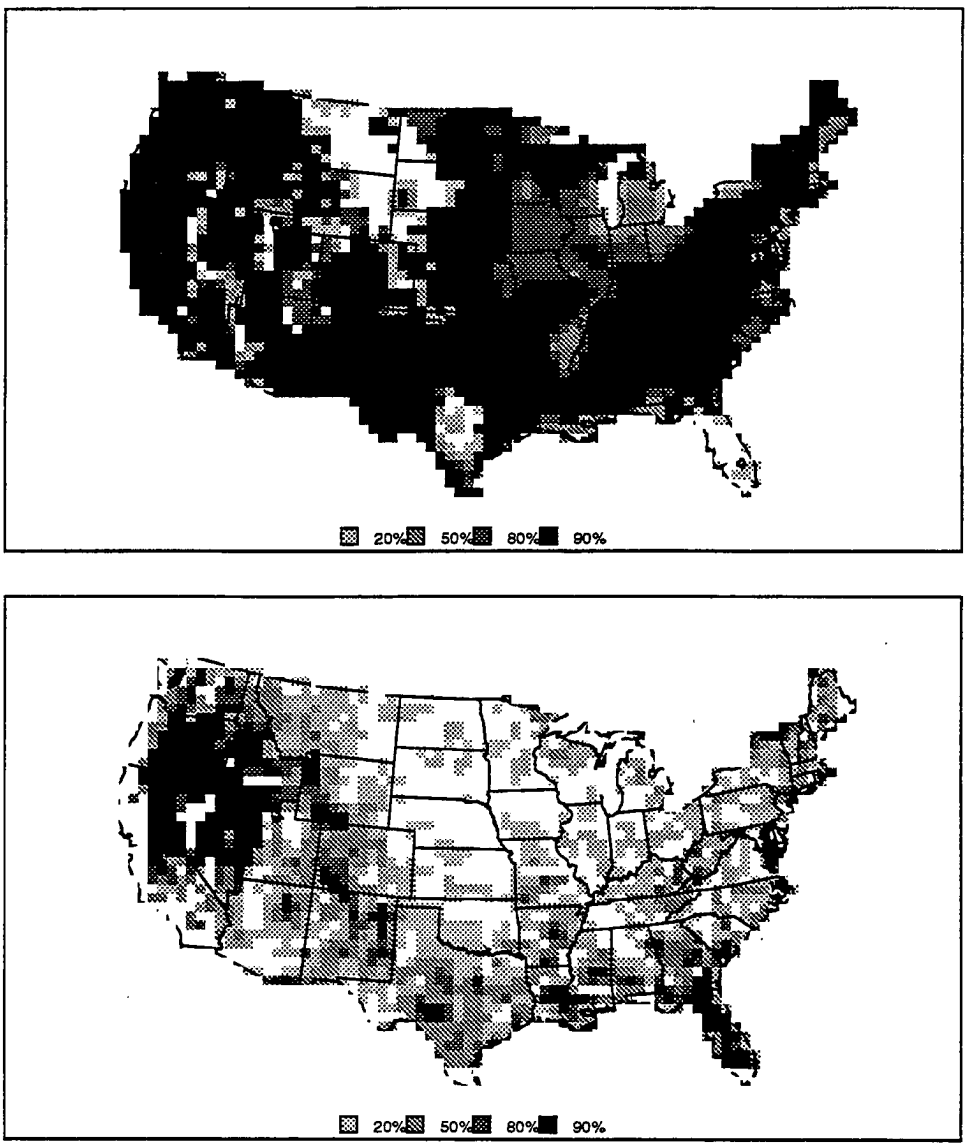

Figure 4.22: The significance levels of differences between mean wind speed for the GRAS scenario from the CNTL scenario top panel) and mean daily convective precipitation rate (bottom panel).

Region	Temperature (K)				Precipitation ($mm \cdot day^{-1}$)			
	CNTL	GRAS	Δ	sig	CNTL	GRAS	Δ	sig
Contiguous U.S.	295.61	295.26	-0.35	90.00	1.91	1.73	-0.18	90.00
Eastern U.S.	296.37	296.11	-0.26	90.00	1.65	0.93	-0.72	90.00
Western U.S.	295.00	294.58	-0.42	90.00	2.11	1.60	-0.51	90.00
Cascades	286.79	286.85	0.06		0.05	0.01	-0.04	80.00
California	290.76	291.07	0.31	20.00	0.17	0.01	-0.16	90.00
Intermountain Basin	293.18	293.56	0.38	50.00	0.49	0.15	-0.34	90.00
Southwestern Deserts	299.55	298.86	-0.69	50.00	2.71	2.47	-0.24	20.00
Northern Rockies	292.67	293.05	0.38	80.00	1.02	0.70	-0.32	90.00
Southern Rockies	295.12	292.30	-2.82	90.00	2.32	1.92	-0.40	90.00
Northern Plains	296.12	296.20	0.08		2.34	2.24	-0.10	50.00
Central Plains	296.15	295.52	-0.63	90.00	3.83	3.47	-0.36	90.00
Southern Plains	298.48	298.80	0.32	90.00	2.49	2.20	-0.29	50.00
Ozark Highlands	298.05	297.97	-0.08	20.00	1.70	1.78	0.08	20.00
Prairie Peninsula	296.74	296.52	-0.22	50.00	1.73	1.77	0.04	20.00
Great Lakes Forests	293.14	292.71	-0.43	20.00	0.93	0.83	-0.10	50.00
Mississippi Valley	298.59	298.40	-0.19	20.00	1.85	1.61	-0.24	90.00
Florida	298.52	298.28	-0.24	50.00	1.72	0.99	-0.73	90.00
Southeast Coastal	298.10	297.76	-0.34	90.00	2.57	2.75	0.18	50.00
Appalachia	296.37	296.32	-0.05		2.29	2.39	0.10	20.00
Mid Atlantic	293.80	293.59	-0.21		1.42	1.21	-0.21	50.00
New England	292.17	291.74	-0.43	50.00	0.49	0.39	-0.10	80.00

Table 4.20: Regional averages, differences and significance levels for mean daily temperature and daily convective precipitation rate for the homogeneous short grass (GRAS) and control scenario (CNTL). Units are degree Kelvin for the temperatures and $mm \cdot day^{-1}$ for precipitation.

of the CNTL mean mixing ratio. The wind speed differences show the effect of roughness length change. Wind speed in all regions increased due to the decrease in roughness length and all differences were above the 90% significance level. The smallest increase occured in the Northern Plains ($0.27m \cdot s^{-1}$) which had a large area of short grass prairie in the CNTL run. The largest increases in wind speed (in excess of $1m \cdot s^{-1}$) occurred in the regions where trees were the dominant vegetation type in the CNTL scenario.

Region	Mixing Ratio ($g \cdot kg^{-1}$)				Wind Speed ($m \cdot s^{-1}$)			
	CNTL	GRAS	Δ	sig	CNTL	GRAS	Δ	sig
Contiguous U.S.	15.46	14.24	-1.22	90.00	1.94	2.66	0.72	90.00
Eastern U.S.	17.47	15.39	-2.08	90.00	1.57	2.36	0.79	90.00
Western U.S.	13.87	11.92	-1.94	90.00	2.23	2.95	0.72	90.00
Cascades	9.31	8.70	-0.61	90.00	1.09	2.61	1.52	90.00
California	12.07	10.80	-1.28	90.00	1.72	3.39	1.67	90.00
Intermountain Basin	10.42	8.98	-1.44	90.00	1.72	2.50	0.78	90.00
Southwestern Deserts	13.36	12.00	-1.36	90.00	2.51	2.87	0.36	90.00
Northern Rockies	11.69	9.86	-1.83	90.00	1.40	2.30	0.90	90.00
Southern Rockies	13.25	9.75	-3.51	90.00	1.55	2.25	0.70	90.00
Northern Plains	15.60	14.66	-0.93	90.00	3.05	3.32	0.27	90.00
Central Plains	17.62	16.08	-1.54	90.00	2.84	3.46	0.62	90.00
Southern Plains	19.45	18.86	-0.59	90.00	2.19	2.98	0.79	90.00
Ozark Highlands	19.35	18.40	-0.96	90.00	1.04	2.21	1.17	90.00
Prairie Peninsula	17.35	16.33	-1.02	90.00	2.26	2.62	0.36	90.00
Great Lakes Forests	14.36	13.26	-1.10	90.00	1.69	2.36	0.67	90.00
Mississippi Valley	19.59	18.95	-0.64	90.00	1.67	2.15	0.48	90.00
Florida	19.48	19.08	-0.40	90.00	1.51	1.80	0.29	90.00
Southeast Coastal	19.38	18.88	-0.50	90.00	1.40	2.32	0.92	90.00
Appalachia	17.97	17.34	-0.63	90.00	0.99	2.17	1.18	90.00
Mid Atlantic	15.27	14.53	-0.74	90.00	1.19	2.00	0.81	90.00
New England	13.46	12.62	-0.84	90.00	1.28	2.44	1.16	90.00

Table 4.21: Regional averages, differences and significance levels for mean mixing ratio and wind speed for the homogeneous short grass (GRAS) and control scenario (CNTL). Units are $g \cdot kg^{-1}$ for mixing ratio and $m \cdot s^{-1}$ for wind speed.

4.6.2 Surface Energy Budget Analysis

The nocturnal net radiation (Table 4.22) shows both regions of increase and decrease in upward net radiation. The regions with an increase in the net upward radiation were generally a result of decreased downward longwave flux. The regions with a decrease in the net upward nocturnal flux were due to a decrease in the emitted longwave flux. The daytime situation was more consistent between all the regions, all but two had a decrease in the net downward flux. All of the regions had an increase in downward shortwave flux due to lower mixing ratios but this was offset by the increase in albedo of the short grass vegetation. In the Southeast Coastal and Southern Plains regions were the two exceptions; in these two regions the albedo increase did not offset the increase in downward shortwave flux. The mean net flux is dominated by the daytime portion. All regions showed a decrease in the mean flux generally from 20-30% of the CNTL scenario mean.

Region	Peak Nocturnal			Peak Daylight			Mean		
	CNTL	GRAS	Δ	CNTL	GRAS	Δ	CNTL	GRAS	Δ
Contiguous U.S.	-74.67	-70.24	4.43	539.90	475.03	-64.87	160.69	136.88	-23.81
Eastern U.S.	-56.40	-58.70	-2.30	455.80	436.99	-18.81	145.83	131.21	-14.62
Western U.S.	-92.08	-85.31	6.77	612.33	519.37	-92.96	172.47	141.74	-30.73
Cascades	-16.13	-41.97	-25.84	453.69	469.95	16.26	167.10	155.11	-11.99
California	-53.94	-71.99	-18.05	621.15	573.00	-48.15	192.86	162.02	-30.84
Intermountain Basin	-93.30	-85.62	7.68	712.35	555.29	-157.06	205.73	153.89	-51.84
Southwestern Deserts	-113.60	-98.58	15.02	665.00	553.17	-111.83	170.21	141.37	-28.84
Northern Rockies	-99.28	-83.00	16.28	648.71	524.83	-123.88	189.17	147.51	-41.66
Southern Rockies	-100.74	-78.35	22.39	703.04	564.19	-138.85	197.21	155.18	-42.03
Northern Plains	-97.62	-94.44	3.18	508.33	472.00	-36.33	142.03	128.38	-13.65
Central Plains	-107.89	-93.68	14.21	565.23	496.00	-69.23	144.91	124.25	-20.66
Southern Plains	-64.27	-72.66	-8.39	487.15	489.10	1.95	141.48	133.88	-7.60
Ozark Highlands	-68.39	-74.68	-6.29	462.12	456.72	-5.40	145.25	129.92	-15.33
Prairie Peninsula	-84.55	-77.09	7.46	546.77	484.05	-62.72	158.91	135.66	-23.25
Great Lakes Forests	-61.02	-70.80	-9.78	511.55	481.81	-29.74	165.28	145.18	-20.10
Mississippi Valley	-54.25	-55.45	-1.20	418.13	389.00	-29.13	134.62	119.32	-15.30
Florida	-22.45	-16.70	5.75	398.35	350.06	-48.29	133.92	116.87	-17.05
Southeast Coastal	-47.40	-56.17	-8.77	397.14	405.82	8.68	129.82	123.57	-6.25
Appalachia	-63.85	-73.19	-9.34	429.01	446.99	17.98	135.64	128.72	-6.92
Mid Atlantic	-52.73	-61.55	-8.82	469.56	454.54	-15.02	151.09	136.97	-14.12
New England	-52.30	-53.19	-0.89	463.81	452.94	-10.87	151.92	142.55	-9.37

Table 4.22: Regional averages and differences and significance levels for net radiation for the control (CNTL) and homogeneous short grass (GRAS) scenarios. Units are $W \cdot m^{-2}$.

The latent heat flux shows the effect of reduced LAI in the large decrease in the daytime latent heat flux for all regions (Table 4.23). The lower mean temperatures

could be an additional factor in reducing the latent heat flux through a reduction in the stomatal conductance. The lower screen height temperatures can also lead to a smaller nocturnal vapor pressure gradient, reducing the evaporation from the soil. Overall the reduction in latent heat flux is around 50% of the CNTL value for each sub-region and the contiguous United States.

Region	Peak Daylight			Peak Nocturnal			Mean		
	CNTL	GRAS	Δ	CNTL	GRAS	Δ	CNTL	GRAS	Δ
Contiguous U.S.	-462.98	-241.93	221.05	-20.71	-6.82	13.89	-189.86	-90.74	99.12
Eastern U.S.	-406.96	-267.08	139.88	-16.95	-7.71	9.24	-167.37	-99.00	68.37
Western U.S.	-508.10	-225.64	282.46	-20.94	-5.67	15.27	-207.67	-84.20	123.47
Cascades	-284.58	-159.33	125.25	-12.93	-3.55	9.38	-122.77	-57.92	64.85
California	-514.95	-228.59	286.36	-9.59	-0.53	9.06	-201.85	-77.57	124.28
Intermountain Basin	-579.06	-180.67	398.39	-11.05	-0.58	10.47	-226.88	-63.50	163.38
Southwestern Deserts	-473.30	-192.55	280.75	-17.73	-2.35	15.38	-183.29	-64.65	118.64
Northern Rockies	-555.33	-187.16	368.17	-16.47	-2.05	14.42	-227.33	-67.52	159.81
Southern Rockies	-630.18	-165.15	465.03	-18.47	-0.91	17.56	-244.77	-55.06	189.71
Northern Plains	-394.04	-274.86	119.18	-25.39	-11.25	14.14	-171.84	-110.93	60.91
Central Plains	-522.04	-319.96	202.08	-29.52	-12.83	16.69	-213.62	-121.10	92.52
Southern Plains	-446.42	-309.16	137.26	-18.42	-8.04	10.38	-179.88	-111.31	68.57
Ozark Highlands	-454.24	-285.35	168.89	-14.28	-4.70	9.58	-180.28	-101.50	78.78
Prairie Peninsula	-502.58	-294.33	208.25	-12.09	-6.35	5.74	-192.59	-105.84	86.75
Great Lakes Forests	-406.07	-245.85	160.22	-13.11	-7.59	5.52	-167.78	-91.91	75.87
Mississippi Valley	-380.56	-258.49	122.07	-13.78	-7.76	6.02	-154.26	-96.14	58.12
Florida	-341.86	-209.97	131.89	-15.95	-11.62	4.33	-139.64	-82.99	56.65
Southeast Coastal	-380.16	-284.11	96.05	-15.26	-8.62	6.64	-158.34	-104.78	53.56
Appalachia	-415.63	-302.23	113.40	-9.67	-5.99	3.68	-168.39	-107.82	60.57
Mid Atlantic	-397.00	-273.96	123.04	-10.49	-5.16	5.33	-156.21	-97.61	58.60
New England	-403.08	-227.63	175.45	-14.79	-6.28	8.51	-165.36	-85.59	79.77

Table 4.23: Regional averages and differences and significance levels for latent heat flux for the control (CNTL) and homogeneous short grass (GRAS) scenarios. Units are $W \cdot m^{-2}$.

The decrease in latent heat flux was much larger than the decrease in the net radiation. This results in a shift to sensible and soil heat fluxes to maintain surface energy balance. This shows up as the much larger upward sensible heat flux in all regions during daylight and in the mean (Table 4.24). At night this shift causes a reduced downward flux. The shift is so large that the direction of the sensible heat flux changes from downward to upward for all regions in the mean and two regions in the nocturnal flux.

The soil heat flux also shows the effect of the imbalance in the net radiation and latent heat fluxes (Table 4.25). The peak nocturnal flux is upward and increases, in part, due to the lower surface temperatures. The daylight flux also increases,

Region	Peak Daylight			Peak Nocturnal			Mean		
	CNTL	GRAS	Δ	CNTL	GRAS	Δ	CNTL	GRAS	Δ
Contiguous U.S.	-58.65	-178.46	-119.81	53.87	21.77	-32.10	10.66	-50.62	-61.28
Eastern U.S.	-27.48	-100.00	-72.52	48.18	14.65	-33.53	16.59	-26.96	-43.55
Western U.S.	-91.88	-249.59	-157.71	67.18	27.41	-39.77	5.96	-69.37	-75.33
Cascades	-151.22	-255.30	-104.08	24.16	-11.00	-35.16	-50.08	-97.53	-47.45
California	-108.20	-316.05	-207.85	58.53	19.53	-39.00	-9.77	-95.25	-85.48
Intermountain Basin	-129.03	-340.71	-211.68	64.89	17.33	-47.56	-11.77	-105.92	-94.15
Southwestern Deserts	-188.77	-336.98	-148.21	76.18	26.98	-49.20	-22.46	-95.70	-73.24
Northern Rockies	-102.03	-283.79	-181.76	55.31	11.48	-43.83	-2.24	-89.38	-87.14
Southern Rockies	-105.00	-372.35	-267.35	58.74	10.42	-48.32	-2.18	-117.21	-115.03
Northern Plains	-76.98	-146.82	-69.84	69.29	45.06	-24.23	12.14	-27.81	-39.95
Central Plains	-22.07	-103.00	-80.93	109.55	53.94	-55.61	51.39	-6.20	-57.59
Southern Plains	-27.77	-119.87	-92.10	84.07	32.27	-51.80	24.51	-25.42	-49.93
Ozark Highlands	-11.74	-102.26	-90.52	59.26	17.07	-42.19	24.36	-25.97	-50.33
Prairie Peninsula	-28.09	-118.25	-90.16	59.11	25.29	-33.82	26.02	-27.04	-53.06
Great Lakes Forests	-72.89	-147.86	-74.97	52.41	18.09	-34.32	1.46	-42.81	-44.27
Mississippi Valley	-19.57	-76.40	-56.83	47.41	11.58	-35.83	14.41	-20.53	-34.94
Florida	-43.16	-97.16	-54.00	28.59	-2.62	-31.21	-4.01	-34.39	-30.38
Southeast Coastal	-4.10	-59.09	-54.99	61.38	11.51	-49.87	23.83	-14.19	-38.02
Appalachia	-3.64	-70.00	-66.36	52.21	16.23	-35.98	27.13	-14.64	-41.77
Mid Atlantic	-46.42	-100.41	-53.99	38.51	11.12	-27.39	3.97	-28.55	-32.52
New England	-36.76	-140.23	-103.47	63.06	12.33	-50.73	15.64	-42.66	-58.30

Table 4.24: Regional averages and differences and significance levels for sensible heat flux for the control (CNTL) and homogeneous short grass (GRAS) scenarios. Units are $W \cdot m^{-2}$.

this time downward, due to the decrease in the latent heat flux. The change in the means are about 50% of the CNTL scenario mean soil heat fluxes and the net effect is to increase the downward flux thus heating the lower soil layers.

4.6.3 Summary

There are three major changes due to replacing all vegetation types with a uniform short grass prairie: increase of the vegetation albedo from a range of 0.1-0.2 for the other vegetation types to a value of 0.26 for short grass; Reduce the leaf area index from 6 to 2; reduce the roughness length from as high as 1m for evergreen needleleaf trees to the short grass value of 0.02m. There are a few locales, of small area, which were originally desert and saw opposite changes, decreased albedo, increased LAI, and increased roughness length. The general result of this sensitivity test was a decrease in mean daily screen height temperature, mixing ratio and precipitation, and an increase in wind speed. The regions which had a decrease in temperature followed Charney's (1975) hypothesis of increased albedo leading

Region	Peak Nocturnal			Peak Daylight			Mean		
	CNTL	GRAS	Δ	CNTL	GRAS	Δ	CNTL	GRAS	Δ
Contiguous U.S.	-15.29	-23.07	-7.78	36.00	57.26	21.26	7.25	10.72	3.47
Eastern U.S.	-8.26	-21.47	-13.21	38.94	70.98	32.04	12.99	17.76	4.77
Western U.S.	-21.10	-26.63	-5.53	33.66	47.82	14.16	2.70	5.14	2.44
Cascades	-16.47	-27.09	-10.62	32.93	55.73	22.80	4.04	6.80	2.76
California	-9.48	-15.66	-6.18	14.22	28.25	14.03	0.61	1.99	1.38
Intermountain Basin	-18.38	-24.33	-5.95	23.64	34.74	11.10	1.34	3.13	1.79
Southwestern Deserts	-23.71	-26.29	-2.58	30.85	35.92	5.07	-1.40	-0.52	0.88
Northern Rockies	-23.94	-31.28	-7.34	36.44	54.11	17.67	4.00	7.82	3.82
Southern Rockies	-19.98	-24.01	-4.03	22.24	31.07	8.83	-1.03	0.27	1.30
Northern Plains	-25.00	-28.87	-3.87	42.27	54.07	11.80	5.29	7.47	2.18
Central Plains	-23.31	-32.72	-9.41	51.21	79.31	28.10	8.14	12.71	4.57
Southern Plains	-16.77	-26.22	-9.45	37.88	62.18	24.30	5.49	9.62	4.13
Ozark Highlands	-10.17	-25.67	-15.50	38.04	74.57	36.53	12.33	17.96	5.63
Prairie Peninsula	-14.39	-26.11	-11.72	43.97	76.45	32.48	13.43	19.43	6.00
Great Lakes Forests	-11.14	-24.58	-13.44	50.08	89.81	39.73	17.22	23.95	6.73
Mississippi Valley	-7.82	-19.19	-11.37	32.84	60.16	27.32	10.85	15.08	4.23
Florida	-10.57	-20.49	-9.92	24.24	43.49	19.25	3.83	5.71	1.88
Southeast Coastal	-5.99	-23.01	-17.02	33.81	65.33	31.52	11.43	14.68	3.25
Appalachia	-6.55	-23.60	-17.05	38.94	77.52	38.58	14.44	19.94	5.50
Mid Atlantic	-6.81	-20.41	-13.60	45.42	80.76	35.34	16.87	22.40	5.53
New England	-4.27	-18.07	-13.80	46.60	85.43	38.83	19.30	24.92	5.62

Table 4.25: Regional averages and differences and significance levels for soil heat flux for the control (CNTL) and homogeneous short grass (GRAS) scenarios. Units are $W \cdot m^{-2}$.

to decreased temperature. The few regions, in the western United States, which had an increase in surface temperature tend to support Wendler and Eaton (1983) in which reduced vegetation (LAI) leads to reduced evapotranspiration, increased sensible heat flux and increased temperatures.

4.7 Natural Landscape Simulation

It was pointed out in Sagan (1975) that even the indigenous pre-European population had modified the natural landscape somewhat. This process has been accelerated in the past two hundred years with the westward spread of settlement and the increased use of the land for agriculture and other economic development. Looking at the current landuse (Figure 3.5) and natural vegetation (Figure 3.6) distribution maps one can clearly see the extent to which eastern forests and central grasslands have been replaced with agricultural cropland. The consequence of the two maps is that 60% of the area of the conterminous United States has a different vegetation type on each of the maps. To examine the effects of this large-scale

change in vegetation cover over the United States I have run a sensitivity scenario that is the same as the CNTL scenario in all ways except that the forcing vegetation is that given by the natural distribution of Figure 3.6.

4.7.1 Screen Height Analysis

The temperature differences for the natural landscape scenario are shown in Figure 4.23. The largest negative differences (where the natural landscape is cooler than the current landscape) are located along the coastal areas of the Gulf of Mexico and the Atlantic Ocean (greater than 0.75°C), in western Oklahoma (greater than 2°C), in southeast Montana (greater than 1°C), and along a line from western Oklahoma to northern Minnesota (greater than 1°C). The area showing an increase in temperature from the CNTL scenario is along the Mexican border where temperatures were from 1.5-3°C warmer in the NATL than in the CNTL scenario. There was also scattered areas of warming and cooling of smaller magnitudes throughout the western United States. The significance levels exceeded the 90% threshold in Oklahoma, Minnesota, and along the Mexican border and coastal areas (Figure 4.24). The mixing ratios decreased by about $0.8g \cdot kg^{-1}$ along the Gulf of Mexico and Atlantic Coasts. It also decreased by more than $1g \cdot kg^{-1}$ in the Central Valley of California, and by more than $1.5g \cdot kg^{-1}$ in the Dakotas and western Kansas and Texas. The areas showing increases in screen height mixing ratio in excess of $1.5g \cdot kg^{-1}$ were located in central Texas and northern Wyoming with the increase in southern Arizona exceeding $4g \cdot kg^{-1}$. All of these areas showed significance above the 90% threshold (Figure 4.24).

The screen height wind speed (Figure 4.25) shows an area of moderate decrease of $0.25m \cdot s^{-1}$ in Iowa and areas of greater decrease in wind speed (greater than $1m \cdot s^{-1}$) in Indiana, Michigan, and along the southeast coast. The greatest decrease in wind speed of more than $2m \cdot s^{-1}$ occurred in central Texas. Increases in wind speed of more than $0.5m \cdot s^{-1}$ occurred in the central valley of California, the Dakotas,

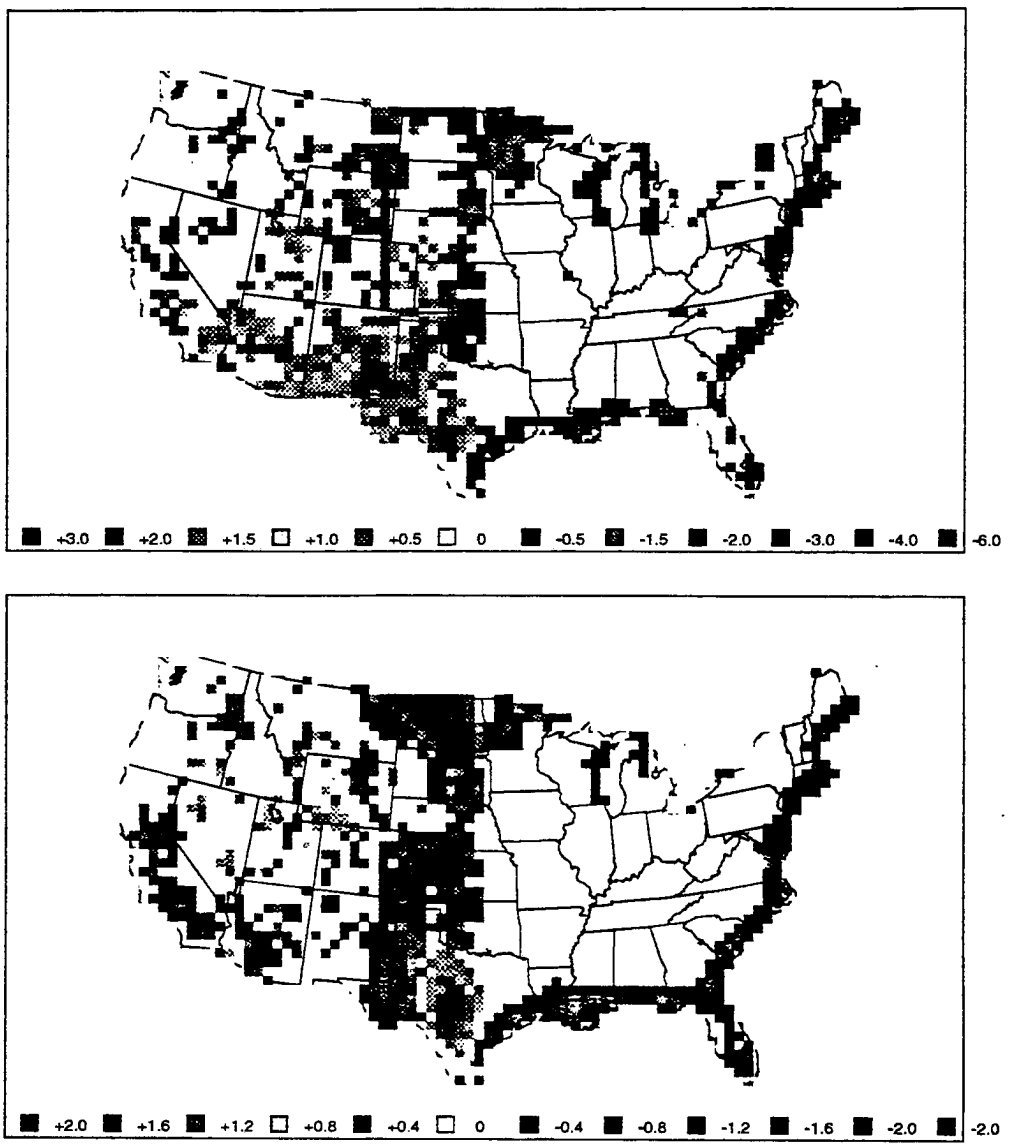

Figure 4.23: The departure of mean daily temperature for the NATL scenario from the CNTL scenario in degrees Celsius (top panel). The departure of mean daily mixing ratio for the NATL scenario from the CNTL scenario in $g \cdot kg^{-1}$ (bottom panel).

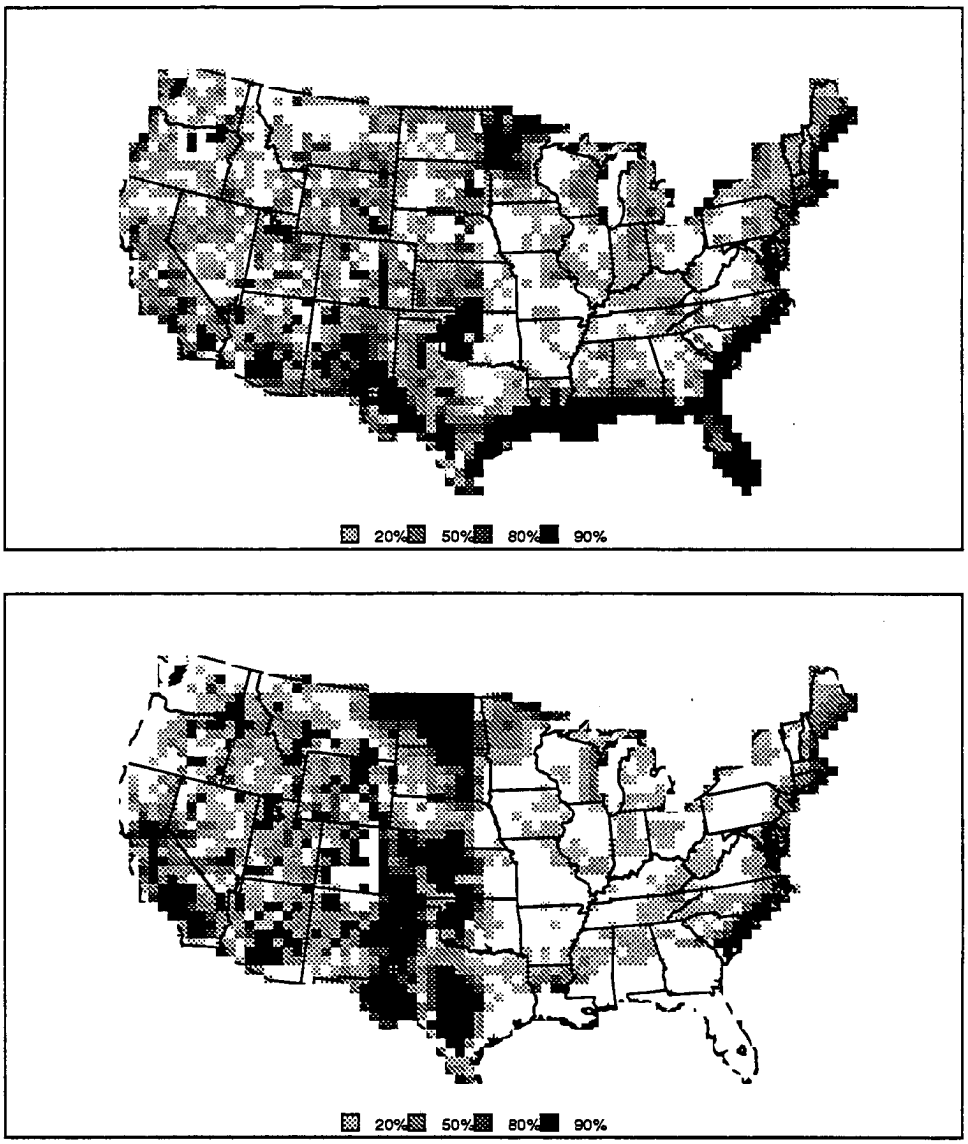

Figure 4.24: Significance test score levels for the departure of mean daily temperature (top panel) and the departure of mean daily mixing ratio (bottom panel).

and western Kansas and Texas. Changes in roughness length accounts for these changes in wind speed. All of these areas showed statistical significance in the mean wind speed difference in excess of the 90% threshold (Figure 4.26). The daily convective precipitation rate (Figure 4.25) indicates an increase in the precipitation rate of more than $0.5mm \cdot day^{-1}$ in northern Georgia, western Texas southeast Arizona, and eastern Colorado. Decrease in precipitation rate of 1-$2mm \cdot day^{-1}$ occurred in Louisiana, the Texas panhandle, and in the southeastern United States. The significance level of these changes exceeded 90% in the southern areas from Arizona, through Texas and Louisiana into Florida (Figure 4.26).

Table 4.26 summarizes the temperature changes for the NATL scenario. Overall there was a slight decrease in mean daily screen height temperature. This was due to a larger decrease in the Eastern United States (0.22°C) than the increase in the Western United States (0.09°C). The largest increase occurred in the Southwest Desert region due to the vegetation fractional coverage difference between the original evergreen shrub (80%) and the natural semi-desert (10%). This results in a much larger contribution of the bare soil to the screen height temperature. Other regions of warming (Southern Plains and Southern Rockies) had an increase in shrub and tree vegetation types and decrease in short grass which serves to decrease the regional albedo thus providing more energy for warming. Regions like the North and Central Plains changed from crop to short grass vegetation saw an increase in albedo thus reducing the net radiation leading to regional cooling. The daily precipitation rate generally decreased in all regions except for two. Overall the precipitation rate decrease was almost $0.1mm \cdot day^{-1}$ and of high (greater than 90%) statistical significance. The decrease in precipitation rate is equal to a 5% loss in precipitation. The decreased precipitation rate can be tied to a decrease in surface temperature and mixing ratio, leading to a more stable drier boundary layer.

The screen height mixing ratio (Figure 4.27) decreased in most regions. This is the result of three processes. The regions where the screen height temperature

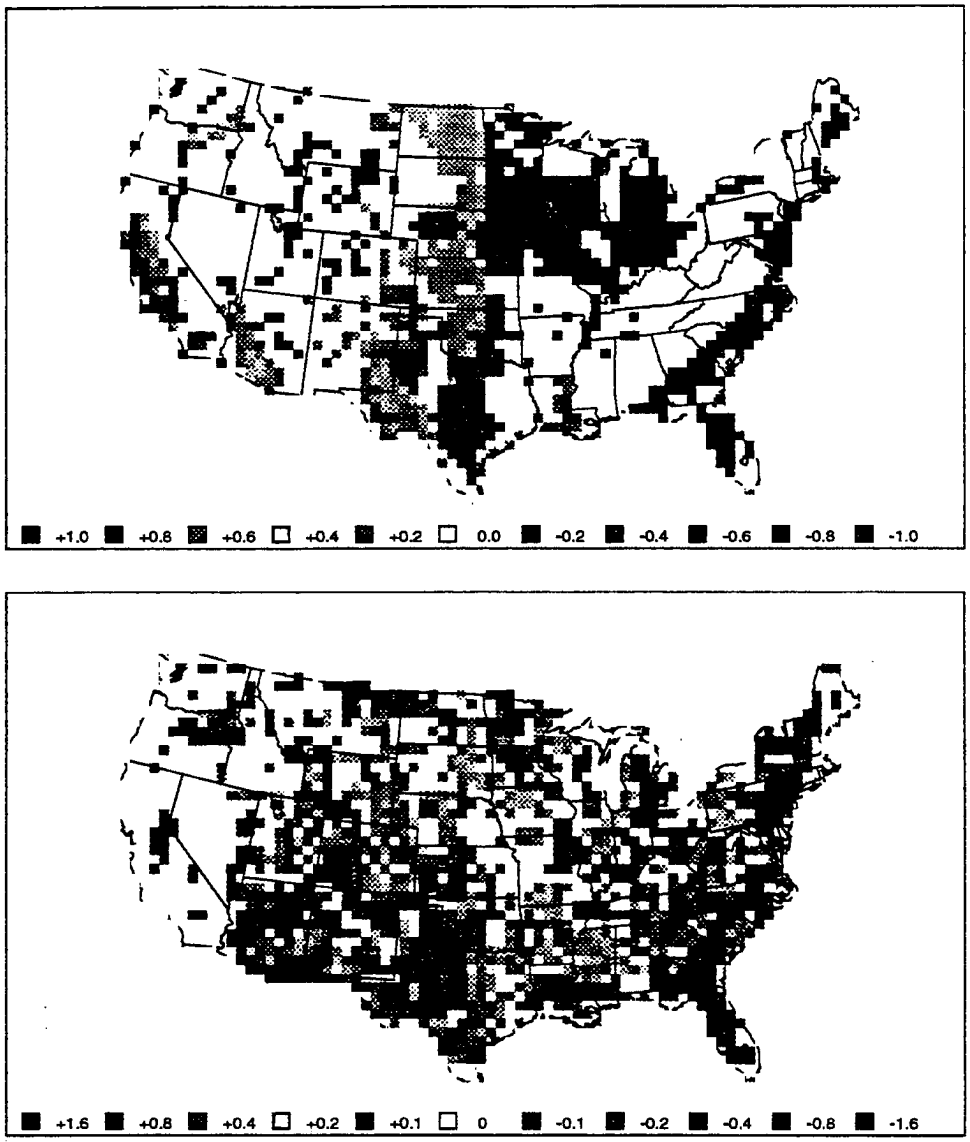

Figure 4.25: The departure of mean wind speed for the NATL scenario from the CNTL scenario in $m \cdot s^{-1}$ (top panel). The departure of mean daily convective precipitation rate for the NATL scenario from the CNTL scenario in $mm \cdot day^{-1}$ (bottom panel).

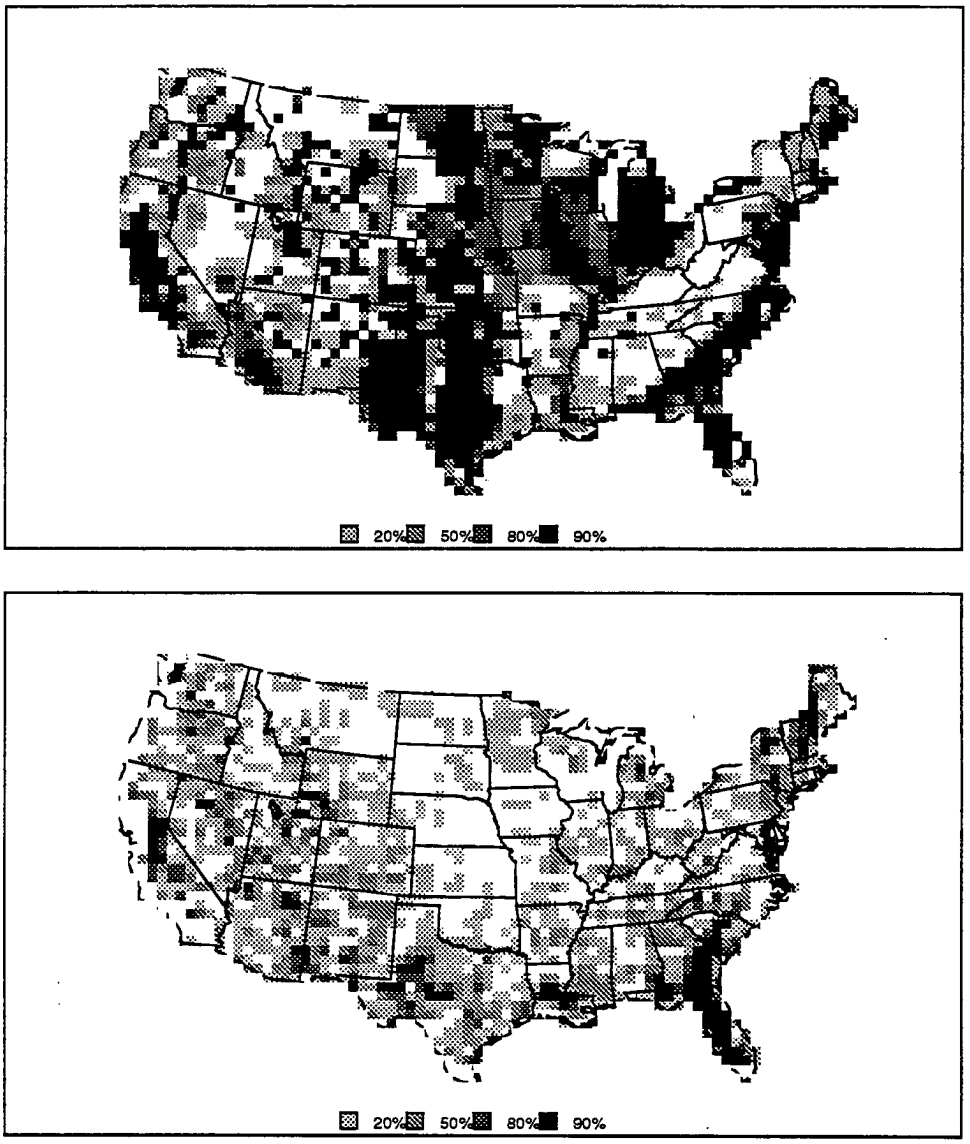

Figure 4.26: The significance levels of differences between mean wind speed for the NATL scenario from the CNTL scenario top panel) and mean daily convective precipitation rate (bottom panel).

Region	Temperature (K)				Precipitation ($mm \cdot day^{-1}$)			
	CNTL	NATL	Δ	sig	CNTL	NATL	Δ	sig
Contiguous U.S.	295.61	295.56	-0.05	20.00	1.91	1.82	-0.09	90.00
Eastern U.S.	296.37	296.15	-0.22	90.00	1.65	1.53	-0.12	90.00
Western U.S.	295.00	295.09	0.09	20.00	2.11	2.05	-0.06	50.00
Cascades	286.79	287.00	0.21		0.05	0.05	-0.00	
California	290.76	290.64	-0.12		0.17	0.11	-0.06	50.00
Intermountain Basin	293.18	293.03	-0.15	20.00	0.49	0.47	-0.02	20.00
Southwestern Deserts	299.55	301.34	1.79	90.00	2.71	2.80	0.09	
Northern Rockies	292.67	292.41	-0.26	50.00	1.02	0.96	-0.06	20.00
Southern Rockies	295.12	295.25	0.13	20.00	2.32	2.24	-0.08	20.00
Northern Plains	296.12	295.80	-0.32	50.00	2.34	2.30	-0.04	20.00
Central Plains	296.15	295.99	-0.16	50.00	3.83	3.65	-0.18	50.00
Southern Plains	298.48	298.66	0.18	90.00	2.49	2.47	-0.02	
Ozark Highlands	298.05	298.08	0.03		1.70	1.73	0.03	
Prairie Peninsula	296.74	296.63	-0.11	50.00	1.73	1.72	-0.01	
Great Lakes Forests	293.14	293.04	-0.10		0.93	0.85	-0.08	50.00
Mississippi Valley	298.59	298.40	-0.19	20.00	1.85	1.66	-0.19	80.00
Florida	298.52	298.08	-0.44	90.00	1.72	0.76	-0.96	90.00
Southeast Coastal	298.10	297.86	-0.24	90.00	2.57	2.34	-0.23	80.00
Appalachia	296.37	296.28	-0.09	20.00	2.29	2.24	-0.05	20.00
Mid Atlantic	293.80	294.02	0.22		1.42	1.29	-0.13	50.00
New England	292.17	291.59	-0.58	80.00	0.49	0.33	-0.16	50.00

Table 4.26: Regional averages, differences and significance levels for mean daily temperature and daily convective precipitation rate for the natural vegetation (NATL) and control scenario (CNTL). Units are degree Kelvin for the temperatures and $mm \cdot day^{-1}$ for precipitation.

also decreased are indicative of a temperature control on the stomatal conductance leading to smaller latent heat flux. The regions where the temperature increased potentially had enough boundary layer growth to provide a greater volume to mix the moisture through. Some of the regions had a greater area of short grass in the NATL scenario than in the CNTL run. This would lead to a reduction of LAI in the region and smaller moisture flux. The wind speed summary (Figure 4.27) shows the general result of roughness length changes. In the east the cropland (roughness length of 0.06m) was replaced by forests (roughness length of 0.8m), while in the west the cropland was replaced mainly by short grass (roughness length of 0.02m). This would account for the overall increase in wind speed in the west and decrease of wind speed in the east. The Southern Plains, Northern Rockies, and Cascade Regions are exceptions to this rule. In those regions the current cropland was replaced by shrubs leading to an increase in roughness length and decrease in wind speed in the NATL scenario.

4.7.2 Surface Energy Budget Analysis

The regional net radiation summary (Table 4.28) shows that during the night there was a slight decrease ($4.5W \cdot m^{-2}$) in the eastern region and a small increase ($3.6W \cdot m^{-2}$) in the western region. The decreases in the nocturnal net upward flux is generally due to more downward longwave from the atmosphere and the increases are due to warmer surface temperatures leading to increased emission. During the daytime the net downward radiation decreased in most regions due to increased surface albedo offsetting any increase in the downward shortwave flux from a drier boundary layer. The few regions which show an increase in the daytime net flux (Prairie Peninsula and Mississippi Valley) are a result of lower vegetation albedo. The overall effect on the mean daily net radiation was a decrease of $1.86W \cdot m^{-2}$ for the contiguous United States.

Region	Mixing Ratio ($g \cdot kg^{-1}$)				Wind Speed ($m \cdot s^{-1}$)			
	CNTL	NATL	Δ	sig	CNTL	NATL	Δ	sig
Contiguous U.S.	15.46	15.20	-0.26	90.00	1.94	1.83	-0.11	90.00
Eastern U.S.	17.47	17.33	-0.14	50.00	1.57	1.25	-0.32	90.00
Western U.S.	13.87	13.51	-0.36	90.00	2.23	2.28	0.05	80.00
Cascades	9.31	9.39	0.08	20.00	1.09	1.05	-0.04	20.00
California	12.07	11.74	-0.34	90.00	1.72	1.85	0.13	50.00
Intermountain Basin	10.42	10.44	0.02		1.72	1.73	0.01	
Southwestern Deserts	13.36	12.33	-1.03	90.00	2.51	2.79	0.28	90.00
Northern Rockies	11.69	11.70	0.01		1.40	1.34	-0.06	50.00
Southern Rockies	13.25	12.70	-0.55	90.00	1.55	1.69	0.14	90.00
Northern Plains	15.60	15.03	-0.57	90.00	3.05	3.14	0.09	80.00
Central Plains	17.62	17.12	-0.51	90.00	2.84	2.96	0.12	90.00
Southern Plains	19.45	19.67	0.22	80.00	2.19	1.72	-0.47	90.00
Ozark Highlands	19.35	19.40	0.05	20.00	1.04	0.94	-0.10	80.00
Prairie Peninsula	17.35	17.42	0.07	20.00	2.26	1.80	-0.46	90.00
Great Lakes Forests	14.36	14.20	-0.16	50.00	1.69	1.16	-0.53	90.00
Mississippi Valley	19.59	19.48	-0.11	20.00	1.67	1.47	-0.20	90.00
Florida	19.48	18.97	-0.51	90.00	1.51	1.05	-0.46	90.00
Southeast Coastal	19.38	19.16	-0.22	90.00	1.40	0.97	-0.43	90.00
Appalachia	17.97	17.94	-0.03		0.99	0.90	-0.09	90.00
Mid Atlantic	15.27	15.21	-0.06		1.19	0.94	-0.25	90.00
New England	13.46	13.14	-0.32	90.00	1.28	1.05	-0.23	90.00

Table 4.27: Regional averages, differences and significance levels for mean mixing ratio and wind speed for the natural vegetation (NATL) and control scenario (CNTL). Units are $g \cdot kg^{-1}$for mixing ratio and $m \cdot s^{-1}$ for wind speed.

Region	Peak Nocturnal			Peak Daylight			Mean		
	CNTL	NATL	Δ	CNTL	NATL	Δ	CNTL	NATL	Δ
Contiguous U.S.	-74.67	-76.23	-1.56	539.90	524.45	-15.45	160.69	156.23	-4.46
Eastern U.S.	-56.40	-51.90	4.50	455.80	444.45	-11.38	145.83	143.97	-1.86
Western U.S.	-92.08	-95.68	-3.60	612.33	593.94	-18.59	172.47	166.32	-6.15
Cascades	-16.13	-27.75	-11.62	453.69	438.93	-14.76	167.10	160.30	-6.80
California	-53.94	-54.56	-0.62	621.15	615.44	-5.71	192.86	187.34	-5.52
Intermountain Basin	-93.30	-93.27	0.03	712.35	717.58	5.23	205.73	207.37	1.64
Southwestern Deserts	-113.60	-121.46	-7.86	665.00	616.02	-48.98	170.21	155.83	-14.38
Northern Rockies	-99.28	-99.77	-0.49	648.71	660.80	12.09	189.17	192.06	2.89
Southern Rockies	-100.74	-97.72	3.02	703.04	682.26	-20.78	197.21	191.64	-5.57
Northern Plains	-97.62	-100.95	-3.33	508.33	484.24	-24.09	142.03	132.43	-9.60
Central Plains	-107.89	-101.65	6.24	565.23	530.89	-34.34	144.91	135.04	-9.87
Southern Plains	-64.27	-61.33	2.94	487.15	483.01	-4.14	141.48	142.26	0.78
Ozark Highlands	-68.39	-66.96	1.43	462.12	459.05	-3.07	145.25	145.48	0.23
Prairie Peninsula	-84.55	-84.70	-0.15	546.77	550.19	3.42	158.91	160.40	1.49
Great Lakes Forests	-61.02	-62.06	-1.04	511.55	479.20	-32.35	165.28	160.45	-4.83
Mississippi Valley	-54.25	-54.05	0.20	418.13	421.05	2.92	134.62	134.47	-0.15
Florida	-22.45	-11.44	11.01	398.35	363.19	-35.16	133.92	123.75	-10.17
Southeast Coastal	-47.40	-38.23	9.17	397.14	382.36	-14.78	129.82	129.15	-0.67
Appalachia	-63.85	-59.79	4.06	429.01	420.16	-8.85	135.64	134.51	-1.13
Mid Atlantic	-52.73	-51.84	0.89	469.56	445.82	-23.74	151.09	143.87	-7.22
New England	-52.30	-37.15	15.15	463.81	423.47	-40.34	151.92	147.47	-4.45

Table 4.28: Regional averages and differences and significance levels for net radiation for the control (CNTL) and natural vegetation (NATL) scenarios. Units are $W \cdot m^{-2}$.

The daytime latent heat flux decreased overall by $29.34W \cdot m^{-2}$ (Table 4.29). This was mainly a result of the large decrease in the western United States due to the change from evergreen shrub in the CNTL scenario to semi-desert in the NATL run in the Southwest Deserts region resulting in a much smaller area of transpiring surface. Regions such as California, Southern Rockies, and Northern and Central Plains all had a decrease in the daytime latent heat flux due to reduced LAI due to replacement of crops and shrubs with short grass. The Southern Plains on the other hand had an increase in daytime latent heat flux due to the replacement of the short grass and crops in the current landuse by shrubs in the natural landscape.

The daytime sensible heat flux increased by almost $28W \cdot m^{-2}$ due mainly to the contribution from the Southwest Desert region (Table 4.29). This was a result of the increased surface temperatures. The changes in the Plains and Rockies regions were mainly due to the partitioning of the heat fluxes with respect to the change in the latent heat flux. The downward nocturnal flux of sensible heat increased in the east and decreased in the west. This was a result of changes in nocturnal temperatures. The Southwest Desert had higher temperatures hence lower downward flux, while

Region	Peak Daylight			Peak Nocturnal			Mean		
	CNTL	NATL	Δ	CNTL	NATL	Δ	CNTL	NATL	Δ
Contiguous U.S.	-462.98	-433.64	29.34	-20.71	-20.21	0.50	-189.86	-179.41	10.45
Eastern U.S.	-406.96	-404.44	2.52	-16.95	-18.79	-1.84	-167.37	-170.48	-3.11
Western U.S.	-508.10	-459.97	48.13	-20.94	-18.55	2.39	-207.67	-186.49	21.18
Cascades	-284.58	-276.78	7.80	-12.93	-12.71	0.22	-122.77	-119.53	3.24
California	-514.95	-474.53	40.42	-9.59	-9.37	0.22	-201.85	-184.98	16.87
Intermountain Basin	-579.06	-570.71	8.35	-11.05	-10.47	0.58	-226.88	-222.29	4.59
Southwestern Deserts	-473.30	-347.65	125.65	-17.73	-18.35	-0.62	-183.29	-139.57	43.72
Northern Rockies	-555.33	-569.91	-14.58	-16.47	-18.56	-2.09	-227.33	-232.72	-5.39
Southern Rockies	-630.18	-550.39	79.79	-18.47	-15.91	2.56	-244.77	-212.26	32.51
Northern Plains	-394.04	-323.92	70.12	-25.39	-15.57	9.82	-171.84	-135.04	36.80
Central Plains	-522.04	-439.67	82.37	-29.52	-24.48	5.04	-213.62	-178.90	34.72
Southern Plains	-446.42	-487.12	-40.70	-18.42	-25.83	-7.41	-179.88	-205.49	-25.61
Ozark Highlands	-454.24	-456.48	-2.24	-14.28	-14.80	-0.52	-180.28	-183.13	-2.85
Prairie Peninsula	-502.58	-523.64	-21.06	-12.09	-13.99	-1.90	-192.59	-203.74	-11.15
Great Lakes Forests	-406.07	-372.77	33.30	-13.11	-15.50	-2.39	-167.78	-163.93	3.85
Mississippi Valley	-380.56	-389.37	-8.81	-13.78	-15.84	-2.06	-154.26	-158.34	-4.08
Florida	-341.86	-317.97	23.89	-15.95	-18.24	-2.29	-139.64	-138.32	1.32
Southeast Coastal	-380.16	-380.77	-0.61	-15.26	-18.00	-2.74	-158.34	-165.96	-7.62
Appalachia	-415.63	-414.28	1.35	-9.67	-10.02	-0.35	-168.39	-166.62	1.77
Mid Atlantic	-397.00	-368.12	28.88	-10.49	-12.21	-1.72	-156.21	-147.24	8.97
New England	-403.08	-344.33	58.75	-14.79	-15.40	-0.61	-165.36	-151.01	14.35

Table 4.29: Regional averages and differences and significance levels for latent heat flux for the control (CNTL) and natural vegetation (NATL) scenarios. Units are $W \cdot m^{-2}$.

Florida and the Southeast Coastal regions had lower temperatures and increased downward heat flux.

The soil heat flux at the top soil layer has a regional consistency not seen in the other fluxes (Table 4.31). The western region had a increase in the nocturnal and daytime soil fluxes due to an increased diurnal range in temperature. The eastern regions, on the other hand, had less nocturnal and daytime flux indicating a reduced diurnal range in temperature. The change in diurnal range was not consistent between regions nor was it symmetric in time about the mean leading to the lack of regional pattern in the mean screen height temperatures (Table 4.26).

4.7.3 Summary

It is difficult to summarize the results of the natural landscape scenario since each of the regions is unique in terms of its landscape type and the balance of energy fluxes that control the screen height atmospheric parameters, but some generalities can still be made. Overall, mean daily temperature decreased for the contiguous

Region	Peak Daylight			Peak Nocturnal			Mean		
	CNTL	NATL	Δ	CNTL	NATL	Δ	CNTL	NATL	Δ
Contiguous U.S.	-58.65	-71.90	-13.25	53.87	48.43	-5.44	10.66	3.76	-6.90
Eastern U.S.	-27.48	-23.05	4.43	48.18	54.60	6.42	16.59	18.65	2.06
Western U.S.	-91.88	-119.84	-27.96	67.18	59.24	-7.94	5.96	-8.04	-14.00
Cascades	-151.22	-141.56	9.66	24.16	21.04	-3.12	-50.08	-47.45	2.63
California	-108.20	-135.61	-27.41	58.53	57.20	-1.33	-9.77	-19.85	-10.08
Intermountain Basin	-129.03	-144.43	-15.40	64.89	62.05	-2.84	-11.77	-19.03	-7.26
Southwestern Deserts	-188.77	-259.33	-70.56	76.18	58.36	-17.82	-22.46	-51.64	-29.18
Northern Rockies	-102.03	-104.27	-2.24	55.31	57.41	2.10	-2.24	-2.08	0.16
Southern Rockies	-105.00	-151.61	-46.61	58.74	44.75	-13.99	-2.18	-25.11	-22.93
Northern Plains	-76.98	-118.76	-41.78	69.29	52.17	-17.12	12.14	-13.30	-25.44
Central Plains	-22.07	-40.92	-18.85	109.55	86.63	-22.92	51.39	32.14	-19.25
Southern Plains	-27.77	-1.27	26.50	84.07	116.32	32.25	24.51	44.99	20.48
Ozark Highlands	-11.74	-9.70	2.04	59.26	60.24	0.98	24.36	25.13	0.77
Prairie Peninsula	-28.09	-23.39	4.70	59.11	67.08	7.97	26.02	31.22	5.20
Great Lakes Forests	-72.89	-75.74	-2.85	52.41	52.62	0.21	1.46	-2.56	-4.02
Mississippi Valley	-19.57	-20.97	-1.40	47.41	49.25	1.84	14.41	13.38	-1.03
Florida	-43.16	-31.73	11.43	28.59	39.76	11.17	-4.01	2.24	6.25
Southeast Coastal	-4.10	8.97	13.07	61.38	79.18	17.80	23.83	31.01	7.18
Appalachia	-3.64	-1.86	1.78	52.21	53.33	1.12	27.13	26.94	-0.19
Mid Atlantic	-46.42	-52.95	-6.53	38.51	34.79	-3.72	3.97	-1.61	-5.58
New England	-36.76	-48.05	-11.29	63.06	60.86	-2.20	15.64	7.26	-8.38

Table 4.30: Regional averages and differences and significance levels for sensible heat flux for the control (CNTL) and natural vegetation (NATL) scenarios. Units are $W \cdot m^{-2}$.

Region	Peak Nocturnal			Peak Daylight			Mean		
	CNTL	NATL	Δ	CNTL	NATL	Δ	CNTL	NATL	Δ
Contiguous U.S.	-15.29	-15.66	-0.37	36.00	37.50	1.50	7.25	7.37	0.12
Eastern U.S.	-8.26	-7.47	0.79	38.94	37.40	-1.54	12.99	12.44	-0.55
Western U.S.	-21.10	-22.25	-1.15	33.66	37.58	3.92	2.70	3.36	0.66
Cascades	-16.47	-16.49	-0.02	32.93	33.56	0.63	4.04	4.31	0.27
California	-9.48	-10.67	-1.19	14.22	16.97	2.75	0.61	0.84	0.23
Intermountain Basin	-18.38	-18.73	-0.35	23.64	24.58	0.94	1.34	1.42	0.08
Southwestern Deserts	-23.71	-24.14	-0.43	30.85	32.55	1.70	-1.40	-0.74	0.66
Northern Rockies	-23.94	-24.41	-0.47	36.44	38.09	1.65	4.00	4.30	0.30
Southern Rockies	-19.98	-20.65	-0.67	22.24	23.45	1.21	-1.03	-0.77	0.26
Northern Plains	-25.00	-27.16	-2.16	42.27	49.06	6.79	5.29	6.22	0.93
Central Plains	-23.31	-27.60	-4.29	51.21	64.02	12.81	8.14	10.18	2.04
Southern Plains	-16.77	-13.93	2.84	37.88	30.38	-7.50	5.49	4.22	-1.27
Ozark Highlands	-10.17	-9.57	0.60	38.04	37.50	-0.54	12.33	12.12	-0.21
Prairie Peninsula	-14.39	-13.97	0.42	43.97	43.91	-0.06	13.43	13.26	-0.17
Great Lakes Forests	-11.14	-10.63	0.51	50.08	48.44	-1.64	17.22	16.48	-0.74
Mississippi Valley	-7.82	-7.19	0.63	32.84	31.99	-0.85	10.85	10.38	-0.47
Florida	-10.57	-8.51	2.06	24.24	20.03	-4.21	3.83	2.85	-0.98
Southeast Coastal	-5.99	-4.62	1.37	33.81	31.30	-2.51	11.43	10.84	-0.59
Appalachia	-6.55	-5.78	0.77	38.94	38.22	-0.72	14.44	14.24	-0.20
Mid Atlantic	-6.81	-6.95	-0.14	45.42	48.00	2.58	16.87	17.13	0.26
New England	-4.27	-2.79	1.48	46.60	42.94	-3.66	19.30	17.80	-1.50

Table 4.31: Regional averages and differences and significance levels for soil heat flux for the control (CNTL) and natural vegetation (NATL) scenarios. Units are $W \cdot m^{-2}$.

United States by 0.05°C. The regions in the NATL scenario that were cooler than the CNTL run were due to an increase in albedo reducing the net radiation available at the surface. The warmer regions were due to the increased sensible heat flux required for energy balance. The imbalance was a result of lower LAI and lower latent heat flux, as well as albedo and roughness differences. The mixing ratio also had an overall decrease from the CNTL scenario of $0.26g \cdot kg^{-1}$. The decrease was generally a result of the lower temperatures but in some regions reduced flux was a consequence of lower LAI.

The wind speed was the only screen height quantity for which the sign of the change could have been predetermined. The wind speed change was opposite to the change in roughness length, with an overall decrease of $0.11m \cdot s^{-1}$. The precipitation rate generally decreased throughout the United States. For the contiguous Unites States the decrease was $0.09mm \cdot day^{-1}$, a change of about 5%. The interesting point about the location of the changes in precipitation rate was that they tended to occur along boundaries between vegetation types. The decrease in precipitation rate occurred along the ecotone separating the mixed woodland and cropland in the current landuse map (Figure 3.5). The increase in precipitation rate in southeastern Arizona occurred at the junction of the desert, semi-desert, and evergreen shrub vegetation types (Figure 3.6).

The results of the natural landscape sensitivity scenario suggest the possibility that the current landuse has caused summertime surface conditions to be warmer and drier than the natural landscape would indicate.

Chapter 5

SUMMARY

5.1 Conclusions

A climate version of RAMS (CLIMRAMS) was developed. CLIMRAMS was verified with a simulation of the month of July 1989. It was then used to evaluate its sensitivity to soil moisture and vegetation distributions.

CLIMRAMS did an excellent job of simulating the surface temperature structure for the month of July 1989. The daily mean temperature had an overall cold bias of 1.35°C when compared with observations. Regionally, 70% of the land area had mean temperatures within 1°C of the observations. This demonstrates the capability of CLIMRAMS to provide high resolution, in space and time, high quality screen height temperature information for ecosystem models. Summertime precipitation on the other hand still leaves a lot to be desired. The Kuo parameterization does a much better job of simulating the pattern of precipitation than the actual amount. The precipitation amounts were generally within a factor of two of observations though locally greater differences exist. For the United States as a whole the simulated precipitation rate of 1.91mm·day^{-1} was close to the observed rate of 2.3mm·day^{-1}. The precipitation results are probably not accurate enough for ecosystem modeling needs.

The first scenario was to test the sensitivity to soil moisture initialization. A decrease in the initial soil moisture throughout the column by 50% led to a decreased soil heat capacity and increased soil temperatures. This in turn led to an increase in mean daily temperature through increased heat flux to the atmosphere.

The decrease in soil moisture was not sufficient to limit transpiration, except in the Cascades. The increase in temperature increased the stomatal conductance leading to greater latent heat flux. The increased moisture flux to the boundary layer did not show up as an increase in the screen height mixing ratio. Instead the higher temperatures led to greater boundary layer growth and the additional moisture was able to mix through a larger volume of atmosphere. The surface wind speed decreased due the warmer boundary layer in the north which reduced the baroclinicity and the wind speeds at the first atmospheric model level, which determine the screen height winds through similarity functions.

The results from the scenario where the top soil layer retained its original initial moisture content but the moisture content of the lower layers was reduced by 50% were very similar to the results of the scenario where the total soil moisture was reduced by 50%. The moist top layer had a moderating effect leading to slightly cooler and more moist screen height conditions with marginally stronger winds than the half total soil moisture scenario. The surface energy fluxes responded in a way consistent with a more moist and cooler surface. The latent heat flux was reduced overall but was higher during the night due to increased evaporation. The sensible heat fluxes during the day (night) were lower (higher) than in the half total soil moisture scenario, consistent with the lower (higher) screen height temperatures. The increase in the diurnal range in the soil heat flux was also consistent with the increase in the top soil layer moisture leading to greater thermal conductivity.

In the homogeneous landscape scenario the current landuse was replaced with a uniform short grass prairie. There were three major changes to the landsurface parameters as a result of the vegetation change: increase in albedo, decrease of the leaf area index, and a decrease in the roughness length. There are a few locales, of small area, which were originally desert and saw opposite changes, decreased albedo, increased LAI, and increased roughness length. The general result of this

sensitivity test was a decrease in mean daily screen height temperature, mixing ratio and precipitation, and an increase in wind speed. The regions which had a decrease in temperature followed Charney's (1975) hypothesis of increased albedo leading to decreased temperature. The few regions, in the western United States, which had an increase in surface temperature tend to support Wendler and Eaton (1983) in which reduced vegetation (LAI) leads to reduced evapotranspiration, increased sensible heat flux and increased temperatures. All regions demonstrated aspects of both theories and it was just in the details which determined which was the dominant process.

The final sensitivity scenario examined the possible effects that changes in the natural landcover may have had on the regional climate. This scenario used a natural vegetation distribution in place of the current landuse. Overall, mean daily temperature decreased for the contiguous United States. The regions in the natural landcover scenario that were cooler than the current landuse run were due to an increase in albedo reducing the net radiation available at the surface. The warmer regions were due to the increased sensible heat flux required for energy balance. The imbalance was a result of lower LAI and lower latent heat flux. The mixing ratio also had an overall decrease as compared to the current landuse scenario. The decrease was generally a result of the lower temperatures but in some regions reduced flux was a consequence of lower LAI. The wind speed was the only screen height quantity for which the sign of the change could have been predetermined. The wind speed change was opposite to the change in roughness length. The precipitation rate generally decreased throughout the United States. The location of the changes in precipitation rate occurred along ecotones. A decrease in precipitation rate in the southeast occurred along the boundary separating mixed woodland and cropland in the current landuse distribution. An increase in precipitation rate in southeastern Arizona occurred at the junction of the desert, semi-desert, and evergreen shrub

vegetation types. The results of the natural landscape sensitivity scenario suggest the possibility that the current landuse has caused summertime surface conditions to be warmer and drier than would occur with the natural landscape.

5.2 Recommendations for Future Work

There is still much work that can be done. Improvements need to be made in the convective parameterization scheme since this is the one weak point in using CLIMRAMS for ecological impact studies. The parameters of the vegetation parameterization need to be better specified. The range in LAI and vegetation fractional coverage is too small, and the results from observational studies indicates that they are wrong for western vegetation types. The seasonality of the LAI in particular needs to better represent that of the actual vegetation; and parameters like albedo and roughness length need a seasonal cycle. The model also needs to be extended into the winter and transitional seasons. To do this a snowcover and frozen soil scheme need to be implemented. Then a verification simulation of a winter season should be undertaken.

As of the writing of this dissertation work is in progress to couple CLIMRAMS with CENTURY to enable a two way coupling between atmospheric and vegetation processes. The coupled model will then be integrated for a period of several years to investigate the interactions between climate and ecosystem dynamics under $1\times CO_2$ and $2\times CO_2$ conditions.

Epilogue

It was shown in figure 4.6 on page 42 the the control simulation precipitation bias had a very spatially distinct distribution. The bias was approximately 200% in the western United States and 50% in the eastern United States. It was felt that a simple experiment could be performed to attempt to correct the precipitation error. To do so an adjustment was made to the precipitation efficiency in the convective parameterization. The original precipitation efficiency, ε_p, was changed as follows:

$$\varepsilon_p^{west} = 0.5\varepsilon_p \tag{E.1}$$

$$\varepsilon_p^{east} = \min \begin{cases} 0.5\varepsilon_p \\ 0.9 \end{cases} \tag{E.2}$$

where ε_p is given by equation 3.13 on page 35 and 97 west longitude is the dividing line between west and east.

The results of the adjusted convective precipitation efficiency run are for only the first half of the month of July. The ratio of simulated to observed precipitation is shown in figure 5.1. The precipitation bias is now more uniformly distributed across the model domain. The bias more clearly shows the western lag in the simulated precipitation systems, which is seen in the observed and simulated precipitation shown in figure 5.2. The model also failed to simulate the region of high precipitation along the gulf coast. This was a result of the model initialization failing to resolve Tropical Storm Allison which made landfall in the first few days of July and accounted for almost all of the observed precipitation in the gulf coastal region for the period. Overall the precipitation increased in the United States with the adjustment to the precipitation efficiency from 87% in the control run to 145%. This precipitation bias remained constant in the eastern and western regions with a bias

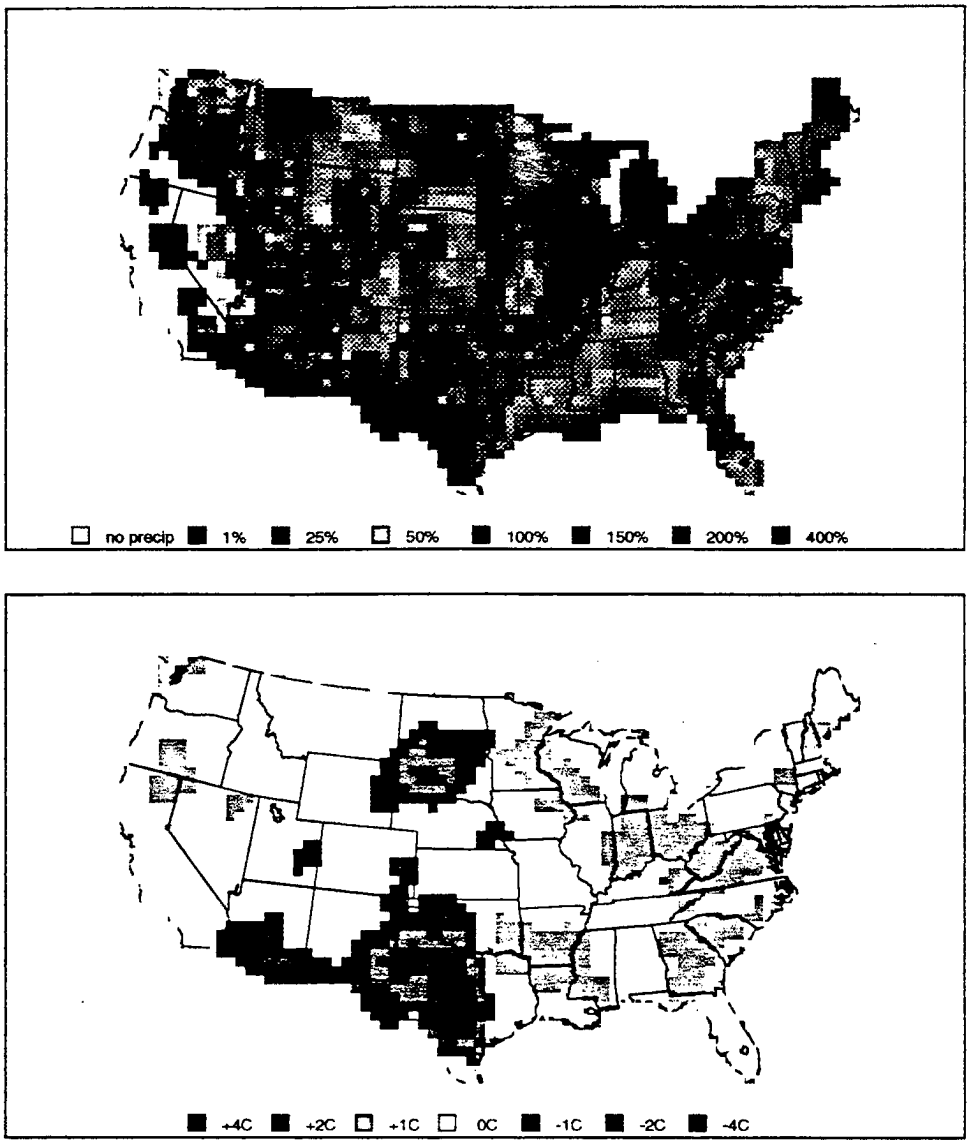

Figure E.1: The ratio of simulated to observed precipitation for July 1-15 1989 (top panel). The departure of mean daily temperature of the precipitation efficiency adjusted scenario from the control scenario; (bottom panel) units are degrees Celsius.

of 145% compared with a precipitation bias of 45% and 220% respectively in the control scenario.

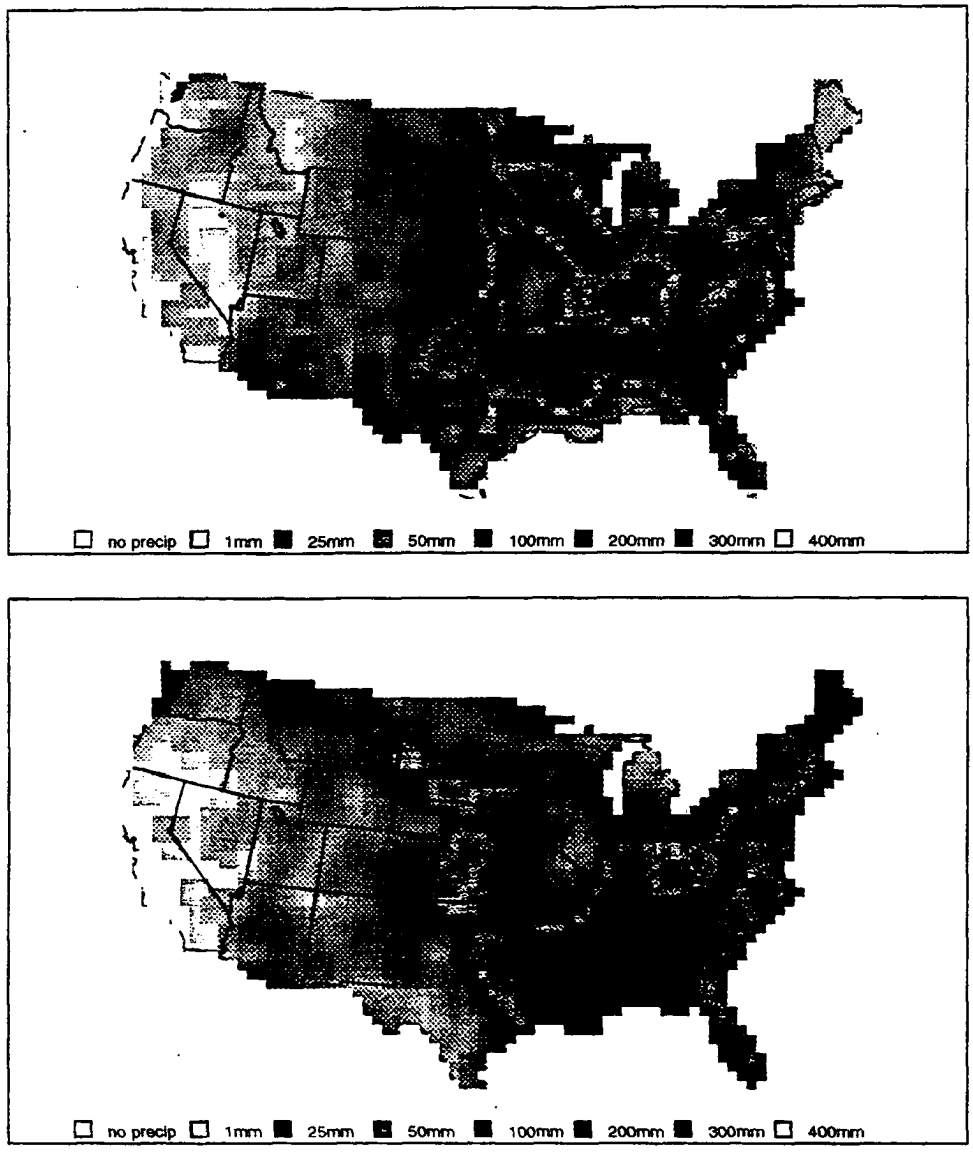

Figure E.2: Simulated precipitation from the precipitation efficiency adjusted scenario for July 1-15 1989 (top panel); units are mm. Observed precipitation for July 1-15 1989 (bottom panel); units are also mm.

The effect of the precipitation change was negligible in all regions except southern Arizona, western Texas and South Dakota(Figure 5.1. These were all areas in which the precipitation amount was also over simulated. There was no clear signal as to the reason for this decrease in mean daily temperature.

Bibliography

Adams, R.M., C. Rosenzweig, R.M. Peart, J.T. Richie, B.A. McCarl, J.D. Glyer, R.B. Curry, J.W. Jones, K.J. Boote, and L.H. Allen, 1990: Global climate change and U.S. agriculture. *Nature*, **345**, 219-224.

Anthes, R.A., 1984: Enhancement of convective precipitation by mesoscale variations in vegetative covering in semiarid regions. *J. Climate Appl. Meteor.*, **23**, 541-554.

Anthes, R.A., E.Y. Hsie, and Y.H. Kuo, 1987: Description of the Penn State/NCAR Mesoscale Model Version 4 (MM4). Technical Report NCAR/TN-282+STR, NCAR, Boulder, Colorado, 66pp.

Arya, S.P, 1988: *Introduction to Micrometeorology.* Academic Press, San Diego, California, 303 pp.

Avissar, R. and Y. Mahrer, 1988: Mapping frost-sensitive areas with a three-dimensional local-scale numerical model. Part I: Physical and numerical aspects. *J. Appl. Meteor.*, **27**, 400-413.

Balling, R.C.Jr., 1988: The climatic impact of a sonoran vegetation discontinuity. *Climatic Change*, **13**, 99-109.

Balling, R.C.Jr., 1989: The impact of summer rainfall on the temperature gradient along the United States-Mexico border. *J. of Appl. Climatology*, **28**, 304-308.

Braham, R.R., 1952: The water and energy budgets of the thunderstorm and their relation to thunderstorm development. *J. Meteorol.*, **9**, 227-242.

Bryant, N.A., L.F. Johnson, A.J. Brazel, R.C. Balling, C.F. Hutchinson, and L.R. Beck, 1990: Measuring the effect of overgrazing in the sonoran desert. *Climatic Change*, **17**, 243-264.

Chang, J.T., and P.J. Wetzel, 1991: Effects of spatial variations of soil moisture and vegetation on the evolution of a prestorm environment: A case study. *Mon. Wea. Rev.*, **119**, 1368-1390.

Charney, J.G, 1975: Dynamics of deserts and drought in the sahel. *Q.J.R.M.S.*, **101**, 193-202.

Chen, C. and W.R. Cotton, 1983: A one-dimensional simulation of the stratocumulus-capped mixed layer. *Bound.-Layer Meteor.*, **25**, 289-321.

Chen, C. and W.R. Cotton, 1983b: Numerical experiments with a one-dimensional higher order turbulence model: Simulation of the Wangara Day 33 case. *Bound.-Layer Meteor.*, **25**, 375-404.

Clark, C.A. and R.W. Arritt, 1994: Numerical simulations of the effect of soil moisture and vegetatiin cover on the development of deep convection. *J. Appl. Meteor.*, submitted.

Collatz, G.J., J.T. Ball, C. Grivet, and J.A. Berry, 1991: Physiological and environmental regulation of stomatal conductance, photosynthesis and transpiration: A model that includes a laminar boundary layer. *Agric. For. Meteorol.*, **54**, 107-136.

Cooter, E.J., B.K. Eder, S.K. LeDuc, and L. Truppi, 1993: General circulation model output for forest and climate change research and applications. *Southeastern Experiment Station Technical Bulletin*, in press.

Cotton, W.R., M.A. Stephens, T. Nehrkorn, and G.J. Tripoli, 1982: The Colorado State University cloud/mesoscale model-1982. Part II: An ice phase parameterization. *J. Rech. Atmos.*, **16**, 295-320.

Cotton, W.R., C.J. Tremback, and R.L. Walko, 1988: CSU RAMS - A cloud model goes regional. *Proc. NCAR Workshop on Limited-Area Modeling Intercomparison*, Nov. 15-18, NCAR, Boulder, CO, 202-211.

Deacon, E.L., 1969: Physical processes near the surface of the earth. *World Survey of Climatology*, **2**, H. Flohn (ed.), Elsevier, New York, New York, 39-100.

Dickinson, R.E., R.M. Errico, F. Giorgi, and G.T. Bates, 1989: A regional climate model for the western United States. *Clim. Change*, **15**, 383-422.

Dickinson, R.E., A. Henderson-Sellers, and P.J. Kennedy, 1993: Biosphere-atmosphere transfer scheme version 1e as coupled to the NCAR community climate model. Technical Report NCAR/TN-387+STR, NCAR, Boulder, Colorado, 72 pp.

Dumenil, L. 1993: Near surface systematic errors in GCMs: Dynamics versus land surface processes. *GEWEX News*, Winter 92/93, 2-3.

EarthInfo, 1993: *Earthinfo NCDC summary of the day: CD-ROM*, EarthInfo, Boulder, Colorado.

Fennessy, M.J., J.L. Kinter, B. Hirtman, L. Marx, S. Nigam, E. Schneider, J. Shukla, D. Straus, A. Vernekar, Y. Xue, and J. Zhou, 1994: The simulated Indian monsoon: a GCM sensitivity study. *J. Climate*, **7**, 33-43.

Fritsch, J.M., and C.F. Chappell, 1980: Numerical prediction of convectively driven mesoscale pressure systems, Part 1 Convective parameterization. *J. Atmos. Sci.*, **37**, 1722-1733.

Foufoula-Georgiou, E., and S. Perica, 1994: Rainfall subgrid scale parameterization: coupling mesoscale meteorology with small-scale scaling descriptions. *Presented at, International GCIP/MAGS Workshop on Scaling in Hydrometeorological/Hydrological Processes and Models*, Victoria, Canada.

Gao, X., and S. Sorooshian, 1994: A stochastic precipitation disaggregation scheme for GCM applications. *J. Climate*, **7**, 238-.

Garratt, J.R., 1993: Sensitivity of climate simulations to land-surface and atmospheric boundary-layer treatments - A review. *J. Climate*, **6**, 419-449.

Giorgi, F., and G.T. Bates, 1989: On the climatological skill of a regional model over complex terrain. *Mon. Wea. Rev.*, **117**, 2325-2347.

Giorgi, F., G.T. Bates, R.M. Errico, and R.E. Dickinson, 1989: Modeling the climate of the western United States with a limited area model coupled to a general circulation model. *Proc., Sixth Conf. on Applied Climatology*, Charleston, 201-208.

Giorgi, F., 1990: Simulation of regional climate using a limited area model nested in a general circulation model. *J. Climate*, **3**, 941-963.

Giorgi, F., 1991: Sensitivity of simulated summertime precipitation over the western United States to different physics parameterizations. *Mon. Wea. Rev.*, **119**, 2870-2888.

Giorgi, F., M.R. Maranuci, and G.T. Bates, 1993a: Development of a second generation regional climate model (RegCM2). Part I: Boundary-layer and radiative transfer processes. *Mon. Wea. Rev.*, **121**, 2794-2813.

Giorgi, F., M.R. Maranuci, G.T. Bates, and G. DeCanio, 1993b: Development of a second generation regional climate model (RegCM2). Part II: Convective processes and assimilation lateral boundary conditions. *Mon. Wea. Rev.*, **121**, 2814-2832.

Giorgi, F., G.T. Bates, and S. Nieman, 1993c: The multiyear surface climatology of a regional atmospheric model over the Western United States. *J. Climate*, **6**, 75-95.

Giorgi, F., C.S. Brodeur, and G.T. Bates, 1994b: Regional climate change scenarios over the United States produced with a nested regional climate model. *J. Climate*, **7**, 375-399.

Goodess, C.M., and J.P. Palutikof, 1992: The development of regional climate scenarios and the ecological impact of greenhouse gas warming. *Advances in Ecological Research*, **22**, 33-62.

Grotch, S.L., and M.C. MacCracken, 1991: The use of general circulation models to predict regional climate change. *J. Climate*, **4**, 286-303.

Hewitson, B., and R.G. Crane, 1992: Regional climates in the GISS global circulation model: Synoptic-scale circulation. *J. Climate*, **5**, 1002-1011.

Hewitson, B. 1994: Regional climates in the GISS general circulation model: Surface air temperature. *J. Climate*, **7**, 283-.

Kellogh, W.W., and Z.C. Zhao, 1988: Sensitivity of soil moisture to doubling of carbon dioxide in climate model experiments, Pt. 1, North America. *J. Climate*, **4**, 348-366.

Kern, J.S. 1994a: Spatial patterns of soil organic carbon in the contiguous United States. *Soil Science Society of America Journal*, **58**, 439-455.

Kern, J.S. 1994b: Geographic patterns of soil water retention in the contiguous United States. *Soil Science Society of America Journal*, in press.

Kiehl, J.T., 1992: Atmospheric general circulation modeling. in Trenberth, K. (ed.), *Climate System Modeling*, Cambridge University Press, New York, 319-369.

Kittel, T.G.F., N.A. Rosenbloom, T.H. Painter, D.S. Schimel, and VEMAP Modeling Participants. 1994. The VEMAP integrated database for modeling United States ecosystem/vegetation sensitivity to climate change. *Global Ecology and Biogeography Letters*, in press.

Koch, S.E., 1985: Synoptic-scale forecast skill and systematic errors in the MASS 2.0 model. *Mon. Wea. Rev.*, **113**, 1714-1737.

Kuchler, A.W., 1964: Potential natural vegetation of the conterminous United States. *Special Publication No. 36*, American Geographical Society.

Kuchler, A.W., 1993: Potential natural vegetation of the conterminous United States. *Digital Vector Data*, US-EPA Environmental Research Laboratory, Corvallis, Oregon.

Kuo, Y.H., 1974: Further studies of the parameterization of the influence of cumulus convection on large-scale flow. *J. Atmos. Sci.*, **31**, 1232-1240.

Lee, T.J., 1992: *The impact of vegetation on the atmospheric boundary layer and convective storms.* Ph.D. dissertation, Colorado State University, Fort Collins, Colorado, 137 pp.

Legates D.R., and C.J. Willmott, 1990: Mean seasonal and spatial variability in guage corrected global precipitation. *Inlt. J. Climatol.*, **10**, 111-127.

Liu, Y., F. Giorgi, and W. Washington, 1994: Simulation of summer monsoon climate over East Asio with an NCAR regional climate model. *Mon. Wea. Rev.*, **122**, 2331-2348.

Louis, J.F., 1979: A parametric model of vertical eddy fluxes in the atmosphere. *Bound.-Layer Meteor.*, **17**, 187-202.

Loveland, T.R., J.W. Merchant, D.O. Ohlen, and J.F. Brown, 1991: Development of a land-cover characteristics database for the conterminous U.S. *Photo. Eng. Rem. Sens.*, **57**, 1453-1463.

Mahrer, Y. and R.A. Pielke, 1977: A numerical study of the airflow over irregular terrain. *Beitr. Phys. Atmos.*, **50**, 98-113.

Marwitz, J.D., 1972: Precipitation efficiency of thunderstorms of the high plains. *J. Rech. Atmos.*, **6**, 367-370.

McCumber, M.C. and R.A. Pielke, 1981: Simulation of the effects of surface fluxes of heat and moisture in a mesoscale model – Part 1. Soil layer. *J. Geophys. Res.*, **86**, 9929-9938.

McGregor, J.L., and K. Walsh, 1993: Nested simulations of perpetual January climate over the Australian region. *J. Geophys. Res.*, **98**, 23,283-23,290.

Meehl, G.A., 1994: Influence of the land surface in the Asian summer monsoon: external conditions versus internal feedbacks. *J. Climate*, **7**, 1033-1049.

Mitchell, J.F.B., S. Manabe, V. Meleshko, and T. Tokioka, 1990: Equilibrium climate change – and its implications for the future, In: *Climate Change, the IPCC Scientific Assessment*, Cambridge University Press, Cambridge, 131-172.

NOAA/USDA, 1989: *Weekly weather and crop bulletin.*, **76**, NOAA/USDA Joint Agricultural Weather Facility, Washington, D.C..

Ojima, D.S., T.G.F. Kittel, D.S. Schimel, C.A. Wessman, B. Curtiss, S. Archer, V.B. Brown, and W.J. Parton, 1992: Global arid and semi-arid ecosystems: Linkage between process models and remote sensing. *International Geoscience and Remote Sensing Symposium*, **2**, 1027-1029.

Over, T.M., V.K. Gupta, and R. Lawford, 1994: Random cascades and stochastic modeling of subgrid-scale precipitation. *Presented at, International GCIP/MAGS Workshop on Scaling in Hydrometeorological/Hydrological Processes and Models*, Victoria, Canada.

Parry, M.L., T.R. Carter, and N.T. Konijn (eds.), 1988: *The Impact of Climate Variations on Agriculture*, Vol. 1, Kluwer Academic Press, 876 pp.

Parton, W.J., D.S. Schimel, C.V. Cole, and D.S. Ojima, 1987: Analysis of factors controlling soil organic matter levels in the Great Plains grasslands. *Soil Sci.*, **51**, 1173-1179.

Pielke, R.A., 1984: *Mesoscale Meteorological Modeling.* Academic Press, 612 pp.

Pielke, R.A., and R. Avissar, 1990: Influence of landscape structure on local and regional climate. *Landscape Ecology*, **4**, 133-155.

Pielke, R.A., C.-H. Yu, R.W. Arritt, and M. Segal, 1984: Mesoscale air quality under stagnant conditions. *Air Pollution Effects on Parks and Wilderness Areas Conference*, 20-23 May, Mesa Verde National Park, Colorado.

Pielke, R.A., M. Segal, R.W. Arritt, C.-H. Yu, and R.T. McNider, 1985: Influence of distant as opposed to local pollution transport on wilderness air quality. *Presented at the National Wilderness Research Conference*, Fort Collins, CO, July 23-25, 1985.

Pielke, R.A., R.W. Arritt, M. Segal, M.D. Moran, and R.T. McNider, 1987: Mesoscale numerical modeling of pollutant transport in complex terrain. *Bound.-Layer Meteor.*, **41**, 59-74.

Pielke, R.A., W.R. Cotton, R.L. Walko, C.J. Tremback, M.E. Nicholls, M.D. Moran, D.A. Wesley, T.J. Lee, and J.H. Copeland, 1992: A comprehensive meteorological modeling system - RAMS. *Meteor. Atmos. Phys.*, **49**, 69-91.

Portman, D.A., W.C. Wang, and T.R. Karl, 1992: Comparison of greneral circulation model and observed regional climates: Daily and seasonal variability. *J. Climate*, **5**, 343-353.

Reed, D.N., 1986: Simulation of time series of temperature and precipitation over eastern England by an atmospheric general circulation model. *J. Climatol.*, **6**, 233-253.

Reynolds, R.W., and T.S. Smith, 1994: Improved global sea surface temperature analyses using optimal interpolation. *J. Climate*, **6**, 929-948.

Roads, J.O., S.C. Chen, A.K. Guetter, and K.P Georgakakos, 1994: Large-scale aspects of the United States hydrologic cycle. *Bull. Amer. Meteor. Soc.*, **75**, 1589-1610.

Robock, A., R.P. Turco, M.A. Harwell, T.P. Ackerman, R. Andressen, H.S. Chang, and M.V.K. Sivakumar, 1993: Use of general circulation model output in the creation of climate change scenarios for impact analysis. *Climatic Change*, **23**, 293-335.

Running, S.W., and E.R. Hunt, 1993: Generalization of a forest ecosystem process model for other biomes, BIOME-BGC, and an application for global-scale models. *Scaling Physiological Processes: Leaf to Globe.*, J.R. Ehleringer and C.B. Fields (eds.), Academic Press, San Diego, California, 141-158.

Sagan, C, O.B. Toon, and J.B. Pollack, 1979: Anthropogenic albedo changes and the earth's climate. *Science*, **206**, 1363-1368.

Schimel, D.S., T.G.F. Kittel, D.S. Ojima, F. Giorgi, A. Metherell, R.A. Pielke, C.V. Cole, and J.G. Bromberg, 1994: Models, methods and tools for regional models of the responses of ecosystems to global climate change. *Proceedings, International Workshop on Sustainable Land Management for the 21st Century.*, Vol. 2, Agricultural Institute of Canada, Ottawa, 227-238.

Segal, M., R.T. McNider, and R.A. Pielke, 1985: Use of a mesoscale primitive equation model in the design of SCCCAMP. ASTeR Report No. 1, 1985, ASTeR Inc., Fort Collins, Colorado 80522.

Segal, M., R. Avissar, M.C. McCumber, and R.A. Pielke, 1988: Evaluation of vegetation effects on the generation and modification of mesoscale circulations. *J. Atmos. Sci.*, **45**, 2268-2292.

Segal, M., W. Schreiber, G. Kallos, and R.A. Pielke, 1989: The impact of crop areas in northeast colorado on midsummer mesoscale thermal circulations. *Mon. Wea. Rev.*, **117**, 809-825.

Segal, M., P. Alpert, U. Stein, M. Mandel, and M.J. Mitchell, 1994: Some assessments of the potential $2\times CO_2$ climate effects on water balance components in the eastern Mediterranean. *Climatic Change*, **27**, 351-371.

Sellers, P., 1992: Biophysical models of land surface processes. in Trenberth, K. (ed.), *Climate System Modeling*, Cambridge University Press, New York, 451-490.

Stocker, R.A., M. Uliasz, and R.A. Pielke, 1994: The validation of the RAMS/NGM meteorological fields used in the MOHAVE field study. *Proc. Aeorsols and Atmospheric Optics: Radiation Balance and Visual Air Quality.*

Stuart, R.A., and G.A. Isaac, 1994: A comparison of temperature-precipitation relationships from observations and as modeled by the general circulation model of the Canadian climate centre. *J. Climate*, **7**, 277-.

Thompson, G., 1993: Prototype real-time mesoscale prediction during 1991-1992 winter season andstatistical verification of model data. Masters Thesis, *Atmospheric Science Paper 521*, 105 pp., Department of Atmospheric Science, Colorado State University, Fort Collins, Colorado.

Tremback, C.J., 1990: Numerical simulation of a mesoscale convective complex: model development and results, PhD dissertation, *Atmospheric Science Paper 465* , 247 pp., Department of Atmospheric Science, Colorado State University, Fort Collins, Colorado.

Tremback, C.J. and R. Kessler, 1985: A surface temperature and moisture parameterization for use in mesoscale numerical models. *Proc. 7th AMS Conference on Numerical Weather Prediction*, June 17-20, Montreal, Quebec, American Meteorological Society, Boston, 355-358.

Tremback, C.J., G.J. Tripoli, and W.R. Cotton, 1985: A regional scale atmospheric numerical model including explicit moist physics and a hydrostatic time-split scheme. *Proc. 7th AMS Conference. on Numerical Weather Prediction*, June 17-20, Montreal, Quebec, American Meteorological Society, Boston, 433-434.

Tremback, C.J., G.J. Tripoli, R. Arritt, W.R. Cotton, and R.A. Pielke, 1986: The regional atmospheric modeling system. *Proc. Inter. Conference. Development and Application of Computer Techniques to Environmental Studies*, November, Los Angeles, California, P. Zannetti, Ed., Computational Mechanics Publications, Boston, 601-607.

Tripoli, G.J. and W.R. Cotton, 1980: A numerical investigation of several factors leading to the observed variable intensity of deep convection over South Florida. *J. Appl. Meteor.*, **19**, 1037-1063.

Tripoli, G.J. and W.R. Cotton, 1981: The use of ice-liquid water potential temperature as a thermodynamic variable in deep atmospheric models. *Mon. Wea. Rev.*, **109**, 1094-1102.

Tripoli, G.J. and W.R. Cotton, 1982: The Colorado State University three-dimensional cloud/mesoscale model-1982. Part I: General theoretical framework and sensitivity experiments. *J. Rech. Atmos.*, **16**, 185-220.

Tripoli, G.J., 1986: A numerical investigation of an orogenic mesoscale convective system. Atmospheric Science Paper No. 401, Department of Atmospheric Science, Colorado State University, Fort Collins, Colorado 80523.

Tripoli, G.J. and W.R. Cotton, 1989a: Numerical solution of the Navier-Stokes equations with topography. *J. Comput. Phys.*, **17**, 276-310.

Von Storch, H., E. Zorita, U. Cusbach, 1993: Downscaling of global climate change estimates to regional scales: An application to Iberian rainfall in winter. *J. Climate*, **6**, 1161-1171.

Wendler, G., and F. Eaton, 1983: On the desertification of the sahel zone. *Climatic Change*, **5**, 365-380.

Wigley, T.M.L., P.D. Jones, K.R. Briffa, and G. Smith, 1990: Obtaining sub-grid-scale information from coarse-resolution general circulation model output. *J. Geophys. Res.*, **95**, 1943-1953.

Wilson, C.A., and J.F.B. Mitchell, 1987: Simulated climate and CO_2-induced change over Western Europe. *Climate Change*, **10**, 11-42.